

THÈSE

présentée au Laboratoire de chimie quantique
UMR 7551 CNRS/ULP
devant la Faculté de chimie
de l'Université Louis Pasteur - Strasbourg I
en vue de l'obtention du
Doctorat de l'Université Louis Pasteur
en Chimie - spécialité Chimie Informatique et Théorique
par
Sébastien VILLAUME

Electronic Spectroscopy and Photochemistry of Small Transition Metal Complexes studied via Coupled Cluster calculations and Wavepacket propagation

soutenue le 5 octobre 2005 devant la commission d'examen:

Chantal DANIEL	Co-directeur de Thèse
Alain STRICH	Co-directeur de Thèse
Alex BOEGLIN	Rapporteur interne
Philippe HIBERTY	Rapporteur externe
Peter SAALFRANK	Rapporteur externe
Ajith PERERA	Examineur

Remerciements/Acknowledgements

Je remercie Chantal Daniel et Alain Strich, mes co-directeurs de thèse, qui ont su me gérer, me canaliser, et tirer le meilleur parti (s'il y en a un) de mes défauts et de mes quelques qualités.

I would like to thank Prof. Rodney J. Bartlett, to have accepted me in his group, for the fruitful discussions and to have got me used to Coupled Cluster theory. I also thank Ajith Perera, for his help, his advice and his patience. This work could not be finished without him.

I want to address my acknowledgements to the members of the jury to have accepted to assess my work.

Je remercie également tout le laboratoire de Chimie quantique de m'avoir accueilli, en particulier mes collègues de bureau, ceux du début, Gaetan et Pascal, et les actuels, Sébastien et Radovan, et ceux qui ont été de passage. Merci aussi à toutes les personnes que j'ai croisées à la fac, les potes du fond de l'amphi, les potes de cafet', les potes de soirées. Chacun se reconnaîtra et se mettra dans la bonne catégorie, voire dans plusieurs! Une petite pensée aussi pour la "fine équipe" autrement connue sous le nom de "belle brochette"! Je remercie en particulier une personne qui se reconnaîtra, trop pudique pour que je la cite et capable de m'égorger pour ça!

I have a thought for all the people in the QTP, and for my Florida friends. I also would like to thank my "american" family, the Fabiani's, to have accepted me in their home, thank you Patti, Rick, Rick Jr, Chris and Alicia. Go Gators!

Je souhaite également remercier ma famille, en particulier mes parents, mais aussi mes petites soeurs qui m'ont toujours soutenu, même dans les moments difficiles ou j'ai été vraiment invivable (et je crois que je le suis toujours!). Sans eux, je ne serais pas ce que je suis aujourd'hui, je leur dois beaucoup.

I also thank the France-USA IGERT and the PROCOPE programs for the financial support during my visiting period in the group of Prof. Bartlett, Quantum Theory Project, Florida and in the group of Prof. Manz, Freie Universität, Berlin.

Contents

French Abstract	9
Introduction	19
1 Methods and Theory	27
1.1 <i>ab initio</i> methods	27
1.1.1 Hartree-Fock Theory	28
1.1.2 Basis set effect	30
1.1.3 Accurate treatments of the electron correlation	30
1.1.4 Density functional theory method	31
1.1.5 Variational methods	31
1.1.6 Perturbational methods	33
1.1.7 Cluster expansion based methods	33
1.1.8 Computing Potential Energy Surfaces	36
1.2 Quantum Dynamics	37
1.2.1 Time Dependent Approach without explicit laser field	38
1.2.2 Representation and Discretization	40
1.2.3 Initial Wave Packet	41
1.2.4 Time propagation: Chebichev propagator	42
1.2.5 Norm, Population, and Probability of dissociation	43
1.2.6 Coupling with Laser field	44
2 Intramolecular Rearrangements in PH₂F₃ revisited through accurate quantum chemical studies	47
2.1 Computational Details	48
2.2 Results	49
2.2.1 Geometry optimization	49
2.2.2 Relative Stabilities of the stereo-isomers	50
2.2.3 Harmonic vibrational frequencies	54
2.3 Conclusion	55

3	Electronic spectroscopy of Cr(CO)₆: Coupled Cluster Calculations	61
3.1	Computational details	62
3.2	Results	63
3.2.1	Basis set	63
3.2.2	Geometry optimization	63
3.2.3	Transition Energies	64
3.3	Conclusion	66
4	Quantum chemical study of the electronic structure of MCH₂⁺ (M=Fe,Co,Ni)	73
4.1	Computational Details	75
4.1.1	Geometry Optimization	75
4.2	Results	76
4.2.1	Electronic Structure	76
4.2.2	Spin Contamination	82
4.3	Conclusion	83
5	Emission spectroscopy of metal-to-ligand-charge-transfer states of HRe(CO)₃(H-DAB)	93
6	Photochemistry of RCo(CO)₄ (R=H,CH₃)	105
6.1	Computational Details	106
6.2	Results	107
6.2.1	Geometry optimization	107
6.2.2	Absorption Spectroscopy of RCo(CO) ₄ (R=H, CH ₃)	108
6.3	Potential Energy Surfaces	108
6.4	Quantum Dynamics	110
6.4.1	Results	114
6.5	Conclusion	114
	Conclusion	123
	Bibliography	132
	A Acronym Glossary	135

French Abstract

LA photochimie est l'étude des réactions chimiques induites par l'absorption de lumière: lorsqu'un photon (ou plusieurs) est absorbé, une molécule peut changer d'état électronique, elle est dans un état excité. Une excitation électronique requiert environ 2eV, les réactions photochimiques sont donc initiées par des photons dans le domaine UV-Visible.

Le principal avantage des réactions chimiques photo-induites par rapport aux réactions thermo-induites est la sélectivité qu'elles permettent. En utilisant une source de photons monochromatique, il est possible d'exciter les molécules dans un état électronique spécifique sans exciter ces molécules (ou d'autres) dans un autre état électronique, conduisant à la formation de produits secondaires non désirés. Cette sélectivité peut donc être atteinte en utilisant une source laser pour laquelle la longueur d'onde, l'intensité, la durée d'irradiation ou encore la polarisation du champ magnétique peuvent être contrôlées afin d'obtenir la source idéale pour une étude photochimique. Au contraire, chauffer un échantillon augmente les énergies vibrationnelles, rotationnelles ou de translation de toutes les molécules sans aucun contrôle possible.

Dans la plupart des cas, l'état électronique fondamental est un singulet avec tous les électrons appariés. Les règles de sélection de spin et les considérations de symétrie montrent que seuls des états singulets de symétrie particulière sont accessibles depuis l'état fondamental.

Plusieurs processus peuvent avoir lieu après une irradiation car la molécule ne peut pas rester dans un état excité indéfiniment, car instable vis-à-vis de l'état fondamental. L'absorption peut initier plusieurs types de processus chimiques. Si l'état vibrationnel excité est au dessus de l'énergie de dissociation de l'état électronique liant excité, la molécule peut se dissocier pour produire de nouvelles espèces chimiques très réactives comme des radicaux. De la même manière, une excitation vers un état électronique excité dissociant peut également conduire à une photo-dissociation ultra-rapide. Des conversions internes ou des croisements intersystème peuvent également conduire de manière indirecte à la photo-dissociation à une échelle de temps plus longue. Enfin, la désexcitation, particulièrement par les voies non-radiatives avec des énergies vibrationnelles relativement élevées, peut induire l'isomérisation. Les voies possibles de désexcitation sont nombreuses et elles ne seront pas toutes décrites ici.

La photochimie et la spectroscopie d'absorption et d'émission ont connu de grandes avancées grâce à l'utilisation de nouvelles sources laser capables de produire des impulsions ultra-brèves de l'ordre de la femtoseconde. Les impulsions à cette échelle de temps ainsi que les progrès réalisés dans l'ajustement des propriétés du laser (longueur d'onde, intensité, phase, etc...) constituent un outil parfaitement adapté pour suivre l'évolution des processus photochimiques ultra-rapides. Parallèlement, de nouveaux scénarii d'impulsions comme les expériences pompe-sonde, ont été développés pour étudier ces phénomènes. Dans une expérience pompe-sonde, une première impulsion excite (ou *pompe*) le système étudié vers un état absorbant particulier, puis une seconde impulsion excite (ou *sonde*) le système vers un état détectable comme par exemple un état ionique. Le délai temporel entre les deux impulsions permet de suivre l'évolution du système et donne de précieuses informations sur les mécanismes mis en jeu. L'objectif à moyen terme est le contrôle quantique des mécanismes par des séquences d'impulsions basées sur les informations expérimentales en utilisant des algorithmes d'apprentissage ou génétiques pour optimiser le dispositif.

Malgré ces avancées spectaculaires dans l'étude des processus photo-induits ultra-rapides, la diversité et la complexité de ceux-ci ne permettent pas de les élucider complètement par les études expérimentales. Pour confirmer ou expliquer les résultats expérimentaux, des calculs de chimie quantique de grande précision sont nécessaires. Ils permettent également d'élucider certains mécanismes inaccessibles avec les résultats expérimentaux seuls.

L'augmentation rapide des moyens de calcul au cours de la dernière décennie permet aujourd'hui d'étudier des systèmes complexes en utilisant des méthodes de grande précision comme les méthodes Coupled Cluster (*CC*) ou Complete Active Space (*CAS*). Ces méthodes de chimie quantique sont utilisées pour calculer les surfaces d'énergie potentielle de l'état fondamental et des états excités, qui serviront de données de départ pour des simulations de dynamique quantique. Les résultats de ces simulations permettent l'assignation des transitions observées sur les spectres expérimentaux, leur nature, ainsi que la caractérisation des chemins de photo-dissociation.

Les complexes de métaux de transition possèdent un nombre très varié de propriétés photochimiques et de processus photo-induits à cause de la diversité des combinaisons possibles entre un ou plusieurs centres métalliques et une quasi infinité de ligands. Les couches d du métal, ainsi que les orbitales moléculaires inoccupées basses en énergie des ligands, conduisent à des états excités qui se situent dans la fenêtre énergétique UV-Visible et à des transitions électroniques de nature très variées (centrée sur le métal, à transfert de charge métal vers ligand, à transfert de charge ligand vers métal, à transfert de charge ligand vers ligand ou encore intra-ligand). Ces transitions peuvent conduire à des chemins de désexcitation intéressants comme la photo-dissociation, la photo-isomérisation, la polymérisation photo-induite ou encore activer des cycles catalytiques.

Il existe dans la littérature scientifique un nombre important de travaux expérimentaux touchant à la photochimie des complexes de métaux de transition. Malgré cela, plusieurs aspects fondamentaux ne sont pas encore expliqués ou compris. L'assignation des bandes d'absorption ou d'émission est encore largement basée sur des lois empiriques et les

complexes de métaux de transition sont généralement caractérisés par une grande densité d'états dans une fenêtre énergétique restreinte conduisant à des spectres compliqués par rapport à celui d'une simple molécule organique de taille similaire. De plus, les premières étapes conduisant à la photo-dissociation ou à d'autres processus photo-induits sont en général difficilement identifiables à cause des différentes interactions possibles entre ce grand nombre d'états électroniques de nature différente (spin, symétrie, etc...), d'autant plus que de récentes études expérimentales résolues en temps ultra-bref (femtoseconde) ont montré que les effets dynamiques ayant lieu dans les premiers instants après l'excitation, gouvernent entièrement le schéma de relaxation ou de fragmentation.

Sur le plan théorique, les complexes de métaux de transition requièrent une attention particulière. La présence d'un centre métallique donne lieu à des difficultés habituellement absentes dans les molécules organiques comme des états à couches ouvertes, des effets de quasi-dégénérescence ou encore des couplages spin-orbite si le métal appartient à la troisième rangée des métaux de transition. Ces effets se traduisent habituellement par des problèmes de convergence, des contaminations de spin ou un caractère multi-configurationnelle de la fonction d'onde.

Ces travaux se positionnent donc à la frontière de l'utilisation standard des calculs de chimie quantique et de dynamique quantique. Le principal but de cette thèse est de comprendre et simuler les processus photo-induits ayant lieu dans les premières femtosecondes après l'irradiation, et d'adapter les méthodes théoriques à l'étude des complexes de métaux de transition. Plusieurs méthodes de la chimie quantique ont été utilisées pour étudier la structure électronique de différents complexes de métaux de transition alors que la dynamique quantique a été utilisée pour calculer les spectres d'absorption et d'émission ainsi que pour simuler des processus de photo-dissociation.

Chapitre 1: Méthodes et Théorie

Ce chapitre expose brièvement les concepts théoriques et les méthodes utilisées pour l'étude des complexes de métaux de transition. La première partie présente les méthodes *ab initio* utilisées, la seconde partie est consacrée à la dynamique quantique.

Chapitre 2: Réarrangements intramoléculaire dans PH_2F_3

Le trifluorophosphorane (PH_2F_3) et ses réarrangements intramoléculaires ont été largement étudiés expérimentalement. La conformation de PH_2F_3 est une bi-pyramide à base

trigonale avec deux atomes de fluor dans les positions axiales et les trois autres ligands occupant les positions équatoriales. Des études de Résonance Magnétique Nucléaire (RMN) à température variable ont montré que des réarrangements intramoléculaires échangeaient les atomes de fluor des positions axiales et équatoriales. Plusieurs mécanismes (en une ou plusieurs étapes) ont été proposés pour expliquer ce réarrangement intramoléculaire. Les études théoriques ont montré qu'un mécanisme en une seule étape était énergétiquement défavorable par rapport aux mécanismes en plusieurs étapes. Elles ont également mis en lumière qu'une pseudo-rotation de Berry était également plus favorable qu'une rotation de Turnstile. Ainsi, deux mécanismes notés M_2 et M_4 , correspondant à une succession de pseudo-rotations de Berry, ont été étudiés au niveau théorique en utilisant des calculs Coupled Cluster avec des fonctions de base de grande qualité. Les structures des trois isomères possibles et des états de transition ont été calculées et identifiées.

La géométrie obtenue pour l'isomère le plus stable est en très bon accord avec celle mesurée expérimentalement. Les structures et les énergies des autres stéréoisomères, ainsi que des états de transition, ont également été caractérisées.

Les deux mécanismes, M_2 et M_4 , ont été parfaitement décrits sur le plan énergétique puisque l'ensemble des intermédiaires et des états de transition a été calculé. La barrière d'activation au niveau de calcul CCSD(T)/cc-pVTZ de M_2 est de 9,70 kcal.mol⁻¹ alors que celle de M_4 est de 7,24 kcal.mol⁻¹. Le mécanisme M_4 est donc celui qui est le plus favorable pour expliquer les réarrangements intramoléculaires.

Les fréquences de vibration de l'isomère le plus stable ont également été calculées en utilisant la méthode CCSD(T) et des fonctions de base de qualité croissante. Les résultats sont en bon accord avec les valeurs expérimentales et avec l'assignation qui avait été proposée précédemment.

Chapitre 3: Spectroscopie électronique de Cr(CO)₆

Le complexe Cr(CO)₆ a été largement étudié tant au niveau expérimental que théorique. C'est un système modèle fréquemment utilisé pour étudier la photochimie et les processus catalytiques photo-induits des complexes métaux de transition - ligand carbonyle. Pourtant, la spectroscopie électronique de ce complexe a été relativement peu étudiée jusque très récemment. Ces nouvelles études ont proposé une autre assignation que celle donnée à l'origine par Beach et Gray.

La dynamique de photo-dissociation de Cr(CO)₆ a aussi été étudiée récemment par l'intermédiaire d'expériences laser pompe-sonde en phase gazeuse. Ces expériences ont montré que suivant les conditions expérimentales, on observait différents schémas de photo-fragmentation: soit une ionisation suivie par une fragmentation conduisant à l'observation de tous les fragments [Cr(CO)_n]⁺, soit une photo-fragmentation ultra-rapide suivie par une ionisation pour laquelle les fragments [Cr(CO)₅]⁺ et [Cr(CO)₄]⁺ ne sont plus observés à cause de leur durée de vie trop courte. Une dernière étude, plus récente, a montré que l'étape primaire était le départ ultra-rapide d'un carbonyle en moins de 100 fs ce qui est

en bon accord avec les observations faites pour d'autres complexes similaires.

Ce chapitre présente donc une étude de la spectroscopie électronique du complexe par l'intermédiaire de calculs Coupled Cluster et Equation Of Motion Coupled Cluster. Nos résultats montrent que les transitions électroniques calculées au niveau EOM-CCSD sont systématiquement surestimées d'environ 0,5eV. Cette surestimation systématique peut avoir différentes origines. La méthode EOM-CCSD est basée sur un unique jeu d'orbitales pour décrire à la fois l'état fondamental et les états excités. Si l'allure des orbitales changent de façon significative entre les différents états, les effets de relaxation orbitalaire peuvent être importants, conduisant à une énergie de relaxation importante également. Il est difficile de jauger les effets de relaxation mais une limite supérieure de 0,015eV a été estimée au moyen de calculs IP-EOM-CC. Les effets relativistes, notamment de couplage spin-orbite, pourraient expliquer cette surestimation systématique. Pourtant ces effets doivent être mineurs pour un métal de transition de la première période. Le dernier facteur pouvant expliquer ce décalage énergétique peut être la corrélation électronique restante qui n'est pas prise en compte au niveau CCSD. Pour l'estimer, des calculs incluant les triples excitations sont nécessaires et sont actuellement en cours.

Les résultats EOM-CCSD ainsi que les résultats MS-CASPT2 confirment la présence d'états singulet MLCT entre 4,5 et 5,0eV, en dessous des états MC calculés à 4,99 et 5,43eV. D'après les calculs CC, l'état absorbant MLCT a^1T_{1u} est quasi-dégénéré avec l'état MC a^1T_{1g} ce qui peut conduire à la dissociation ultra-rapide d'un ligand carbonyle, mais cette hypothèse doit encore être confirmée par les calculs des surfaces d'énergie potentielle.

Chapitre 4: Étude de la structure électronique de MCH_2^+ (M=Fe,Co,Ni)

Les petits complexes de type MCH_2^+ ont été largement étudiés tant au niveau expérimental que théorique. Le principal but de ces études était de comprendre et d'expliquer le rôle fondamental de ces complexes de métaux de transition possédant une sphère de coordination insaturée dans les réactions catalytiques de formation d'alcanes. En effet, le schéma catalytique dépend fortement du choix du centre métallique du complexe. Par exemple, le processus catalytique est endothermique avec un métal de la première période alors qu'il est exothermique avec un métal de la troisième période.

Les études théoriques précédentes se sont surtout intéressées à la liaison métal-carbone (énergies, longueur de liaison, etc.). En fonction du centre métallique, la nature de la liaison varie entre deux cas extrêmes: une liaison purement covalente ou une liaison purement dative. Dans la situation covalente, la liaison σ peut être vue comme le recouvrement entre une orbitale hybride (s+d) du métal contenant un électron et une orbitale hybride sp^2 du carbone contenant également un électron. La liaison π est un recouvrement entre une orbitale d du métal et une orbitale p du carbone contenant chacune un électron. Ce type de complexe porte le nom de complexe de Schrock ou complexe métal-méthylidène. Dans

la situation dative, une orbitale sp^2 doublement occupée interagit avec une orbitale $(s+d)$ vide du métal induisant une rétrodonation d'une orbitale d doublement occupée du métal vers une orbitale p vide du carbone. Ce sont les complexes de Fischer ou complexe de type métal-carbone. Les deux types de complexes ont une réactivité totalement différente, les complexes de Schrock peuvent servir de catalyseur dans les réactions nucléophiles comme la polymérisation des oléfines alors que les complexes de type Fischer sont plutôt des centres catalytiques électrophiles.

Les propriétés spectroscopiques dans ces complexes ont, au contraire, été relativement peu étudiées bien qu'intéressantes. Ces complexes sont connus pour être caractérisés par une très grande densité d'états électroniques dans un domaine d'énergie restreint avec beaucoup d'états quasi-dégénérés. Pour les trois complexes qui nous intéressent, l'état fondamental n'est jamais clairement identifié. Une description précise de la structure électronique est donc nécessaire pour déterminer quel est l'état fondamental de chaque complexe et quelle est la nature de la liaison M-C.

Récemment, des études de photo-fragmentation ont montré que le cation MCH_2^+ ($M=Fe, Co, Ni$) avait trois voies de dissociation possibles. Le départ de CH_2 est le plus favorable mais on peut également observer le départ de H ou de H_2 . Ce schéma de fragmentation nous donne une série de petits complexes très intéressants pour étudier la compétition entre les différentes voies de fragmentation. La taille du système, ainsi que le petit nombre de degrés de liberté, autorisent l'utilisation de méthodes de chimie quantique hautement corrélées, particulièrement les méthodes CCSD et EOM-CCSD. La complexité de la structure électronique de ces systèmes est également un défi pour l'emploi des méthodes CC, jamais employées pour ce type de problèmes.

Ce chapitre présente donc une étude préliminaire de la structure électronique des complexes MCH_2^+ ($M=Fe, Co, Ni$). De plus, la contamination de spin de certains états est discutée et une solution simple pour y remédier est présentée.

L'état fondamental électronique de chaque complexe a été caractérisé, ainsi que la nature de la liaison métal-carbone. La liaison σ_{M-C} est un recouvrement entre l'orbitale $3d_{z^2}$ du métal et l'orbitale $2p_z$ du carbone alors que la liaison π est un recouvrement entre l'orbitale $3d_{yz}$ du métal et l'orbitale $2p_y$ du carbone.

Les fonctions d'onde calculées en UHF présentent dans certains cas une forte contamination de spin. Une analyse détaillée de ces fonctions d'onde montre qu'au niveau de calcul HF, le système est mal décrit: l'orbitale π liante est remplacée par deux orbitales simplement occupées, une orbitale $3d_{yz}$ sur le métal et une orbitale $2p_y$ sur l'atome de carbone. Cette description incorrecte peut être corrigée par l'utilisation d'orbitales KS qui ne présentent pas cette anomalie. La nouvelle fonction d'onde CCSD obtenue avec ces orbitales KS est nettement moins contaminée mais la contamination de spin ne disparaît pas complètement. L'inclusion des triples excitations dans le calcul devrait retirer la contamination de spin résiduelle, les calculs sont en cours.

L'écart énergétique entre l'état fondamental et le premier état excité a été rationalisé pour la série MCH_2^+ ($M=Fe, Co, Ni$). Le nombre de trous dans les orbitales $3d$ du métal influence directement l'écart énergétique: partant d'une situation à 3 trous dans les orbitales $3d$ de l'état fondamental de l'atome de fer à une situation à un seul trou dans le complexe du

nickel, l'écart énergétique passe d'une situation d'états quasi-dégénérés à un écart de 2200 cm^{-1} .

L'étape suivante sera le calcul des surfaces d'énergie potentielle dans le but d'étudier la photo-fragmentation de ces complexes.

Chapitre 5: Spectroscopie d'émission de $\text{HRe}(\text{CO})_3(\text{H-DAB})$

Les spectres d'émission et d'absorption théoriques du complexe $\text{HRe}(\text{CO})_3(\text{H-DAB})$ (H-DAB= 1,4-diaza-1,3-butadiène), système modèle pour toute une classe de composés α -diimine de métaux de transition, ont été construits par propagation de paquets d'ondes sur le potentiel $V(q)$ ($q=[\text{Re-H}]$) calculé au niveau CASSCF/MR-CI pour l'état fondamental et l'état absorbant $^1\text{MLCT}$ correspondant principalement à une excitation $5d_{\text{Re}} \rightarrow \pi_{\text{H-DAB}}^*$. Les spectres issus de ces simulations comportent les principales caractéristiques des spectres expérimentaux couramment observés, c'est-à-dire une bande d'absorption intense située entre 20 000 et 25 000 cm^{-1} , attribuée à cet état MLCT, et une bande d'émission correspondante, décalée vers le rouge. La contribution des états triplets dissociant $^3\text{SBLCT}$ et liés $^3\text{MLCT}$ n'est pas prise en compte dans ces simulations préliminaires, dont le but est de comprendre la contribution de la transition $^1\text{MLCT}$ (absorbant) vers l'état fondamental dans le spectre d'émission expérimental. Ce processus peut entrer en compétition avec la rupture homolytique de la liaison Re-H via l'état $^3\text{SBLCT}$ couplé par spin-orbite à l'état absorbant. Enfin, le spectre d'émission stimulé théorique résolu en temps, accessible expérimentalement par des expériences laser pompe-sonde pour ce type de molécule, est également présenté.

Chapitre 6: Photochimie de $\text{RCo}(\text{CO})_4$ ($\text{R}=\text{H}, \text{CH}_3$)

La photochimie de $\text{RCo}(\text{CO})_4$ a déjà été largement étudiée dans la littérature en tant que système modèle pour comprendre et expliquer les mécanismes de dissociation des ligands carbonyles ayant lieu après une irradiation. Des expériences en matrice à basse température ont montré que la perte d'un ligand carbonyle est plus favorable que la rupture homolytique de la liaison Co-H avec un rapport de branchement de 8:1. Malgré cela, les études théoriques ont toujours échoué à reproduire ce résultat expérimental. Plusieurs explications peuvent être avancées pour expliquer cet échec. Le nombre de degrés de liberté pris en compte, les distances Co-R et Co-CO_{axial}, ne suffisent pas à décrire complètement la flexibilité du système. De plus, le nombre d'états électroniques pris en compte est également trop faible et l'espace actif choisi pour les calculs CASSCF est trop petit pour décrire correctement l'ensemble des états électroniques.

Dans ce chapitre, nous présentons donc une nouvelle étude de la structure électronique de $\text{RCo}(\text{CO})_4$ ($\text{R}=\text{H}, \text{CH}_3$) basée sur de nouveaux calculs CASSCF/MS-CASPT2 utilisant de

meilleures bases. Les résultats sont comparés à ceux obtenus par TD-DFT. Nous présentons également une simulation préliminaire de dynamique quantique à deux dimensions sur $\text{HCo}(\text{CO})_4$.

Les énergies de transition obtenues au niveau MS-CASPT2 sont en bon accord avec les valeurs expérimentales, les résultats TD-DFT sous-estiment les énergies de transition par plus de 0,5eV. Les principales caractéristiques du spectre expérimental sont qualitativement reproduites. Les surfaces d'énergie potentielle de $\text{HCo}(\text{CO})_4$ ont été obtenues grâce à 400 points calculés au niveau CASSCF(10e/11a). L'angle du parapluie formé par les carbonyles équatoriaux n'a pas encore été inclus dans les calculs, seules les distances Co-H et Co-CO_{axial} sont considérées. Les deux premiers états ^1E sont dissociants dans les deux directions.

Les simulations par paquets d'ondes que nous avons réalisées n'ont pas mis en évidence le départ du carbonyle mais confirment les résultats précédents, c'est-à-dire la rupture de liaison Co-H. Des calculs sont en cours avec un espace actif plus grand et en prenant en compte plus d'états pour vérifier que nos résultats ne sont pas dus à un manque de flexibilité du système.

Le principal but de ce travail était d'étudier la spectroscopie électronique et la photochimie de complexes de métaux de transition en utilisant d'une part les méthodes Coupled Cluster pour les calculs de chimie quantique, et d'autre part la propagation de paquets d'ondes pour la dynamique quantique.

Les méthodes CC ont été appliquées avec succès à plusieurs systèmes (PH_2F_3 , $\text{Cr}(\text{CO})_6$, MCH_2^+), mettant en lumière certaines difficultés (choix des bases, choix de la troncature pour les excitations, etc.). Plusieurs points peuvent être dégagés: les bases utilisées doivent être de très bonne qualité, c'est-à-dire au moins de niveau triple- ζ , pour obtenir des résultats précis; l'inclusion des triples excitations, au moins de façon perturbative, est également nécessaire pour calculer les états excités. Enfin, dans le cas de fonction d'onde à couches ouvertes fortement contaminées de spin, l'utilisation d'orbitales KS comme référence du calcul CC permet de réduire significativement cette contamination. Concernant le second aspect de ce travail, il apparaît de façon claire qu'on ne peut faire l'économie de la qualité et de la précision des calculs de chimie quantique si on veut obtenir des résultats au moins qualitatifs. De même, le choix des degrés de liberté importants est également primordial pour la construction des surfaces d'énergie potentielle et pour les simulations.

Introduction

PHOTOCHEMISTRY is the study of chemical reactions induced by light absorption. When a photon (or many photons) is absorbed, a molecule may be promoted to an excited electronic state. Since an electronic excitation usually takes about 2eV, photochemical reactions are initiated by UV or visible photons [1].

One major advantage of the photo induced chemical reactions compared to thermal reactions is the selectivity. By using monochromatic light, it is possible to excite a molecule to a selected excited state without exciting other molecules while avoiding other undesired excited states which leads to side products. This selectivity can be achieved by using a laser source in which the wavelength, the intensity, and the pulse duration or the polarization of the electromagnetic field can be tuned to obtain an ideal source for photochemical studies. In contrast, heating a sample increases vibrational, rotational or translational energies of all the molecules without any control.

In most cases, the electronic ground state is a singlet with all electrons spin paired. The selection rule $\Delta S=0$ and symmetry considerations shows that the allowed excited electronic states are also singlets with particular symmetry properties.

As depicted in figure 1, several processes may occur after irradiation because the molecule cannot persist in an excited state indefinitely, since it represents a situation unstable with respect to the electronic ground state. After light absorption, the molecule is usually in a vibrationally excited state of an electronic excited state. In solution, intermolecular collisions can transfer this extra vibrational energy to other molecules (see red zigzag arrows in Fig. 1). This process is radiationless and called **vibrational relaxation**. In gas phase, however, the number of collision is low and vibrational relaxation is not efficient. The excited molecule can lose its electronic energy by spontaneously emitting a photon. When the emission corresponds to a transition between two states of the same spin multiplicity, the process is called **fluorescence** (see green arrows in Fig. 1). Since all closed shell molecules have singlet ground state noted as S_0 , fluorescence is most frequently observed from singlet excited states, noted as S_1 , S_2 , ... Fluorescence is favoured in low pressure gas phase, where the time between collision is long. A typical life time of an electronic excited state is 10^{-8} s in the absence of collisions. If a lower electronic state of the same multiplicity (excited or ground state) is accessible, the molecule can make a radiationless transition to this lower state, this process is called **internal conversion** (see light green arrows in Fig. 1). If the lower state is not of the same multiplicity, the radiationless transition can still occur but its probability is very small. This type of transition is called **intersystem**

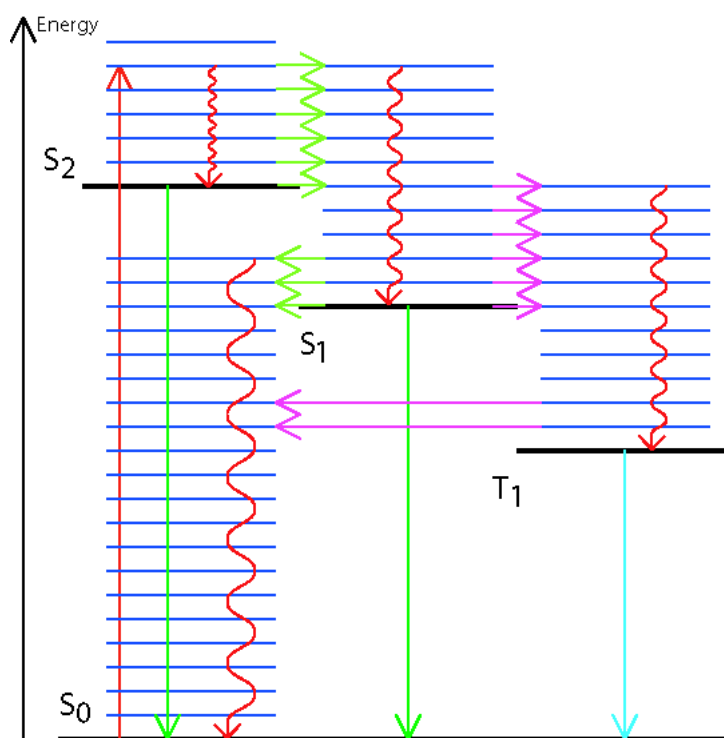


Figure 1: Jablonski diagram.

crossing (see purple arrows in Fig 1). From this state, an intersystem crossing to the high vibrational level of the electronic ground state is possible, but its probability is very low since the spin multiplicity changes. The molecule can also emit a photon and fall to the electronic ground state. This emission with a change of spin multiplicity is called **phosphorescence** (see cyan arrow in Fig. 1). The life time of a low lying electronic excited state with a spin different from the electronic ground state spin is typically 10^{-3} to 1 s in the absence of collisions.

Besides this typical picture of physical processes, absorption of light can cause several kinds of chemical processes. If the vibrational excited state is above the dissociation energy of the bound electronic excited state, the molecule may dissociate to produce new reactive species that may further react. In the same way, excitation to a repulsive (or dissociative) electronic excited state can initiate an ultra fast dissociation. Internal conversions or intersystem crossings may lead indirectly to dissociative state and then dissociation. During the de-excitation process, particularly radiationless transition with high vibrational energy levels, the molecule may isomerize. The number of channels are numerous and it is not within the context of this chapter to describe all possibilities.

During last decades, photochemistry and absorption and emission spectroscopy experiments have moved from the picosecond to the femtosecond timescale, and almost to the attosecond timescale [2, 3]. Pulse duration of few femtoseconds and pulse shaping are now routinely used in research groups [4–17], giving scientists a perfect tool to follow the ultra-fast photochemical processes. Better control of the frequency width and other properties of the laser such as the phase or the polarization improve the control or the excitation process and hence the selectivity (possibility to populate a particular state selected in an energy region characterized by a high density of absorbing states). New techniques, like pump-probe experiments [11–14], have been developed to study catalytic processes, polymerisations, electronic spectroscopy, or photodissociation [18, 19]. In pump-probe experiments, a first pulse excites the system to a particular absorbing state which is probed with a second laser pulse to a detectable state like an ionic state. The time delay between pulses gives useful information on the behaviour of the molecule under irradiation. The ultimate goal is the quantum control of processes by selective excitation based on experiments using genetic, adaptive or learning algorithms [9, 10, 20–22] (see the detailed review of Goswami on Optimal pulse shaping approaches to coherent control [23]).

Even with the advances made in experiments studying photo induced response of molecules, the physical and chemical processes that they undergo after light absorption is so complex and diverse, the experiments alone is not capable enough to fully resolve them. The experiments must be complemented by accurate theoretical calculations. When sufficiently accurate and predictive, theoretical methods can not only be used to complement or rationalize experimental findings, but also to describe processes that are difficult to access by experiments.

As discussed further in the following chapter, practical theoretical solutions are approximations with varying quality of accuracy and cost, loosely grouped into two branches commonly referred to as electronic structure theory and quantum dynamics. Theoretical photochemistry requires fully characterization of ground and excited state structures; realm of the electronic structure theory, and simulating the interaction between the ground and excited states under the influence of photons; realm of quantum dynamics.

During the last few years, computer power has grown rapidly and now it is possible to study more complex systems with accurate electronic structure techniques such as Coupled Cluster (CC) or Complete Active Space (CAS) methods. The primary role of the electronic structure calculations is to elucidate ground and excited state structures and energetics. Often, with this information alone one might be able to confirm the experimental assignments of observed bands or assist in making such assignments. Furthermore, the electronic structure theory is employed to compute the potential surfaces, which serves as an input for standard quantum dynamics simulations, and their properties such as allowed or forbidden states, coupling with other state etc. The results from these calculations yield the band structures in absorption or emission spectrum, assist in identifying the nature of bands and the characterizing photofragmentation paths, a powerful alternative to complement the experiments. The potential energy surfaces alone are not sufficient to fully understand the photochemistry; they give guidance to what the photochemical process could be. The quantum dynamics can give informations reliable to experimental quantities and validate

or invalidate the scheme assessed by the shape of the PES. The propagation of wave packets on potential energy surfaces allows for the determination of several important quantities, some of them being directly comparable to experimental data:

- The time scale of the primary reactions occurring after irradiation
- The main features of the absorption and emission spectra
- The branching ratio between concurrent reactions
- The time scale of non radiative transitions

Transition metal complexes exhibit a numerous photochemical properties and processes due to an almost infinite combination of metal centers with a large variety of ligands. The d-shell of the metal and the low lying unoccupied orbitals of the ligands lead to excited states in the UV-Visible spectral window and to electronic excited states of various characters. Different types of transitions may coexist:

- a transition from a d-shell to another d-shell is called *Metal Centered Transition* (MC).
- a transition from the metal to a ligand is called *Metal to Ligand Charge Transfer* (MLCT).
- a transition from a ligand to the metal is called *Ligand to Metal Charge Transfer* (LMCT).
- a transition between two ligands is called *Ligand to Ligand Charge Transfer* (LLCT).
- a transition centered on one ligand is called *Intra-Ligand* (IL).

These transitions may lead to interesting channels such as photodissociation, photoisomerization, photo induced polymerization or to initiate catalytic cycle.

A large number of experimental studies concerning the photochemistry of transition metal complexes are available in the literature. Despite this, several fundamental aspects of the photo-induced processes are not fully understood yet. Assignment of bands in absorption or emission spectra is usually speculative and based on empirical laws. The high density of electronic states in a small energy windows leads to complicated spectra compared to organic molecules or simple diatomics. The primary steps leading to dissociation or other chemical processes are usually not clearly identified due to the complex interplay between all these electronic states of different nature, spin or symmetry. Recent fast time resolved experiments have shown that the dynamical effects occurring at the early stage of the photolysis govern entirely the relaxation and fragmentation scheme of transition metal complexes and need to be identified to get a clear picture [9, 24–28].

From the theoretical point of view, transition metal complexes require a particular attention

and extra care. The presence of a metal center creates unusual difficulties like open shell states, quasi degeneracy effects, or spin-orbit coupling in the case of third row metals [29–31]. These aspects require special efforts and attentions since the calculations usually reveal convergence problem, spin contaminations, or multi reference character.

This work, which is manifold, but the theme lies at the frontier of the standard use of quantum chemical calculations and quantum dynamics. The goal is to understand and simulate photo-induced phenomena of transition metal complexes, which occur in the first femtoseconds and to adapt existing theoretical techniques to this complex field.

Several quantum chemical calculations have been applied to different transition metal complexes. The Coupled Cluster method and Equation of Motion Coupled Cluster method (EOM-CC) have shown promising results and a good accuracy in the Franck Condon Region but needs improvements to treat dissociation regions adequately. The CASPT2 method have shown its limitations in the description of strong avoided crossings. Quantum dynamics has been applied to study absorption/emission spectrum or to control the branching ration of two competitive photodissociation processes. A new simulation of a time-resolved emission spectroscopy has been presented for the first time.

This work is organized as follows:

The first chapter reviews the basic theoretical concepts used in this work. Practical aspects of quantum chemical calculations and wave packet propagation techniques are also briefly presented.

The second chapter deals with the intra molecular rearrangements of trifluorophosphoranes PH_2F_3 . The PH_2F_3 system is used to assess the quality of CC calculations. The prior computational work on this system were done at low level Hartree-Fock method, and hence not reliable. The structure of the three trigonal bipyramidal isomers, the interconnecting tetrapyramidal transition states, vibrational spectrum and energetics are presented.

In chapter three, we present a CC study of excited states of chromium hexacarbonyls complex, $\text{Cr}(\text{CO})_6$, which exhibits degeneracy of many states. A comparison of basis sets was performed for both ground and excited states. The structures were optimized at the CC level and vibrational calculations were performed. A comparison of transition energies with other methods such as CASSCF, CASPT2, TDDFT, and experiment is presented.

The fourth chapter deals with the study of the electronic structure of small transition metal complexes, the MCH_2^+ series ($\text{M}=\text{Fe}, \text{Co}, \text{Ni}$). The CC and EOM-CC calculations were performed to elucidate the electronic structure of these small systems. For the first time, the Kohn-Sham orbitals were used as reference function for the CC treatment. The results show that, for each complex, the ground state is always quasi degenerate and have a large spin contamination. The use of Kohn-Sham orbitals significantly decreases the spin contamination. Gas phase photo-decomposition experiments have been done on these systems and have shown that several photo-dissociation channels are possible leading to the departure of either H, H_2 or CH_2 . Preliminary work on the photofragmentation of these small system have been performed.

Chapter five presents an application of quantum dynamics. The absorption and emission

spectra of $\text{HRe}(\text{CO})_3(\text{H-DAB})$ are obtained from wave packet propagation. A time resolved emission spectrum of this complex is also presented, showing the fine structure and the evolution in time.

The last chapter, chapter six, deals with the study of the competitive photodissociation in $\text{RCo}(\text{CO})_4$ complex ($\text{R}=\text{H}, \text{CH}_3$). A simple simulation of a laser driven photodissociation is presented, showing the possibility of controlling the branching ratio.

The final chapter is followed by a conclusion. Beside summarizing the overall results of the preceding chapters and presenting concluding remarks, we also look ahead and present some perspectives of the role of theory in the field of photochemistry.

Chapter 1

Methods and theory

THIS chapter primarily reviews all theoretical concepts used in this work. As it was stated in the introduction, it is necessary to use highly accurate quantum chemical methods to study the electronic spectroscopy and the photochemistry of transition metal complexes. Photochemical processes of this type of complexes are varied and need to be treated by well balanced methods¹. These methods have to describe our system with enough accuracy, since processes like laser induced dissociation (photodissociation) that can be direct and very fast if the complex is excited directly to a dissociative state or indirect and much slower if the complex goes through non adiabatic transitions². The quantum chemical methods used in this work are introduced in the first part of this chapter while the quantum dynamical methods are presented in the second part.

1.1 *ab initio* methods

The electronic structure or related properties³ are described by the wave function $|\Psi(q, Q)\rangle$, solution of the Schrödinger equation:

$$\hat{\mathcal{H}}|\Psi(q, Q)\rangle = E|\Psi(q, Q)\rangle \quad (1.1)$$

where q and Q are respectively all electronic and nuclear coordinates and $\hat{\mathcal{H}}$ is the time independent Hamiltonian defined by:

$$\hat{\mathcal{H}} = \hat{\mathcal{T}}_q + \hat{\mathcal{T}}_Q + \hat{\mathcal{V}}_{qq} + \hat{\mathcal{V}}_{qQ} + \hat{\mathcal{V}}_{QQ} \quad (1.2)$$

where $\hat{\mathcal{T}}$ and $\hat{\mathcal{V}}$ are the kinetic energy and the potential energy operators. This equation is an eigenvalue problem where E is the eigenvalue and $|\Psi(q, Q)\rangle$ is the eigenvector that satisfy (1.1). Mathematical techniques to solve differential equations such as equation 1.1 exactly

¹it means the energy or other properties have to be computed in the same way

²internal conversions, intersystem crossings, ...

³energy, electronic transition, oscillator strength, transition dipole moments, ...

are not available. But we can obtain approximate solutions using different approaches and approximations giving different levels of accuracy. The first common approximation is the Born-Oppenheimer approximation [32] which is a separation of variables. The approximation is based on the difference in mass between electrons and nuclei, and assumes that the electrons follow the nuclear movement instantaneously. We can now rewrite the Hamiltonian as:

$$\hat{\mathcal{H}} = \hat{\mathcal{T}}_Q + \hat{\mathcal{H}}_{el} \quad (1.3)$$

where $\hat{\mathcal{T}}_Q$ depends only on nuclear coordinates and is a constant term and where $\hat{\mathcal{H}}_{el}$ depends on electronic coordinates and mixed term of electronic and nuclear coordinates. The wave function $|\Psi(q, Q)\rangle$ can be decomposed into a product of a nuclear wave function $\Xi(Q)$ with an electronic wave function $\Phi_{el}(q, Q)$ ⁴ parametrically dependent on nuclear coordinates:

$$\Psi(q, Q) = \Xi(Q)\Phi_{el}(q, Q). \quad (1.4)$$

This leads to a new simplified electronic Schrödinger equation:

$$\hat{\mathcal{H}}_{el}|\Phi_{el}(q)\rangle = E|\Phi_{el}(q)\rangle. \quad (1.5)$$

We can now find approximate solutions for chosen different sets of nuclear coordinates and build potential energy hypersurfaces. There are different quantum chemical methods available to solve this equation, based on various formalisms and giving energies at different levels of accuracy. Quantum chemical methods used in this work are presented in the next section. All of them start with the same initial wave function, the Hartree-Fock wave function. The Hartree-Fock theory is first presented, followed by Complete Active space (CAS), Configuration Interaction (CI) and Coupled Cluster (CC) theories.

1.1.1 Hartree-Fock Theory

The Hartree-Fock theory [33] is built on a simple idea, the Hartree product, which defines a polyelectronic wave function as a product of mono-electronic wave functions ϕ_i describing one electron:

$$\Theta(1, 2, \dots, n) = \phi_1(1)\phi_2(2) \dots \phi_n(n) \quad (1.6)$$

where indices i from 1 to n represent electrons. Each ϕ_i is a molecular orbital describing the three space coordinates of a single electron q_r, q_θ, q_ϕ ⁵. It is an approximation since, in the Hartree product, mono-electronic wave functions are independent. From the physical point of view, each electron interacts with all other electrons in the molecule. To satisfy normalization and antisymmetry, the polyelectronic wave function is built as following:

$$\Phi(1, 2, \dots, n) = (n!)^{-1/2} \hat{\mathcal{A}}\Theta(1, 2, \dots, n) \quad (1.7)$$

⁴we will drop Q in the following equations for simplicity

⁵in spherical coordinates

where $(n!)^{-1/2}$ and \hat{A} are respectively the normalization factor and the antisymmetry operator.

Each molecular orbital is defined as a linear combination of atomic orbital (LCAO) or a linear combination of basis functions which is simply a guess function developed on a basis of orthogonal functions χ_p :

$$\phi_i = \sum_{p=1}^N C_{pi} \chi_p \quad (1.8)$$

where N represents the total number of basis functions.

To solve equation (1.5), we have to determine the coefficients C_{pi} that minimize the energy, it is the variational principle:

$$E[\Phi(q)] = \frac{\langle \Phi(q) | \hat{\mathcal{H}} | \Phi(q) \rangle}{\langle \Phi(q) | \Phi(q) \rangle} \geq E_0 \quad (1.9)$$

where E_0 is the exact energy of the electronic ground state.

We can define a new operator, the total Fock operator $\hat{\mathcal{F}}$ which replaces the electronic Hamiltonian $\hat{\mathcal{H}}_{el}$ with the benefit that this new operator can be decomposed into a sum of monoelectronic operators:

$$\hat{\mathcal{F}} = \sum_{i=1}^n \hat{f}_i \quad (1.10)$$

where \hat{f}_i is a monoelectronic operator defined by:

$$\hat{f}_i = -1/2 \nabla_i^2 - \sum_{A=1}^M \frac{Z_A}{r_{iA}} + v^{HF}(i) \quad (1.11)$$

∇_i is the Laplacian for electron i , and $v^{HF}(i)$ is the Hartree Fock electrostatic potential created by other electrons. This leads directly to the Hartree Fock equations:

$$\hat{f}_i \phi_i = \epsilon_i \phi_i \quad (1.12)$$

where ϵ_i is the eigenvalue (or orbital energy) corresponding to the eigenvector (or molecular orbital) ϕ_i . The total energy E is not directly the sum of energies ϵ_i and the wave function Φ_0 can be built upon molecular orbitals ϕ_i . If we solve this system of equations, one can obtain a solution but approximations lead to a small error on the energy. Unfortunately, this small error is extremely important when we want to study excited states and the photochemistry because it is not systematic and constant, it varies depending on the geometry and the electronic state. This error is a consequence of the approximations made to develop the HF equations and then to solve them.

1.1.2 Basis set effect

A part of the energy error in Hartree Fock theory and post Hartree Fock theories comes from the basis set: in practice the HF equations are solved by expanding the mono-electronic wave functions as a linear combination of orthogonal basis functions (to be exact Gaussian functions). This treatment is correct only if the basis set is infinite which is not the case. This finite size of the basis set induces a systematic bias on the energy.

In the particular case of computing excited states, we have to take into account several factors in the choice of the basis set: the basis set must treat both ground and excited state in a balance manner. Diffuse functions may be necessary in the case of low lying Rydberg state and polarisation functions may help to describe the change of the electron density (charge transfer) between the ground and excited states.

Transition metal complexes also require some attention: first row transition metals can be treated with basis sets built based on an average of the electron density over several states. Second and third row metals exhibit relativistic effects and, are adequately described by basis sets built based on relativistic calculations. Relativistic effects are primarily responsible for the photochemistry of the transition metal complexes that contain heavy elements. The choice of the basis is also dependent on the quantum chemistry method. For Hartree Fock or low level perturbational method like MP2, small basis sets are satisfactory. For more accurate and correlated methods like CASSCF, CASPT2 or MRCI, Atomic Natural Orbital (ANO) are well adapted. Coupled cluster methods are quite demanding in terms of basis set quality.

The compromise between the computational cost, the accuracy and then the size of the basis set is not easy and required some experience.

1.1.3 Accurate treatments of the electron correlation

To describe a molecular system accurately, we have to take into account the electron correlation by going beyond the HF approximation. There are different approaches to solve this problem leading to different strategies and mathematical formalisms. The methods used in this work are briefly presented together with derived methods or extensions.

The choice of the method is always a compromise between several factors. The level of accuracy is the first and foremost and then the computational cost. For instance, it is faster to compute energies, transition dipole moments and oscillator strengths with Time Dependent Density functional Theory (TDDFT) than with multi State Complete Active Space Self Consistent Field (MS-CASPT2) method, but the results are less accurate. The computational cost grows with the size of the system and the level of accuracy required. The DFT methods are less accurate than CC or CAS methods, but may be the only choice for larger systems when latter methods are prohibitively costly. The validity of some approximations are important points to consider: perturbational methods will fail at dissociation distances and cannot be used to compute potential energy surfaces but can be useful to study the Franck Condon region and transition energies. Moreover, this

approach needs a zeroth order wave function of high quality describing the physico-chemical properties under study correctly.

The methods commonly used in electronic spectroscopy in transition metal complexes can be divided into 4 main families based on different mathematical approaches:

- Density functional based method like TD-DFT.
- variational methods based on a multiconfigurational wave function like CASSCF or Configuration Interaction (CI) methods.
- perturbational methods based on a second order perturbation applied to a zeroth order variational wave function. Single state CASPT2 and Multi State CASPT2 use a CASSCF wave function as reference function.
- Couple Cluster methods based on a cluster expansion and their extensions like EOM-CC, STEOM-CC.

Each method has its advantages and its limitations. Some care is needed to decide which method is the best compromise and in that sense, these methods cannot be used as black box methods and the results have to be analysed carefully.

1.1.4 Density functional theory method

Time Dependent Density Functional Theory TDDFT

The density functional theory [34] is a general one particle representation of the Schrödinger equation and the HF method is simply a special case. However, in the literature the DFT and HF methods are presented as two very different approaches derived from two distinctly different philosophies (density and wave function). Within the DFT formalism, linear response theory is used to extract the excitation energies and properties such as polarizabilities and transition moments. The advantages of DFT lies in its modest computational cost compared to wave function based correlated methods. However, the quality of the results very much depends on the choice of the functional, the exchange correlation potential and the atomic basis set. Charge transfer excitation are very difficult to compute with a good accuracy with conventional functionals and should be compared and validated by *ab initio* methods.

Despite the sensitivity of the method, the description of the electronic structure and the absorption spectrum can be achieved in a reasonable time since the computational cost is very low and the TDDFT provides good preliminary data.

1.1.5 Variational methods

Complete Active Space Self Consistent Field Theory (CASSCF)

The CASSCF method [35] is based on the partitioning of the occupied molecular orbitals into different sets:

1. Inactive molecular orbitals
2. Active molecular orbitals
3. Virtual molecular orbitals

Inactive molecular orbitals are always doubly occupied in the wave function. Active molecular orbitals can be doubly, singly or unoccupied while the virtual orbitals are never occupied and simply span the orbital space defined by the size of the basis set. Electrons in the active orbitals are called active electrons. The number of active electrons and orbitals, commonly referred to as the *size*, dictates the computational cost and the accuracy. This method is a multiconfigurational variational method which improves the SCF wave function and energy by taking into account a part of the electron correlation. The wave function is a linear combination:

$$\Phi^{CASSCF} = \Phi_0 + \sum \Phi_i \quad (1.13)$$

where Φ_0 is usually the SCF wave function and Φ_i are the wave functions obtained from Φ_0 by occupying the active orbitals with active electrons in all possible ways with symmetry restrictions. The success of this method lies in the concept of active space. All the important configurations that are relevant to describe the processes under consideration must be in the active space. Choosing a suitable active space for a given chemical process is not straightforward unless the chemical system and the processes under study are rather simple. Complex processes, like photochemistry of transition metal complexes, require experience, sound intuitive knowledge of the electronic structure and in some cases targeted *trial and error* calculations. The choice of the active orbitals will depend on the physico-chemical problem under investigation: orbitals involved in bond interaction, in isomerization processes or in absorption/emission spectra for instance.

An important feature of this method is that we can compute excited states and transition dipole moments which control the photochemistry of the molecules. There are two different approaches; we can use different sets of orbitals for each excited state (state specific) or only one set of averaged orbitals (state average). The advantage of the second approach is that transitions properties are easily computed with only one set. On the other hand, the number of computed states is limited by the constraint on the averaged orbitals. This error can be fully recovered by additional treatment as it is discussed below.

Multi Reference Configuration Interaction (MR-CI)

The CASSCF results are only of qualitative values, but we can go beyond this with a multireference configuration interaction (MRCI) treatment [36]. Using a selected space of configurations (for instance the most important configurations of a CASSCF wave function that contain the relevant informations about the studied physical phenomenon), a new wave function is built by generating single and double excitations within this restricted space.

The method introduces mixing between configurations allowing interactions of reference states with each other. If the CASSCF treatment takes into account the static electron correlation of the system, the MR-CI built on the CASSCF reference wave function handles for the remaining dynamical correlation effects due to the short range instantaneous interactions of electrons.

The validity of this method is strongly dependent on the quality of the zeroth order wave function, usually a CASSCF wave function. If an important reference configuration is missing or if the active space is too small and not flexible enough, electronic state inversion or convergence problems may occur. The MR-CI can give excellent results when the active space is adequate and representative. However, as for MCSCF, the choice of active space remains in the hands of the user.

The high computational cost and a slow convergence of the method are also a major disadvantage and a perturbative treatment like CASPT2 can provide a good alternative.

1.1.6 Perturbational methods

CASPT2 Method

Starting with a CASSCF reference wave function, the dynamic correlation effects are obtained by means of second order perturbation theory. The method is strongly dependent on the quality of the CASSCF reference wave function. We can also face intruder state problems. Intruder states are those configurations that have large unphysical contributions to the energy, and hence they effectively invalidate the perturbative treatment. One possible way to avoid this is to increase the size of the active space, but it is not always possible due to technical reasons. If we are facing a weak intruder state, the best solution is to use a level shift technique, but the final energy will have a negligible dependence on the shift parameters.

The CASPT2 method is very accurate in the Franck Condon region and is quasi size-extensive, but can be inadequate at avoided crossings. Recent development of the method is the Multi-State CASPT2 (MS-CASPT2) which usually solves this problem [37]. The idea is to perform an interaction between CASPT2 states leading to new states. These new states are simply a linear combination of regular CASPT2 states. This improvement has shown a very good promise for complex systems like transition metal complexes and can be applied to generate potential energy surfaces.

1.1.7 Cluster expansion based methods

Coupled Cluster Theory

Unlike multi configurational methods, the coupled cluster theory is not based on a linear expansion of the wave function but on an exponential expansion [36]:

$$\Phi = e^{\hat{T}}\Phi_0 \quad (1.14)$$

where Φ is the exact non-relativistic electronic wave function of the ground state and Φ_0 is a starting reference wave function, usually the HF wave function, but not necessarily. The operator $e^{\hat{T}}$ is defined by a Taylor expansion:

$$e^{\hat{T}} \equiv 1 + \hat{T} + \frac{\hat{T}^2}{2!} + \frac{\hat{T}^3}{3!} + \dots = \sum_{k=0}^{\infty} \frac{\hat{T}^k}{k!} \quad (1.15)$$

and the *cluster* operator \hat{T} by:

$$\hat{T} \equiv \hat{T}_1 + \hat{T}_2 + \dots + \hat{T}_n \quad (1.16)$$

where n is the number of electrons. Operators \hat{T}_n are the n -excitation operators, for instance, the *mono-excitation operator* \hat{T}_1 and the *di-excitation operator* \hat{T}_2 , we obtain:

$$\hat{T}_1\Phi_0 = \sum_{a=n+1}^{\infty} \sum_{i=1}^n t_i^a \Phi_i^a \quad (1.17)$$

$$\hat{T}_2\Phi_0 = \sum_{b=a+1}^{\infty} \sum_{a=n+1}^{\infty} \sum_{j=i+1}^n \sum_{i=1}^{n-1} t_{ij}^{ab} \Phi_{ij}^{ab} \quad (1.18)$$

where Φ_i^a is a singly excited Slater determinant where one electron from an occupied orbital i^6 was promoted to a virtual orbital a^7 , and the t_i^a 's are called *amplitudes*, and they depend on orbitals i and a . The action of excitation operators on the reference generates a linear combination of all possible single, double and higher order excitations. Equation (1.16) contains n operators \hat{T} which correspond to the maximum number of electron we can excite.

The operator $e^{\hat{T}}$ acts on Φ_0 to produce a linear combination of Φ_0 and all possible excitations from occupied to virtual orbitals of Φ_0 , which is identical to the expansion commonly refers to as the full configuration interaction (full CI). The intermediate normalization $\langle \Phi | \Phi_0 \rangle$ ensures that the CI coefficient for the reference state is one, and the remaining coefficients corresponding to the excited determinants are expected to be smaller, reflecting that the excited determinants are correlation corrections to the reference wave function. Technically full CI calculations are limited to small systems as a result of the rapid increase in the demand for computational resources due to the fact that number of determinants grows exponentially with the number of electrons. In order to handle larger systems, one has to select configurations to truncate the series subjected to constrain that the loss of accuracy is minimized.

Beginning with inserting equation (1.14) in (1.5), and multiplying both sides by $exp(-\hat{T})$, we can write:

$$e^{-\hat{T}} \hat{\mathcal{H}} e^{\hat{T}} \Phi_0 = E \Phi_0 \quad (1.19)$$

⁶indices i, j, k, \dots represent an electron in an occupied orbital of Φ_0

⁷indices a, b, c, \dots represent an electron in a virtual orbital of Φ_0

since

$$e^{-\hat{T}} E e^{\hat{T}} = E. \quad (1.20)$$

The operator on the left-hand side of (1.19) can be rewritten using a Hausdorff commutator expansion. As shown elsewhere, the series is not infinite and truncate exactly after five terms:

$$\begin{aligned} e^{-\hat{T}} \hat{\mathcal{H}} e^{\hat{T}} &= \hat{\mathcal{H}} + [\hat{\mathcal{H}}, \hat{T}] + \frac{1}{2} [[\hat{\mathcal{H}}, \hat{T}], \hat{T}] \\ &+ \frac{1}{3!} [[[\hat{\mathcal{H}}, \hat{T}], \hat{T}], \hat{T}] + \frac{1}{4!} [[[[\hat{\mathcal{H}}, \hat{T}], \hat{T}], \hat{T}], \hat{T}]. \end{aligned} \quad (1.21)$$

Given that, only by truncating \hat{T} , we can reduce the number of terms in the expansion given in (1.21). The most appropriate and the most useful truncation is to include only the single and double excitations:

$$\hat{T} \approx \hat{T}_1 + \hat{T}_2 \quad (1.22)$$

Limiting to \hat{T}_1 has no effect on correlation energy since singly excited determinants do not couple with reference state, and are not useful except for property calculations. The main part of the electron correlation is coming from \hat{T}_2 . This truncation is the basis of the CCSD method (Coupled Cluster Single and Double), widely used in quantum calculations.

Unaffordable cost prevents the full inclusion of higher excitations only for few small systems with adequate basis sets. Including \hat{T}_3 gives the CCSDT model, including \hat{T}_4 the CCSDTQ and so on. There are some derived methods like CCSD(T) where the triple excitations are not treated exactly but as a perturbation of the CCSD equation or the CCSDT-3 where only the most important contributions of the triple excitations are computed. These methods that include approximate triple excitation effects can be useful when CCSD inadequately describes the near-degeneracy effects.

So far our discussion of CC methods limited to ground state calculations. the extension of CC methods to excited states and properties have been accomplished recently, and that is the topic of the next section.

Equation Of Motion Coupled Cluster

This method [38] starts from a very simple and common expression where the final excited state is given by:

$$|\Phi_x\rangle = \mathcal{R}|\Phi_g\rangle \quad (1.23)$$

where x and g refer to excited and ground state wave function, respectively and \mathcal{R} is a linear *Excitation operator* defined by:

$$\mathcal{R} = \mathcal{R}_0 + \mathcal{R}_1 + \mathcal{R}_2 + \dots \quad (1.24)$$

with:

$$\mathcal{R}_n = \frac{1}{n!^2} \sum_n r_{ijk\dots}^{abc\dots} a^\dagger_i b^\dagger_j c^\dagger_k \dots \quad (1.25)$$

Using (1.23) and (1.24) with (1.14) in (1.5), we have:

$$\hat{\mathcal{H}}\mathcal{R}exp(\hat{T})|\Phi_0\rangle = E\mathcal{R}exp(\hat{T})|\Phi_0\rangle \quad (1.26)$$

This equation is in principle exact, but in order to be practically useful we must truncate both \hat{R} and \mathcal{T} , which in effect leads to approximate solutions. Limiting \hat{T} and \hat{R} only to single and double excitations yields the now widely used EOM-CCSD method. It is interesting to note that the special case where $\hat{R} \equiv 1$, equation (1.26) is equivalent to the ground state CC equation.

This approach can be used to determine properties and transition dipole moments between electronic states. It is an important point that we should be able to compute transition dipoles to study photochemical properties of molecules. A potential weakness of this method is that all electronic states are computed with a common set of orbitals, which can introduce a small error by not having the flexibility to describe distinct electronic environments of excited states by different sets of basis functions.

1.1.8 Computing Potential Energy Surfaces

The potential energy surfaces (PES) have a central role in the understanding of chemical or photochemical processes since the nuclear motions are determined by the shape of the PES. The ground and excited PES are needed to study and understand absorption/emission spectroscopy and processes like photodissociation. Standard *ab initio* calculations can be used to determine the PES with a few limitations. Excited states have complicated landscape due to local minima, saddle points, avoided crossings or conical intersections resulting from non-adiabatic interactions between surfaces. In these critical regions, the nature of the electronic wave function may change rapidly as a function of the nuclear coordinates and the Born Oppenheimer approximation becomes invalid.

These critical regions and other effects like spin orbit interactions lead to transition between two or more PES. These couplings have to be determined accurately and are strongly dependent on the quality of the electronic structure calculations. A poor accuracy of the calculations would result in a biased description of the PES and a wrong description of the photochemical and photophysical processes.

The choice of the relevant nuclear coordinates is also crucial. The perfect treatment would be to take into account all nuclear coordinates, but it is only feasible for diatomics since the number of nuclear coordinates growth as $3N - 5$ for a non linear N -atoms molecule resulting in a hypersurface with $3N - 5$ dimensions. A partition of the nuclear coordinates has to be made: the active/important coordinates are fully treated while the other coordinates are fixed. The choice of the relevant coordinates is driven by the chemical or physical process under study. In the case of competitive dissociations, the bond distances would be a clever choice while in the case of photoisomerisation, a set of complex coordinates built on the true cartesian coordinates would be more suitable. The remaining nuclear coordinates, the less relevant ones, are usually fixed at their equilibrium values.

Relaxation effects may also have to be taken into account: Couplings between coordinates

may occur in some cases and the energy given by photons to a particular bond or normal vibrational mode of the molecule can be redistributed to other bonds or modes during the time evolution after the excitation. It is safe to assume that in the most cases, the coordinates are decoupled or weakly coupled and can be approximated by harmonic potential. The validity of the harmonic potential can be assessed quickly by computing single point energies at few displaced geometries from the equilibrium and then evaluating the quality of the harmonic profile connecting these points. Furthermore, if the modes are weakly coupled, they can be neglected for processes that are ultra fast in relaxation time scale. Photodissociation occurring within few a few hundreds of femtoseconds after the excitation pulse can be considered as a valid case for such an approximation.

1.2 Quantum Dynamics

New experiments in the field of *femtochemistry* like pump dump experiments or laser control techniques require adequate and accurate theoretical simulations for interpretation and validation. Several techniques have been available for theoretical simulation of femtosecond processes approximately. Recent growth in computer power has contributed to the improvement of the quality of these simulations.

These methods can be divided into two different classes, a semi classical treatment or a full quantum treatment. The semi classical methods are more approximate methods and will not be discussed in details here. Within the full quantum treatment, the study can be done in the time-independent picture by diagonalisation of the Hamiltonian or in the time-dependent picture by propagation of a wave packet on the potential energy surfaces. Exact numerical methods are limited to triatomics since the computational cost grows exponentially with the number of degrees of freedom. The exponential scaling can be reduced by approximate techniques.

Two techniques are widely used, the Time Dependent approach [39] described in further details in the next sections and the Multi Configurational Time Dependent Hartree method (MCTDH) [40]. The first takes into account only few nuclear degrees of freedom (usually one or two) but there are treated in an exact way on an *ab initio* grid while the second takes into account more degrees of freedom using fitted analytical potential energy surfaces.

The MCTDH method is based on the Time Dependent Hartree method (TDH) by expanding the wave function as:

$$\Psi(Q_1, Q_2, \dots, Q_f, t) = a(t)\psi_1(Q_1, t)\psi_2(Q_2, t) \dots \psi_f(Q_f, t) \quad (1.27)$$

where $a(t)$ is a time-dependent complex number, Q_i are the nuclear coordinates and ψ_i are known as single-particle functions. The product $\psi_1 \dots \psi_f$ is the so called Hartree product. The performance of the TDH method is rather poor and can be improved using a multiconfigurational approach, the MCTDH method. In this extension, the wave function is

expressed as a linear combination of Hartree products:

$$\Psi(Q_1, Q_2, \dots, Q_f, t) = \sum_{j_1=1}^{n_1} \sum_{j_2=1}^{n_2} \dots \sum_{j_f=1}^{n_f} A_{j_1 j_2 \dots j_f}(t) \prod_{\kappa=1}^f \psi_{j_\kappa}^{(\kappa)}(Q_\kappa, t) \quad (1.28)$$

where A_{j_1, j_2, \dots, j_f} denote the MCTDH expansion coefficients. Increasing the number of degrees of freedom and the number of Hartree product leads to more accurate propagation of the wave function and converges to the exact solution. In practice, it is rarely the case since the computational effort and disk space requirements grow rapidly.

The weakness of this method is that the potential surface is represented by a fitted analytical function. The fitting itself is an approximation which results in loss of information. When the number of important coordinates is one or two, and when the other coordinates are decoupled from these important ones, the regular treatment on an accurate grid and a propagation of a wave packet is a good compromise between accuracy and computational cost. This technique is described in the following sections.

1.2.1 Time Dependent Approach without explicit laser field

The time dependent Schrödinger equation without explicit laser field describes the time evolution of each property of a quantum system [39] and can be written as:

$$i\hbar \frac{\partial}{\partial t} \chi(Q, t) = \hat{\mathcal{H}}_f(Q) \chi(Q, t) \quad (1.29)$$

where $\chi(Q, t)$ is a wave packet evolving on an arbitrary electronic state and $\hat{\mathcal{H}}_f(Q)$ is the Hamiltonian depending only on nuclear coordinates Q for the state f . This Hamiltonian is the sum of the nuclei kinetic energy operator and the electronic potential computed as explain in the preceding section (in this work, only one or two nuclear coordinates are allowed to vary while the other remaining coordinates are fixed at the experimental or optimized value).

Wave packet propagation gives a robust method to study the photochemistry and the time evolution of the system after the interaction between light and molecules [41, 42]. A wave packet, for a short timescale in the range of few hundreds of femtoseconds, is a group of classical trajectories evolving on potential energy surfaces. This method is well adapted to the simulation of absorption and emission spectroscopy and photodissociation processes.

Formally, a wave packet is a coherent superposition of eigenstates which change in time through an exponential factor depending on time:

$$\chi(Q, t) = \int dE_f \sum_n c_f(n) \Gamma_f(Q, E_f(Q), n) e^{\frac{-iE_f t}{\hbar}} \quad (1.30)$$

where $\Gamma_f(Q, E_f(Q), n)$ are the eigenfunctions of $\hat{\mathcal{H}}_f(Q)$ with corresponding eigenvalues $E_f(Q, n)$ of vibrational state n . The coefficients $c_f(n)$ are independent of time and nuclear coordinates, and depend only on the initial conditions. The wave packet itself is a solution

of the time dependent Schrödinger equation.

The first step in wave packet propagation is the choice of the initial conditions, and therefore, the coefficients $c(E_f, n)$. Usually, at its start, the promoted wave packet is simply the vibrational ground state of the initial electronic state $\Gamma_i(Q, E_i(Q), n = 0)$ multiplied by the transition dipole moment between initial (i) and final states (f) $\mu_{i \rightarrow f}$:

$$\chi(Q, t = 0) = \mu_{i \rightarrow f} \Gamma_i(Q, E_i(Q), n = 0) \quad (1.31)$$

$\chi(Q, t = 0)$ is not an eigenstates of the excited state anymore, it starts to move on the excited state. Using these initial conditions, it implies that $c(E_f, n)$ are defined by:

$$c(E_f, n) = (2\pi\hbar)^{-1} \langle \Gamma_f(Q, E_f, n) | \mu_{i \rightarrow f} | \Gamma_i(Q, E_i, n = 0) \rangle \quad (1.32)$$

We can now introduce one of the most important function in quantum dynamics, the autocorrelation function $S(t)$ [41] which provides:

- the theoretical absorption or emission spectrum as shown by Heller
- the absorption or emission cross section
- the evolution of the wave packet on excited states.

The autocorrelation function is defined as the overlap between the wave packet at time t and the initial wave packet:

$$S(t) = \langle \chi(0) | \chi(t) \rangle \quad (1.33)$$

The total absorption spectrum, measuring the strength of a molecule to interact with photons of certain frequency ω is obtained from the Fourier transform of the total autocorrelation function:

$$\sigma_{tot}(\omega) \propto \int_{-\infty}^{\infty} e^{i(E_0(0) + \hbar\omega)\frac{t}{\hbar}} S_{tot}(t) dt \quad (1.34)$$

where $E_0(0)$ is the energy of the vibrational ground state of the electronic ground state and ω is the frequency of the absorbed photon.

The main interest of this method is the possibility to follow the movements of the wave packet on the potential energy surface. These movements can be viewed as a group of classical trajectories which facilitate the understanding of photochemical processes. In the following sections, we briefly address the three main aspects, namely,

- representation and discretization of the potential energy surfaces and of the wave packet
- the method to calculate the initial wave packet
- the different time propagators

that must be considered before an implementation and then successful application of this method.

1.2.2 Representation and Discretization

All quantities, the coordinates, the potential energy surfaces (or curves in one dimension), the Hamiltonian, and the wave packet must be discretized [43]. The continuous range of coordinates Q are replaced by a grid of discrete values using the simple scheme:

$$Q_i = i\Delta Q \quad (1.35)$$

where ΔQ is the uniform spacing between points. The grid in coordinate space can be transformed in a grid in momentum space using a Fourier Transformation. In this representation, the expression of the kinetic energy takes a very simple form as it is a diagonal matrix. The grid size in coordinate space determines the grid size in momentum space:

$$\Delta k = \frac{2\pi}{N\Delta Q} \quad (1.36)$$

where N is the number of grid points in one coordinate and has to be odd. This expression determines also the smallest frequency or longest wavelength that can be described in momentum space since $\lambda_{max} = N\Delta Q$. The mid point in the momentum space is taken as $k=0$, with an equivalent distribution of positive and negative values. We can define an index n going from the highest negative value of k to the highest positive value. The relationship between n and N is:

$$2n = N - 1 \quad (1.37)$$

The number of points and the range of each coordinate have to be chosen very carefully. The size of the grid has to be enough large to prevent out of bound problem: if the wave packet reaches end of the grid, results will be poor due to unphysical effects introduced by the boundary (unphysical reflexion of the wave packet). Consequently, the minimum number of grid points is determined by the range of each coordinates and their spacing.

Fourier Grid Hamiltonian method

We start from the Hamiltonian expression [43]:

$$\hat{\mathcal{H}} = \hat{T} + \hat{V}_Q = \frac{\hat{p}^2}{2m} + \hat{V}_Q \quad (1.38)$$

where \hat{V}_Q is the potential energy surface obtained from electronic structure calculations. As mentioned in the previous section, the kinetic operator has a very simple form in the momentum space, but not for the potential energy operator in equation (1.38) which is represented in the coordinate space. The ability to switch from one representation to the other by using Fourier transformation is often taken advantage, and perhaps the single most important feature of the Fourier Grid Hamiltonian method. For example, we can switch in the momentum space, compute the kinetic part of the Hamiltonian (asking advantage of the simpler form in Fourier space), use a back transformation to come back in the coordinates

representation and add the potential energy part. It can be shown that a matrix element of $\mathcal{H}_{QQ'}$ (Q and Q' denote arbitrary values of two different degree of freedom) can be represented as:

$$\mathcal{H}_{QQ'} = \langle Q|\hat{\mathcal{H}}|Q'\rangle = \frac{1}{2\pi} \int_{-\infty}^{\infty} e^{ik(Q-Q')} T_k dk + V(Q)\delta(Q-Q') \quad (1.39)$$

where T_k is a matrix element between k and k' in the momentum space:

$$\langle k'|\hat{T}|k\rangle = T_k \delta(k-k') \equiv \frac{\hbar^2 k^2}{2m} \delta(k-k') \quad (1.40)$$

and the matrix element for the potential term is:

$$\langle Q'|V(Q)|Q\rangle = V(Q)\delta(Q-Q') \quad (1.41)$$

We can discretize this expression of the Hamiltonian matrix element using (1.35), (1.36) and 1.37), we get:

$$\mathcal{H}_{QQ'} = \frac{1}{\Delta Q} \left\{ \sum_{l=-n}^n \frac{e^{il2\pi(Q-Q')/N}}{N} T_l + V(Q)\delta_{QQ'} \right\} \quad (1.42)$$

where

$$T_l = \frac{\hbar^2}{2m} (l\Delta k)^2 \quad (1.43)$$

1.2.3 Initial Wave Packet

The relation (1.42) can be simplified by combining negative and positive value in exponential term and normalizing [43] to get:

$$\mathcal{H}_{QQ'}^0 = \frac{2}{N} \sum_{l=1}^n \cos(l2\pi(Q-Q')/N) T_l + V(Q)\delta(QQ') \quad (1.44)$$

where the superscript 0 stands for the renormalization form of $\mathcal{H}_{QQ'}$ and using

$$T_l = \frac{2}{m} \left(\frac{\hbar\pi l}{N\Delta Q} \right)^2 \quad (1.45)$$

The expectation value of the Hamiltonian (equation (1.29) can be written as:

$$E = \frac{\sum_Q \sum_{Q'} \Gamma_Q^* \mathcal{H}_{QQ'}^0 \Gamma_{Q'}}{\sum_Q |\Gamma_Q|^2} \quad (1.46)$$

Using the variational principle, we can define a set of secular equations that give the vibrational energies E_λ and eigenfunctions $\Gamma_{Q'}^\lambda$:

$$\sum_{Q'} [\mathcal{H}_{QQ'}^0 - E_\lambda \delta_{QQ'}] \Gamma_{Q'}^\lambda = 0 \quad (1.47)$$

Now we have our initial eigenfunction to build the initial wave packet. The next step is to propagate it in time. To do so, we have to solve the time dependent Schrödinger equation. There are different techniques based on different time propagators. One of them, the Chebichev propagator, is presented in the next section.

1.2.4 Time propagation: Chebichev propagator

To solve the time dependent Schrödinger equation (1.29), there are several techniques based on the same approximations [?]. The first step is to consider a time independent Hamiltonian and in this case, the general solution of (1.29) is:

$$\chi(t - t_0) = e^{-i\hat{\mathcal{H}}(t-t_0)/\hbar}\chi(t_0) \quad (1.48)$$

The main idea is to use this equation to calculate the wave packet at time t using the previous wave packet at a time t_0 . With this scheme, we can use a recurrence procedure to compute the wave packet at time $t_0 + \Delta t$, $t_0 + 2\Delta t$, \dots $t + n\Delta t$ with a fixed Δt .

Propagation techniques differ from each other in the way the exponential term is expanded. In Chebichev method [44, 45], the exponential term is developed as:

$$\exp\left(\frac{-i\hat{\mathcal{H}}t}{\hbar}\right) = \exp\left(\frac{-it\bar{E}}{\hbar}\right)\exp\left(\frac{-i\Delta Et\hat{\mathcal{H}}_{norm}}{\hbar}\right) \quad (1.49)$$

where

$$\exp\left(\frac{-i\Delta Et\hat{\mathcal{H}}_{norm}}{\hbar}\right) = \sum_{n=0}^{\infty} C_n J_n(\Delta Et/2\hbar) T_n(-i\hat{\mathcal{H}}_{norm}) \quad (1.50)$$

with $C_n = 1$ for $n = 0$ and $C_n = 2$ for $n \geq 1$. J_n are the n -order Bessel functions of the first type and T_n are the Complex Chebichev polynoms.

The Hamiltonian has to be renormalized because Chebichev polynoms are defined in an interval $[-i, i]$. We defined new quantities $\hat{\mathcal{H}}_{norm}$, ΔE , and \bar{E} as follow:

$$\hat{\mathcal{H}}_{norm} = \frac{\hat{\mathcal{H}} - \hat{I}\bar{E}}{\Delta E} \quad (1.51)$$

$$\Delta E = \frac{E_{max} - E_{min}}{2} \quad (1.52)$$

$$\bar{E} = \frac{E_{max} + E_{min}}{2} \quad (1.53)$$

where

$$E_{max} = \frac{p_{max}^2}{2\mu} + V_{max} \quad (1.54)$$

$$E_{min} = V_{min} \quad (1.55)$$

The Chebichev method is very stable in the case of long time propagation with large values of Δt (1 to 10 fs) and it is the method of choice in our simulation.

1.2.5 Norm, Population, and Probability of dissociation

In this section, some quantities and properties relevant the study of photochemical processes are defined. These can be used to extract values that can be compared to experimental data.

The general decomposition of a wave packet can be an expansion in term of vibrational eigenstates of an electronic state i is given by:

$$\chi(Q, t) = \sum_{E_i} \sum_{v_i} C_{v_i}(t) \Gamma(Q, E_i(Q), v_i) \quad (1.56)$$

where $\Gamma(Q, E_i(Q), v_i)$ is a vibrational eigenstate with quantum vibrational number v_i of an electronic state of energy E_i as defined previously.

The norm of the wave packet along one dimension can be written as:

$$\langle \chi(t) | \chi(t) \rangle = 1 \quad (1.57)$$

We can project the total wave packet on each vibrational eigenstate $\Gamma(Q, E_i, v_i)$ using this simple projection:

$$\langle \Gamma(Q, E_i, v_i) | \chi(t) \rangle = C_{v_i}(t) \quad (1.58)$$

With this, we can express the part of the wave packet on an electronic state as a sum of all projections on each vibrational eigenstate of this state:

$$\chi_{E_i}(t) = \sum_{v_i=0}^v C_{v_i}(t) \Gamma(Q, E_i, v_i) \quad (1.59)$$

The population of an electronic state at a time t using this can be written as:

$$\begin{aligned} P_{E_i}(t) &= \int_{-\infty}^{\infty} \chi_{E_i}^*(t) \chi_{E_i}(t) dQ \\ &= \int_{-\infty}^{\infty} \sum_{v_i=0}^v C_{v_i}^*(t) \Gamma^*(Q, E_i, v_i) C_{v_i}(t) \Gamma(Q, E_i, v_i) dQ \\ &= \sum_{v_i} |C_{v_i}(t)|^2 \end{aligned} \quad (1.60)$$

and the total population over all the states is 1.

The probability of dissociation can also be defined similarly (Eqn. 1.61) as the norm of the wave packet which lies between chosen dissociation distance Q_{diss} and the asymptotic region of the surface:

$$P_{diss}(t) = \int_{Q_{diss}}^{\infty} \chi_{E_i}^*(t) \chi_{E_i}(t) dQ \quad (1.61)$$

where in practice, Q_{diss} is chosen as three times the equilibrium value of the coordinate of interest or the point where the orbitals of the fragments do not significantly overlap. We can follow the probability of dissociation as a function of time for the often complex photodissociation pathways and dissociation times, both of which are experimentally observed.

1.2.6 Coupling with Laser field

Up to this point, the laser was not explicitly taken into account in the Hamiltonian. The wave packet builds in equation (1.56) is not a true wave packet that represents the interaction between light and molecules, but states created by an infinitely short pulse in time. If we want to use explicit laser pulses of finite duration, we can define the electric field of a pulse as:

$$e(t) = e_0 \frac{e^{i\omega t} + e^{-i\omega t}}{2} \quad (1.62)$$

where e_0 is the amplitude and ω the central frequency of the electric field. In the electric field approximation, only the electric field is considered since the interaction between molecules and magnetic field is much smaller and negligible. The new term (laser field) is treated as a perturbation of field free Hamiltonian since only a small fraction of the population get excited. The light can interact with molecules through the dipole moments μ . The new Hamiltonian in the presence of a laser field can be written as:

$$\hat{\mathcal{H}}_{laser} = \hat{\mathcal{H}} - \mu e(t) \quad (1.63)$$

This new Hamiltonian implies that a new set of coupled equations has to be solved during propagation. Under the new scheme, wave packets can move to other electronic states if the frequency ω is resonant with the difference in energy between two states and the interaction become negligible and can be ignored if the frequency is far from the resonance regime. In the case of a two levels system, the coupled equations are:

$$i\hbar \frac{\partial}{\partial t} \chi_0(t) = \hat{\mathcal{H}}_0 \chi_0(t) + e_0(t) \mu_{01} \frac{e^{i\omega t} + e^{-i\omega t}}{2} \chi_1(t) \quad (1.64)$$

$$i\hbar \frac{\partial}{\partial t} \chi_1(t) = e_0(t) \mu_{10} \frac{e^{i\omega t} + e^{-i\omega t}}{2} \chi_0(t) + \hat{\mathcal{H}}_1 \chi_1(t) \quad (1.65)$$

where $\hat{\mathcal{H}}_i = \hat{T}_{nucl} + V_i$ and $\chi_i(t)$ is the wave packet moving on the potential energy surface i . The off diagonal elements, containing the electric field, show that a fraction of the wave packet comes from other states under the influence of the laser pulse. The initial conditions are $\chi_0(0) = 1$ and $\chi_1(0) = 0$ since at the beginning, only the ground state is populated. At the end of the laser pulse, the off diagonal terms vanish and the two equations become decoupled, and reduce to the situation that these are no interacting laser pulses.

Chapter 2

Intramolecular Rearrangements in PH_2F_3 revisited through accurate quantum chemical studies

TRIFLUOROPHOSPHORANE PH_2F_3 and its intramolecular rearrangements have been widely studied during past decades by both experiment and theory. Variable temperature NMR experiments have shown that the molecule undergoes intramolecular rearrangements exchanging the axial and the equatorial fluorines [46]. *Ab initio* studies have concluded that trifluorophosphorane PH_2F_3 adopts a trigonal bipyramidal structure (TBP) with two fluorine atoms in axial positions, the other three ligands occupying the equatorial positions (TBP1) (see figure 2.2) [47]. Different mechanisms have been proposed to explain these rearrangements. Based on observations made by prior work, we concluded that one-step mechanism is not energetically favorable and we choose not to consider that possible furthermore [48]. It has also been shown that Berry's pseudo-rotation [49] is most favorable compared to Turnstile rotation mechanism [50]. The two multi-step mechanism corresponding to M_2 and M_4 (according to the nomenclature of Musher [51], depicted in figure 2.1) consist of a succession of Berry's pseudo-rotations which interconvert two TBP structure via a tetragonal pyramid (TP).

The first experimental study on phosphorane has been done by Holmes and coworkers [52, 53], who reported the first IR and NMR spectra. Gilje and coworkers [46] were the first to suggest and study intramolecular rearrangements in PH_2F_3 by means of experimental and theoretical ^1H variable temperature NMR spectroscopy. Treichel et al. also reported an IR along with mass spectra, and attempted to correctly assign the vibrational modes of PH_2F_3 [54]. Christen et al. determined the experimental geometry of PH_2F_3 and other fluorophosphorane from gas phase electron diffraction experiments [47]. Most of the theoretical studies focused on the stable isomer TBP1 and its vibrational modes of the $\text{PH}_n\text{F}_{5-n}$ series. Previously, Strich studied the possible mechanisms of intramolecular rearrangement, and concluded the one-step mechanism is energetically unfavorable [48]. Strich's early work was limited to HF-SCF with small basis sets. Keil and Kutzelnigg

published a study of the nature of the chemical bond in fluorophosphorane using estimated geometries from related fluorophosphoranes [55]. Breidung et al. computed the vibrational modes of TBP1 with a SCF/6-31G** method/basis set and they reevaluated the prior experimental assignments [56]. The recent work of Wasada and Hirao has shown that perturbational theory method such as MP2, MP3 or MP4 failed to describe the rearrangement path between TBP1, the transition state TP2, and TBP2 [57]. They found a small barrier at the SCF level of 0.13 Kcal/mol between TBP2 and TP2 and a barrier of 12.03 Kcal/mol between TBP1 and TBP2 which is larger than that of at the correlated level.

This chapter reports highly accurate *ab initio* CC calculations with various high quality basis sets (cc-pVDZ, cc-pVTZ) of the structures of the trifluorophosphorane isomers. The frequencies of the vibrational modes of TBP1 are calculated at the same level of theory. A stability diagram and a rearrangement path between different structures is proposed.

2.1 Computational Details

The stereo-isomers of PH_2F_3 participating in multi-step mechanism determined by Strich [48] have been revisited. They constitute three trigonal bipyramids TBP1 (C_{2v}), TBP2 (C_s) and TBP3 (D_{3h}) and three tetragonal pyramids TP1 (C_{2v}), TP2 (C_s) and TP3 (C_s) (see Fig. 2.3).

The equilibrium structures and harmonic vibrational frequencies are obtained at the Coupled Cluster singles and doubles augmented by perturbative correction for the connected triple excitations (CCSD(T)). The geometry optimizations were performed by analytical gradients combined with classical Newton Raphson search algorithm guided by Hessian updates. The transition states were obtained using an *eigenvector following* algorithm [58] implemented in ACES II [59].

Correlation consistent basis sets, namely cc-pVDZ, cc-pVTZ and cc-pVQZ were used for both optimization and frequency calculations (see Table 2.1).

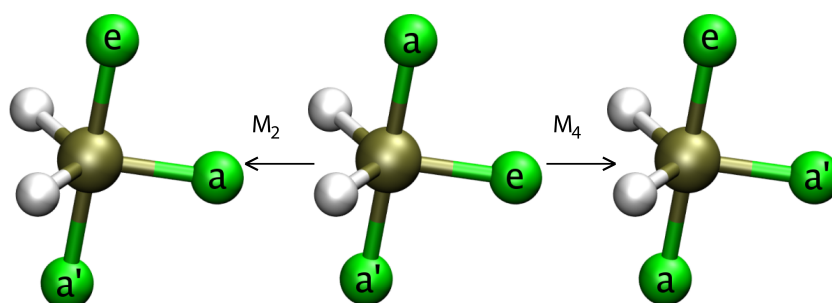


Figure 2.1: The two rearrangement modes M_2 and M_4 of PH_2F_3 .

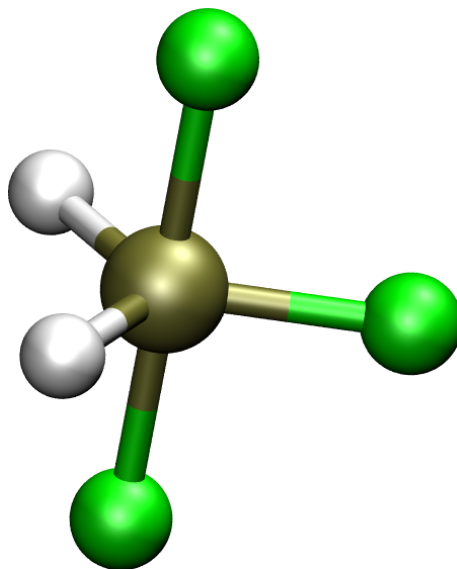


Figure 2.2: The most stable isomer of PH_2F_3 : a trigonal bipyramidal structure with two fluorine atoms in axial positions, the other three ligands occupying the equatorial positions.

2.2 Results

In this section, we will discuss the structures of the six isomers obtained at different levels of theory using different basis sets, their relative stabilities, which intramolecular rearrangement mode is the most favorable and the harmonic vibrational frequencies of TBP1.

2.2.1 Geometry optimization

The optimized structures of the six stereo-isomers of PH_2F_3 are depicted in Figure 2.3, and the corresponding optimized parameters are reported in Table 2.2 together with other results from previous calculations.

The TBP1 structure, which is the most stable isomer, is compared with a theoretical and experimental data in Table 2.3. TBP2 and TBP3 are the isomers with one or both hydrogen atoms in axial positions respectively. The TP1 is the transition state between TBP1 and TBP3, TP2 is the transition state between TBP1 and TBP2, and TP3 is the transition state between two TBP2 structures. There is no possible Berry's pseudo-rotation between TBP2 and TBP3 (see Fig. 2.4 and 2.6). The amplitudes in the CCSD wave functions near the equilibrium structures of isomers were of small magnitude showing that these molecules can be adequately treated with single reference correlation methods.

The CCSD(T)/cc-pVTZ geometry of TBP1 is in good agreement with the experiment. Bond lengths are shortened compared to the values with the double zeta basis set, which is a generally observed trend for improving basis set quality. The bond angles are less affected by the basis set quality and are already closed to the experimental values even

atom label	cc-pVDZ	cc-pVTZ
P	12s8p1d/4s3p1d	15s9p2d1f/5s4p3d1f
F	9s4p1d/3s2p1d	10s5p2d1f/4s3p2d1f
H	4s1p/2s1p	5s2p1d/3s2p1d

Table 2.1: Description of the basis sets used in this work and the contraction scheme: primitives/contracted.

with smaller basis sets. The geometry from Breidung and coworkers agrees very well with experiment [56], which might be from an unexpected error cancellation that occurs between the method (RHF) and the basis set (6-31G**).

For each isomer (TBP1, TBP2 and TBP3) and transition state (TP1, TP2 and TP3), we optimized the same parameters (bond lengths and bond angles) as Strich [48] with one exception concerning TP1: Strich was unable to locate the transition state connecting TBP1 and TBP3 and extrapolated its structure by calculating points on the reaction path connecting the two TBP structures. Geometries are close to the RHF geometries obtained by Strich with limited basis set showing that the correlation corrections do not play a bigger role in geometry. We were unable to find a structure for TP2 since it is not a true transition state but an intermediate structure between TBP1 and TBP2.

2.2.2 Relative Stabilities of the stereo-isomers

The relative stabilities of each structure calculated at the CCSD(T)/cc-pVTZ level are reported in Table 2.4 together with the previous results.

The TBP1 structure is the most stable as known from previous calculations. TBP2 and TBP3 lie at 5.77 and 6.95 kcal mol⁻¹ higher respectively. TBP2 is more stable than TBP3 with regards of the basis at the CCSD(T) level. The order of stability of the TBP's, TBP1 < TBP2 < TBP3 is not in agreement with previous calculations of Strich where TBP3 was found to be more stable than TBP2. Our results shows that the correlation energy is very important to determine the correct order of relative stabilities, and to describe adequately the electronic structure. This order follows the empirical rules favoring as many as possible electronegative atoms in axial position [60, 61].

It is important to note that TBP2 is not fully optimized: two bond angles, namely H_{ax}-P-H_e and F_{ax}-P-H_e, are fixed at 90° to maintain a trigonal bipyramid structure. A Relaxation of these angles could potentially stabilize TBP2 but its structure could become closer to TBP1 since TP2 is not a true transition state by judging from its relative energy which is in between that of the TBP1 and TBP2 at the RHF level.

	symmetry	optimized parameters	RHF	CCSD(T)	
			[48]	cc-pVDZ	cc-pVTZ
TBP1	C_{2v}	PF _{ax}	1.610	1.659	1.624
		PF _e	1.562	1.605	1.558
		PH	1.368	1.401	1.388
		α	90.6	91.0	91.3
		β	117.5	116.8	116.8
TBP2	C_s	PF _{ax}	1.595	1.643	1.597
		PF _e	1.562	1.614	1.562
		PH _{ax}	1.368	1.428	1.411
		PH _e	1.384	1.416	1.397
		α	120.3	119.4	119.8
TBP3	D_{3h}	PF	1.586	1.631	1.590
		PH	1.378	1.411	1.395
TP1	C_{2v}	PF _{ap}	1.579	1.617	1.572
		PF _b	1.594	1.639	1.601
		PH	1.375	1.410	1.395
		α	111.2	113.8	112.6
		β	98.3	93.4	94.3
TP2	C_s	PF _b	1.604	.	.
		PF _{b'}	1.572	.	.
		PH _{ap}	1.366	.	.
		PH _b	1.375	.	.
		α	96.1	.	.
		β	105.5	.	.
		γ	112.4	.	.
TP3	C_s	PF _{ap}	1.548	1.592	1.542
		PF _b	1.594	1.640	1.590
		PH	1.392	1.423	1.410
		α	100.0	101.8	102.8
		β	105.1	101.6	102.0
		γ	86.2	88.4	89.2
		δ	92.7	95.6	94.4

Table 2.2: Optimized geometries. Bond lengths are given in Angstroms and bond angles in degrees

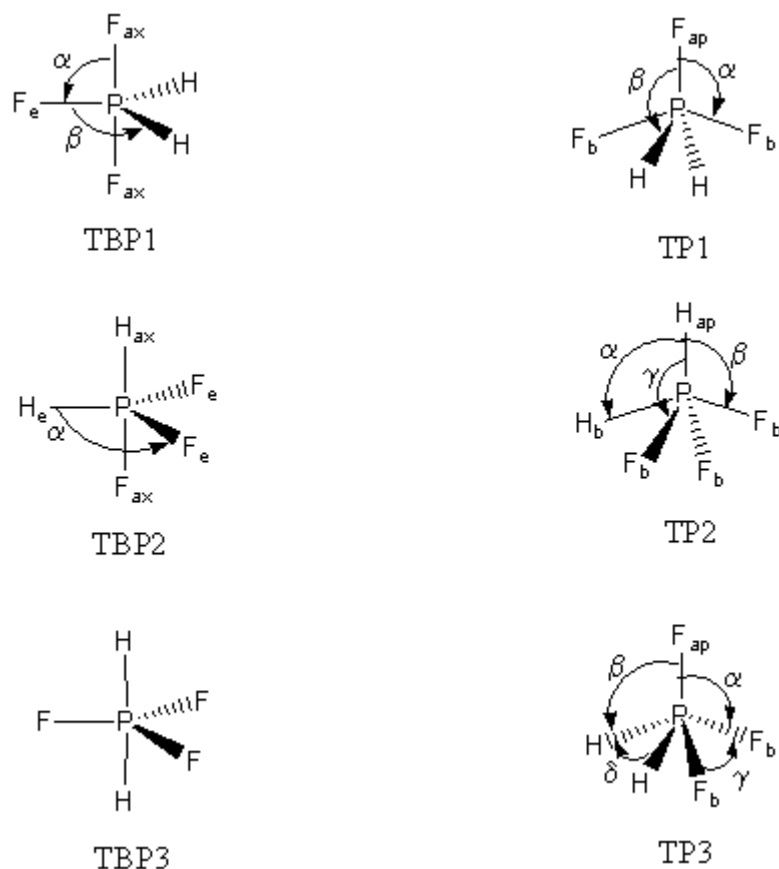


Figure 2.3: The detailed parameters of the six isomers of PH_2F_3 .

The stereo-isomer with the highest energy relative to TBP1 is TP3 ($9.70 \text{ kcal mol}^{-1}$). This transition state plays a role in the M_2 mode interconverting a TBP2 into an another TBP2 structure. Since TBP2 is $5.77 \text{ kcal mol}^{-1}$ above TBP1, the barrier between two TBP2 structure is $3.93 \text{ kcal mol}^{-1}$.

According to the relative energies of TBP2 and TP3, there is no metastable structure between two TBP1 in the M_2 mode. The activation energy of this mode is the relative energy between TBP1 and TP3 (see Fig. 2.5).

The activation barrier of the intramolecular rearrangement is determined by the highest energy of the intermediates relative to TBP1. In the M_4 mode, starting from TBP1, the isomer TBP3 is obtained by a Berry's pseudo-rotation where TP1 is the intermediate transition state. From this geometry, a second Berry's pseudo-rotation converts TBP3 to the final TBP1 (see Fig. 2.5 and 2.6). Starting and final TBP1 differ from each other by an exchange of the three Fluorine atoms. The activation barrier of the M_4 mode is then the energy of TP1 relative to TBP1 which is $7.24 \text{ kcal mol}^{-1}$. The energy difference of $0.29 \text{ kcal mol}^{-1}$ between TP1 and TBP3 suggest that TBP3 is metastable and the conversion back to TBP1 is rather easy. This result disagrees with the results of Wasada and Hirao [57]:

	RHF [48]	RHF [56]	CCSD(T) cc-pVDZ	CCSD(T) cc-pVTZ	exp [47]
PF _a	1.610	1.611	1.659	1.624	1.618
PF _e	1.562	1.553	1.605	1.558	1.539
PH	1.368	1.373	1.401	1.388	1.375
α	90.6	90.4	91.0	91.3	91.9
β	117.5	117.4	116.8	116.8	117.1

Table 2.3: Comparison of experimental and calculated geometries of TBP1 isomer. Bond lengths are give in Angstroms and bond angles in degrees.

isomers	RHF [48]		CCSD(T)/cc-pVTZ	
	Energy (a.u.)	Stability	Energy (a.u.)	Stability
TBP1	-640.0816	0.0	-641.3930	0.0
TBP2	-640.0625	12.0	-641.3838	5.77
TBP3	-640.0667	9.31	-641.3820	6.95
TP1	-640.0654	10.2	-641.3815	7.24
TP2	-640.0726	5.63	.	.
TP3	-640.0546	16.9	-641.3776	9.70

Table 2.4: Energies and Relative stabilities of the isomers at the CCSD(T)/cc-pVTZ level. The stabilities relative to TBP1 are given in kcal mol⁻¹.

they found that TP1 is more stable than TBP3 by few tens of cal mol⁻¹ at the MP2, MP3, MP4(DQ), MP4(SDQ), MP4(SDTQ), SDCI and SDCI with Davidson’s correction using a DZP basis set and SCF optimized geometries. They concluded that the Berry’s pseudo-rotation is not a possible mechanism to explain the intramolecular rearrangement, and that the correlation energy is important but not essential. On the basis of our calculations, we do not believe these conclusions are correct. As we have shown, a better method (CCSD(T)) with flexible basis sets, lead us to reach different conclusions. Also note that all the structures are optimized at CCSD(T) level of theory.

The difference between the two activation barriers of the modes M₂ and M₄ is 9.70 and 7.24 Kcal mol⁻¹ respectively, which shows that the most favorable intramolecular rearrangement of axial and equatorial Fluorine atoms is the mode M₄. This result is in good agreement with previous work of Strich but gives a better estimate of the barrier.

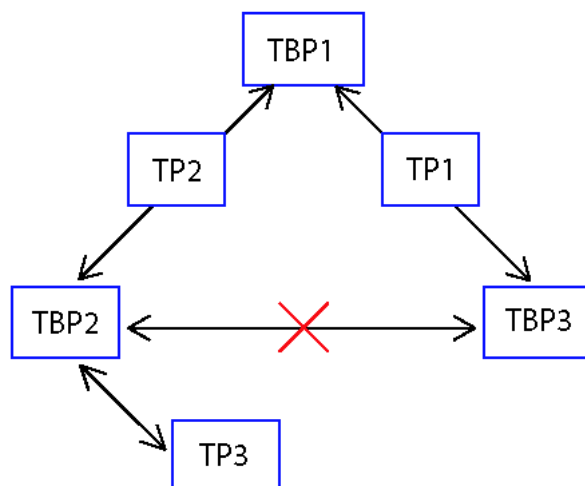


Figure 2.4: The interconverting relation between stable isomers and transition states. There is no pathway between TBP2 and TBP3.

2.2.3 Harmonic vibrational frequencies

The theoretical vibrational spectrum of TBP1 have been calculated using a numerical gradient with different basis sets of increasing quality. The vibrational CCSD(T) frequencies are presented in Table 2.5 with previous work and experimental data. Each spectrum is calculated using the optimized CCSD(T) geometry obtained with the corresponding basis set.

The results are in good agreement with the experimental values. The experimental work [53] was done with limited accuracy and new high resolution experiments are needed to confirm our results. Improving the quality of the basis set and the accuracy of the optimized geometry gives a better precision on the frequencies. The largest deviation is only 79 cm^{-1} for the ν_1 mode at the CCSD(T)/cc-pVTZ level. Each mode can be clearly assigned using symmetry, the intensities and the nuclear displacements. We confirm the assignment of Breidung and coworkers.

The calculated intensities reproduce the behaviour reported from the experimental spectrum and from the previous work of Breidung et al. The significant difference is observed for the ν_9 mode: RHF/6-31G** and CCSD(T)/cc-pVDZ overestimate the intensity where CCSD(T)/cc-pVTZ correct this to come into agreement with the weak intensity in the experimental spectrum. The ν_6 mode is forbidden in IR spectroscopy since its symmetry is A_2 , the experimental value is determined from Raman Spectroscopy. The modes ν_2 and ν_{11} have very strong intensities as expected while ν_8 is less intense but still strong. The weak/medium intensities are not correctly reproduced, but our values are in better agree-

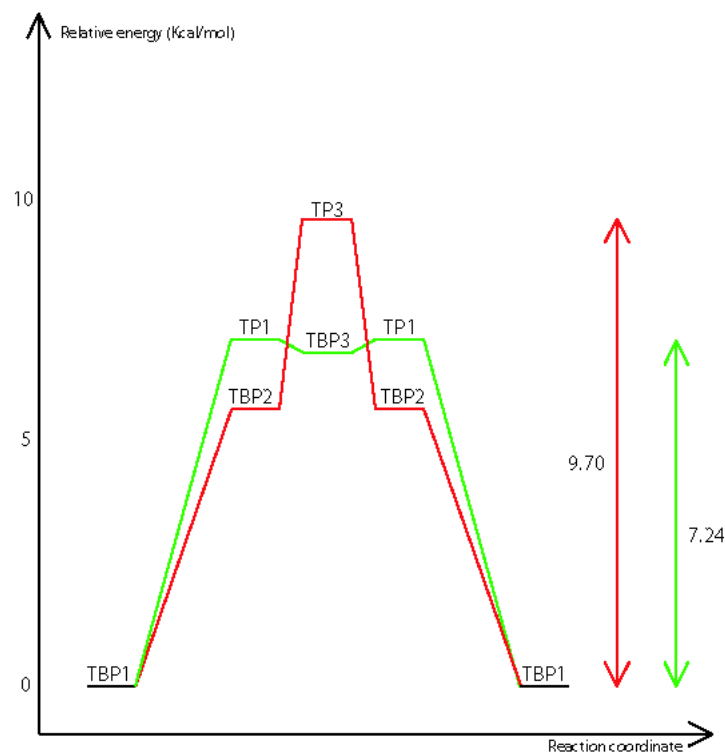


Figure 2.5: Relative stabilities of each isomers through M_2 and M_4 modes at the CCSD(T)/cc-pVTZ level.

ment with the experimental observation than the previous work.

2.3 Conclusion

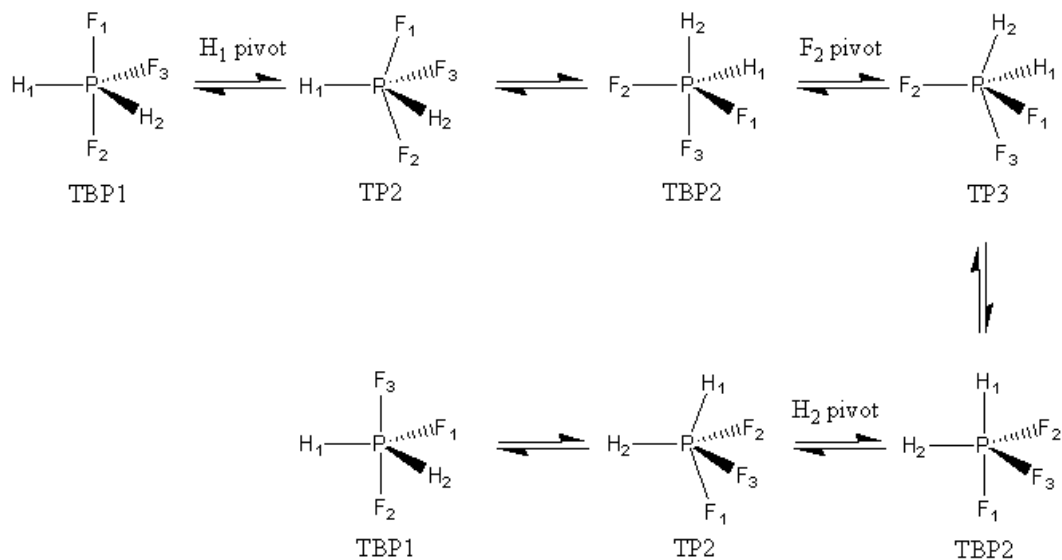
A new study of the intramolecular rearrangements in Trifluorophosphorane has been carried out. Accurate calculations including electron correlation have been performed, using CCSD(T) and large basis set of triple zeta level. The geometry of six stereo-isomers was optimized at the same level of theory. The optimized geometry of TBP1, the most stable isomer, is in good agreement with the experimental one.

The two possible modes of rearrangement, M_2 and M_4 , have been studied by characterizing the transition states and metastable intermediates. The activation barrier of M_2 is $9.70 \text{ kcal mol}^{-1}$ where the M_4 mode has an activation barrier of $7.24 \text{ kcal mol}^{-1}$. The mode M_4 , exchanging the three fluorine atoms is the most favorable one.

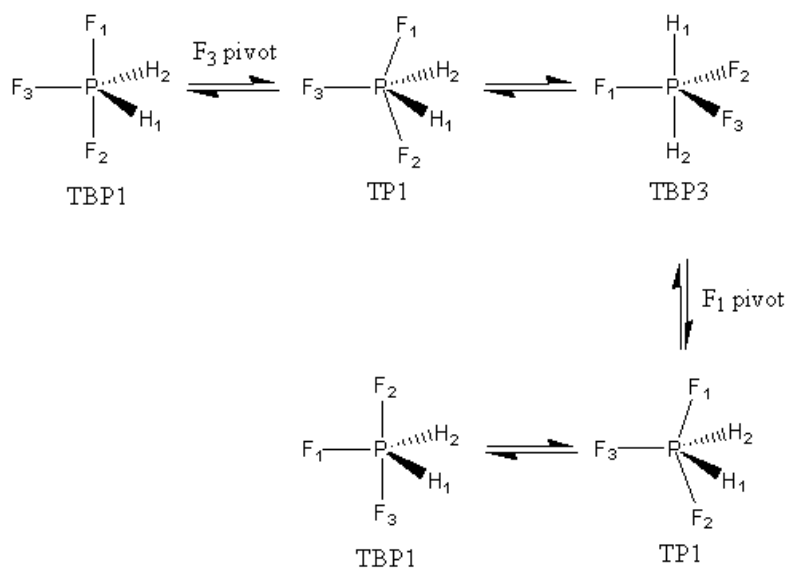
The Harmonic vibrational spectrum of TBP1 has been calculated at the CCSD(T) level of theory. The vibrational frequencies as well as the intensities are in good agreement with experiment, and confirm the previous assignment of Breidung and coworkers.

Normal Mode	Symmetry	RHF [56]	cc-pVDZ	cc-pVTZ	experimental [54]	Assignment
ν_1	A ₁	2767 (33)	2561 (18)	2561 (18)	2482 (m)	s-stretch eq.
ν_2	A ₁	1118 (236)	987 (189)	1014 (179)	1005 (vs)	scissors eq.
ν_3	A ₁	945 (27)	833 (10)	872 (14)	864 (m)	PF stretch
ν_4	A ₁	698 (1)	653 (1)	649 (2)	614 (w)	s-stretch ax.
ν_5	A ₁	351 (20)	301 (16)	315 (16)	335 (m)	s-bending ax.
ν_6	A ₂	1361 (-)	1222 (-)	1269 (-)	1233 (-)	PH ₂ wag.
ν_7	B ₁	2812 (79)	2618 (52)	2612 (46)	2549 (m)	a-stretch eq.
ν_8	B ₁	844 (119)	735 (88)	766 (83)	767 (s)	PH ₂ rock. eq.
ν_9	B ₁	354 (28)	333 (22)	349 (22)	308 (w)	a-bending ax.
ν_{10}	B ₂	1443 (46)	1285 (37)	1323 (12)	1291 (w)	PH ₂ deform.
ν_{11}	B ₂	957 (525)	903 (423)	871 (443)	825 (vs)	a-stretch. ax.
ν_{12}	B ₂	503 (10)	442 (10)	474 (10)	472 (m)	PF deform

Table 2.5: Normal modes of vibration of TBP1 at the CCSD(T) level. Frequencies are given in cm⁻¹. The relative intensities are given in parenthesis with the code vs=very strong, s=strong, m=medium, w=weak, vw=very weak, - =forbidden.



Scheme I



Scheme II

Figure 2.6: The M_2 and M_4 modes describe in details.

Chapter 3

Electronic spectroscopy of $\text{Cr}(\text{CO})_6$: Coupled Cluster Calculations

THE geometry, the binding energy and the vibrational spectroscopy of $\text{Cr}(\text{CO})_6$ have been widely studied in the past 20 years by various methods of quantum chemistry [62–71]. This complex is a model system to study the synthesis, the photochemistry and catalytic processes such as polymerization of alkynes or alkenes by transition metal carbonyls [72]. However, little attention has been given to the electronic spectroscopy of this complex until recently. CASSCF/CASPT2 and TD-DFT studies have proposed a new assignment to the commonly accepted original assignment of Beach and Gray.

The Absorption spectrum of $\text{Cr}(\text{CO})_6$ is dominated by two very intense bands which can be assigned as *metal to ligand charge transfer* (MLCT) excitations corresponding to spin-allowed ${}^1\text{A}_{1g} \rightarrow {}^1\text{T}_{1u}$ transitions. Beside these bands, a number of weak bands can be observed as shoulders at the low energy window. These bands were originally assigned by Beach and Gray [73] as vibronic ${}^1\text{A}_{1g} \rightarrow {}^1\text{T}_{1g}, {}^1\text{T}_{2g}$ transitions (Metal Centered or MC). On the Basis of the CASPT2 calculations of Pierloot et al. [74] and the recent TD-DFT study of Baerends and coworkers [75], these shoulders should be assigned to forbidden ${}^1\text{A}_{1g} \rightarrow {}^1\text{E}_u, {}^1\text{A}_{2u}, {}^1\text{T}_{2u}$ MLCT transitions or spin-forbidden ${}^1\text{A}_{1g} \rightarrow {}^3\text{T}_{1u}$ transitions.

The photodissociation dynamics of $\text{Cr}(\text{CO})_6$ has been recently studied through multiphoton ionization pump/probe laser experiments in gas phase [25, 76]. Depending on the experimental conditions, two photodissociation dynamics characterized by different photofragmentation schemes can be observed: a ionization followed by a fragmentation leading to the observation of all $[\text{Cr}(\text{CO})_n]^+$ fragments ($n=5..0$) [25] or an ultrafast photodissociation followed by a ionization where the $[\text{Cr}(\text{CO})_5]^+$ and $[\text{Cr}(\text{CO})_4]^+$ have too short lifetimes to be observed in ps experiments [76]. Recent low intensity laser probe in gas phase concluded that the primary step is the ultrafast loss of one carbonyl within 100 fs which is in good agreement with the results of other transition metal carbonyls. Theoretical investigations based on trajectory surface hopping on schematic PES obtained from experimental fittings [25] and limited CASSCF calculations have been done [77]. The proposed scheme is an absorption followed by an internal conversion to a dissociative state in an ultra short timescale leading to the loss of one carbonyl.

O_h	D_{2h}
A_{1g}, A_{2g}, E_g	A_g
T_{1u}, T_{2u}	B_{1u}, B_{2u}, B_{3u}
T_{1g}, T_{2g}	B_{1g}, B_{2g}, B_{3g}
A_{1u}, A_{2u}, E_u	A_u

Table 3.1: Correlation between D_{2h} and O_h symmetry groups.

While a large number of experimental and theoretical studies have been done, the electronic spectroscopy is still not fully understood. The CASSCF/CASPT2 work of Pierloot [74] based on mixed active spaces and the TD-DFT study of Baerends [75] have to be taken with care to explain the photodissociation dynamics. This chapter aims at calculating the low lying electronic transitions using CC approach, namely CCSD and EOM-CCSD calculations. The main advantage of the CC framework is that all states (ground, MLCT and MC states) are treated in the same level of electron correlation, tackling the controversial use of selected active spaces used by Pierloot et coworkers [74]. The first part of this chapter is dedicated to the computational details. In the second part, results are presented: a brief study of the basis set is discussed followed by a geometry optimization comparison. EOM-CCSD transition energies are presented and compared with CASPT2 and TD-DFT results. The last section is devoted to a discussion on the assignment of the absorption spectrum.

3.1 Computational details

The calculations were performed using both experimental and optimized geometries. The calculations are done in D_{2h} abelian subgroup of the full point group O_h of $\text{Cr}(\text{CO})_6$ since symmetry handling in the ACES program system [59] is limited to abelian subgroups. The correlation between D_{2h} and O_h groups are presented in Table 3.1.

Several basis sets, namely Wachters+f (Cr), cc-pVDZ (C, O), Ahlrichs (Cr, C, O) and ANO-S (Cr, C, O) were used for geometry optimization or CCSD and EOM-CCSD calculation. The Cr-C and C-O bond lengths were optimized and the O_h symmetry was kept by means of fixed C-Cr-C and Cr-C-O angles.

	Ahlrichs	Wachters+f/ cc-pVDZ	Wachters+f/ PBS	ANO-S
Cr	14s9p5d 5s3p2d	14s11p6d3f 8s6p4d1f	14s11p6d3f 8s6p4d1f	17s12p9d4f 8s7p7d4f
C	7s4p1d 3s2p1d	9s4p1d 3s2p1d	10s6p4d 5s3p2d	10s6p3d 7s6p3d
O	7s4p1d 3s2p1d	9s4p1d 3s2p1d	10s6p4d 5s3p2d	10s6p3d 7s6p3d
${}^1A_{1g}$	-1721.255512	-1722.298329	-1722.647561	-1723.512348
${}^1T_{2u}$	-1721.072312	-1722.132931	-1722.482923	-1723.346403
${}^1A_{1g} \rightarrow {}^1T_{2u}$	4.98	4.50	4.48	4.52

Table 3.2: Description of the various basis sets and CCSD calculated values of the total energies (in a.u.) of the ${}^1A_{1g}$ electronic ground state, the first ${}^1T_{2u}$, and the transition energy ${}^1A_{1g} \rightarrow {}^1T_{2u}$ (in eV) as a function of the basis sets.

3.2 Results

3.2.1 Basis set

CCSD (${}^1A_{1g}$) and EOM-CCSD (${}^1T_{2u}$) calculations on the experimental geometry of $\text{Cr}(\text{CO})_6$ [78] using various basis sets are presented in Table 3.2. The ${}^1A_{1g} \rightarrow {}^1T_{2u}$ transition is also reported. As expected, ANO-S, the largest basis set used in terms of primitives and contracted functions, gives the lowest absolute energy. The transition energies show that the description of the electronic structure is equivalent for ANO-S, Wachters+f/cc-pVDZ, and Wachters+f/PBS with a transition energy around 4.5eV. The smallest basis set, namely Ahlrichs basis set, is too small and overestimates the transition energy compared to other basis sets. On the basis of these observations, we used the Wachters+f/cc-pVDZ basis set to save computational effort while maintaining accuracy.

3.2.2 Geometry optimization

Geometry optimization was performed using the basis set selected in the previous section, namely a Wachters+f basis set on Cr and cc-pVDZ on C and O atoms. The octahedral geometry was kept by means of Cr-C-O and C-Cr-C fixed angles. Cr-C and C-O bond

	Experimental			CCSD	DFT			MCPF	CCSD	CCSD(T)
	[79]	[80]	[78]	this work	[67]	[71]	[75]	[63]	[63]	[63]
Cr-C	1.914	1.918	1.916	1.938	1.910	1.918	1.904	1.940	1.949	1.939
C-O	1.140	1.141	1.142	1.146	1.153	1.150	1.156	1.145	1.168	1.178

Table 3.3: Experimental and theoretical Cr-C and C-O bond distances in Å of $\text{Cr}(\text{CO})_6$ in O_h symmetry.

lengths were optimized using an analytical gradients. Our results are presented in Table 3.3 together with previous optimizations.

Experimental data on the molecular structure is available in the literature and a recent work reported a bond length of 1.916 Å for metal ligand distance and a C-O bond length of 1.142 Å which is in the usual range [78]. Density functional, modified coupled pair functional (MCPF) and CC calculations were also reported [63]. DFT optimized geometries [67,71,75] are in good agreement with experimental values while MCPF and old CC bond lengths are overestimated by 0.02-0.03 Å for the metal-C and the C-O distances. These geometries were obtained with limited basis sets and a basis set effect could explain this behaviour.

Our geometry optimization using Wachters+f/cc-pVDZ basis sets gives bond distances of 1.938 and 1.146 Å for Cr-C and C-O respectively. The values are improved relative to the previous CCSD(T) calculations with smaller basis set.

3.2.3 Transition Energies

The ground state is a $^1A_{1g}$ closed shell state. Its electronic configuration is $(8a_{1g})^2 (7t_{1u})^6 (1t_{2g})^6 (1t_{2u})^6 (1t_{1g})^6 (5e_g)^4 (8t_{1u})^6 (2t_{2g})^6$ where $7t_{1u}$, $1t_{2g}$, $1t_{2u}$ and $1t_{1g}$ correspond to the 12 π_{CO} orbitals, $8a_{1g}$, $5e_g$ and $8t_{1u}$ correspond to the 6 σ_{Cr-C} bonding orbitals and $2t_{2g}$ corresponds to the 3 occupied d-type orbitals of the chromium atom and is the highest occupied molecular orbital (HOMO). Occupied orbitals are represented in Figure 3.1. The low lying virtual orbitals are plotted in Figure 3.2. The low lying virtual orbitals $9t_{1u}$, $2t_{2u}$, and $2t_{1g}$ correspond to the π_{CO}^* orbitals while $3t_{2g}$ is a mixing of π_{CO}^* and correlated unoccupied d-type orbital. The $6e_g$ orbital is a very diffused unoccupied d-type orbital, the $9a_{1g}$ has mainly a 5s orbital character of the Chromium atom.

According to this order, the low lying excited states are characterized by excitations from the $2t_{2g}$ d orbitals of the metal to π_{CO}^* orbitals (MLCT transitions) or to the remaining vacant $6e_g$ d-type orbitals (MC transitions). EOM-CCSD calculations on the experimental geometry with Wachters+f/cc-pVDZ basis sets are presented with previous theoretical works in Table 3.4. We have also used the MOLPRO package [81] with limited ANO basis sets to compute a large number of states at the EOM-CCSD level (oscillator strengths calculation is not available in this package). The MS-CASPT2, based on an average CASSCF

with a large active space, is the theoretical reference work [82]. The CASPT2 calculation of Pierloot [74], based on different active spaces, underestimates the transition energies.

As expected, low lying transitions are mainly of MLCT character while the MC transitions are higher in energy. All transitions correspond to excitations from the d-shell orbital $2t_{2g}$ of the chromium atom. According to the group theory of the octahedral symmetry, all transitions are forbidden except those to ${}^1T_{1u}$ states. Starting from the t_{2g} orbital, there are only two different excitations which give a ${}^1T_{1u}$ state: $t_{2g} \rightarrow t_{1u}$ and $t_{2g} \rightarrow t_{2u}$. An excitation from a t_{2g} to a t_{1u} orbital generates more than one state, namely, a A_{2u} , a doubly degenerate E_u , and two triply degenerate T_{1u} and T_{2u} states (change $1u$ by $2u$ and vice versa to get a transition from a t_{2g} to a t_{2u}). Within these conditions, only one component of these transitions is active. Only two computed excitations satisfy this, a $2t_{2g} \rightarrow 9t_{1u}$ excitation and a $2t_{2g} \rightarrow 2t_{2u}$ excitation found at 5.12 and 6.24eV respectively (5.05 and 6.07eV with Molpro). These transitions correspond to $d_{Cr} \rightarrow \pi_{CO}^*$ excitations. Molpro calculations gives a third allowed transition at 6.64eV corresponding to a $2t_{2g} \rightarrow 9t_{1u}$ excitation but we do not have the oscillator strength to confirm a strong or weak absorption. The values of the allowed transitions of both EOM-CCSD calculations are overestimate by 0.5eV with respect to the experimental values of the observed bands at 4.46 and 5.5eV, the highest computed transition at 6.64eV remaining not assigned. The calculated oscillator strengths of these states are in good agreement with the experimental ones: we found a ratio of 1:5 while the experimental ratio is 1:9.

Other transitions were also computed but are in principle forbidden by symmetry. A proposed assignment is presented in Table 3.4. The transitions highlighted in red, correspond to the four components of a $2t_{2g} \rightarrow 9t_{1u}$ excitation. In the same way, the green, orange, violet and navy blue transitions correspond to the components of excitations from $2t_{2g} \rightarrow 2t_{2u}$, $3t_{2g}$, $10t_{1u}$ and $2t_{1g}$ respectively. The fourth component of the $2t_{2g} \rightarrow 2t_{1g}$ excitation is too high in energy and was not computed. All of these transitions have MLCT character. Two metal centered (MC) transitions calculated at 4.99 and 5.43eV (5.15 and 5.58eV with Molpro), correspond to the $2t_{2g} \rightarrow 6e_g$ excitation. This order is in good agreement with the most recent MS-CASPT2 calculations but shifted by 0.5eV to higher energies. The two EOM-CCSD calculations do not give the same position in the order of these states. This effect might be explain by a lack of flexibility in the Molpro calculations due to limited basis sets. The $a^1A_{1g} \rightarrow b^1T_{1g}$, a^1E_g , and c^1T_{2g} corresponding to a $2t_{2g} \rightarrow 3t_{2g}$ excitation have also a MC transition character since $3t_{2g}$ is a mixing between d-type orbital of Cr and π_{CO}^* orbitals.

According to the experimental absorption spectrum, electronically forbidden but vibronically allowed transitions should be found at about 3.66, 3.91, and 4.82eV in order to reproduce the observed shoulders. The lowest transition found in EOM-CCSD calculation lies at 4.53eV (4.48eV with Molpro) which is too far from the lowest shoulder. However, we found a density of states in the 4.53-4.57eV, 4.99eV, and 5.35-5.88eV energies windows. Compared to the experimental absorption spectrum, our transition are shifted to higher energy by about 0.5eV. Excitations to these electronic forbidden states combined with adequate vibrational modes excitations might lead to allowed vibronic transitions. In order

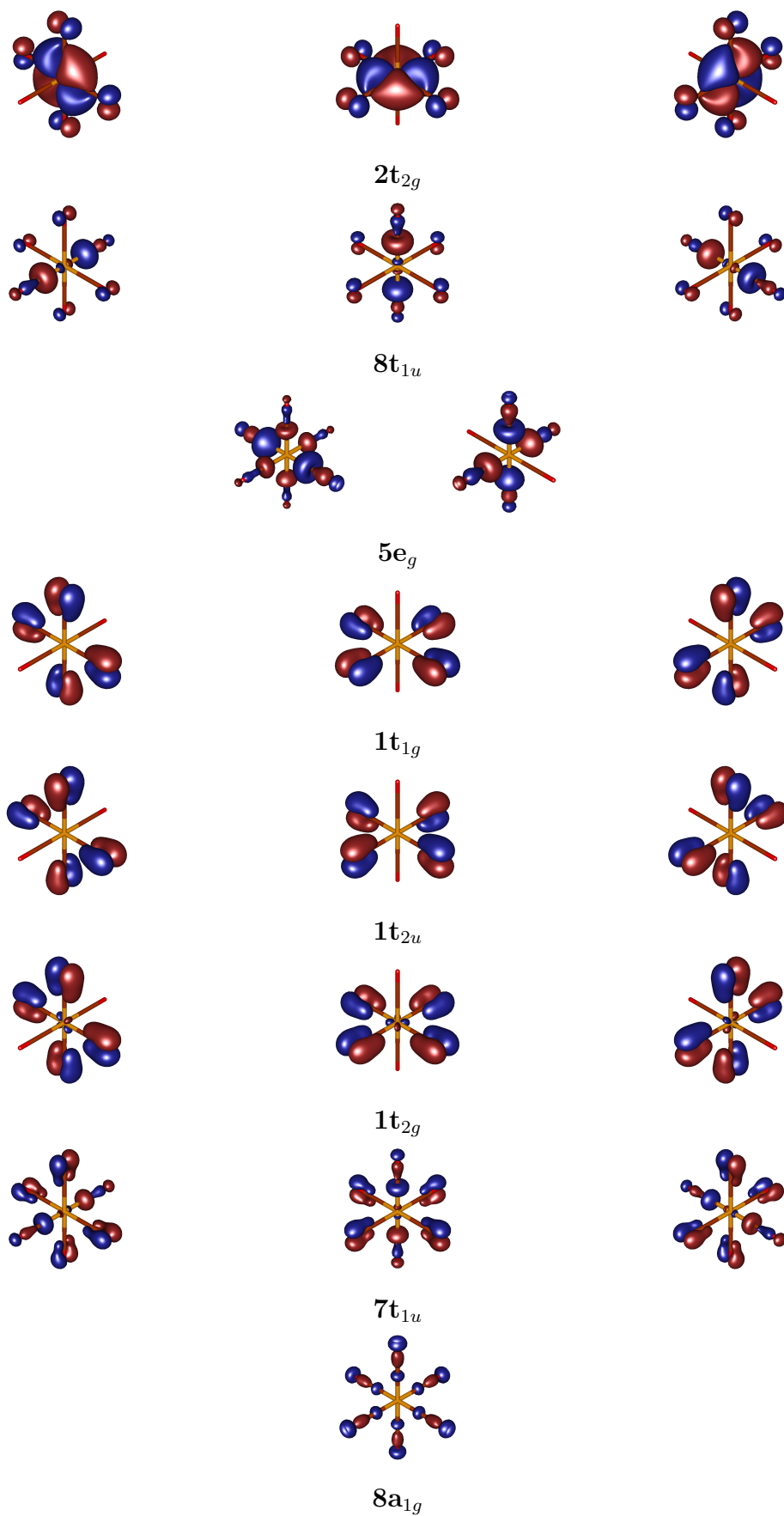
to verify this possibility, this work is on the way.

3.3 Conclusion

Transition energies calculations at the EOM-CCSD level have been done. Our results have shown that the EOM-CCSD transition energies are systematically shifted by 0.5eV at higher energies. This systematic shift might be explained by different factors. The EOM-CCSD method is based on one set of orbitals to describe the ground and the excited states. If the shape of the orbitals is significantly different between the ground and the excited states, the relaxation effects (and the relaxation energy) might be important. It is hard to estimate relaxation effects because of all degeneracies and the multiconfigurational character of these excited states. However, an upper limit of 0.015eV has been estimated by means of IP-EOM-CC calculations [83]. This does mean that this effect does not explain the discrepancy between the calculated EOM-CCSD values and the experimental data.

A second factor to explain this shift is the relativistic (spin orbit) effects. These effects should be minor for a molecule with a first-row transition metal [84]. The presence of low lying triplets calculated at 4.29 and 5.05eV (³A_{1g}), 4.45 and 5.55eV (³T_{1u}) and 4.57 and 5.04eV (³T_{2g}) [83] may explain the occurrence of the shoulders at 3.66, 3.91 and 4.82eV if we assume the same shift of 0.5eV observed with the singlets. Both improved MS-CASPT2 [82] and the present EOM-CCSD calculations confirm the presence of low-lying singlet MLCT states between 4.5 and 5.0eV below the MC states calculated at 4.99 and 5.43eV. According to CC calculations, the a¹T_{1u} absorbing state is nearly degenerate with the a¹T_{1g} MC state which should lead to the ultra fast dissociation of a carbonyl ligand observed experimentally. This has to be confirmed by the calculation of associated potential energy surfaces.

The last factor could be the remaining correlation effects that are not taken into account at the CCSD level. To estimate the missing correlation, it is necessary to go beyond double excitations with the inclusion of the triples. This work is on the way [83].

Figure 3.1: Occupied orbitals of $\text{Cr}(\text{CO})_6$ (see text for details).

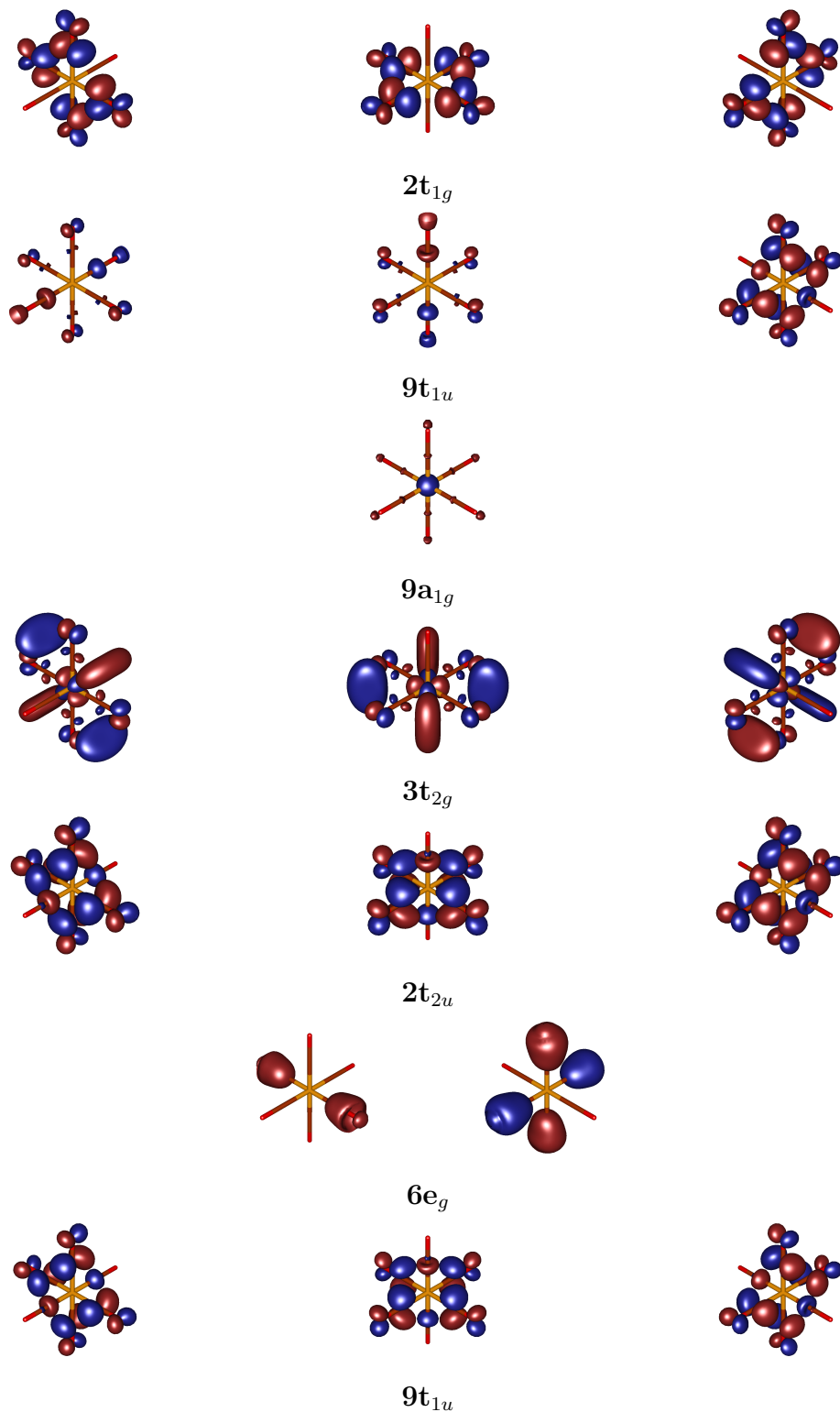


Figure 3.2: Low-lying unoccupied orbitals of $\text{Cr}(\text{CO})_6$ (see text for details).

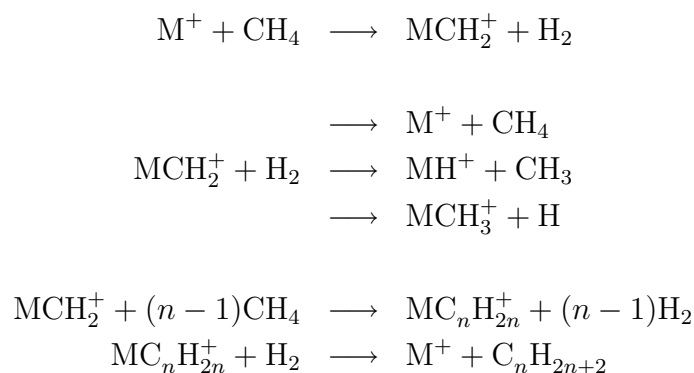
Transition	Excitation	EOM-CCSD		CASPT2	MS-CASPT2	TD-DFT		Exp
		ACES	Molpro			[82]	[75]	
$a^1A_{1g} \rightarrow a^1E_u$	$2t_{2g} \rightarrow 9t_{1u}$		4.48		3.96			
$a^1A_{1g} \rightarrow a^1A_{2u}$	$2t_{2g} \rightarrow 9t_{1u}$	4.53	4.51		3.98			
$a^1A_{1g} \rightarrow a^1T_{2u}$	$2t_{2g} \rightarrow 9t_{1u}$	4.57	4.52	3.70-3.56	4.12	4.21		
$a^1A_{1g} \rightarrow a^1T_{1u}$	$2t_{2g} \rightarrow 9t_{1u}$	5.12(0.141)	5.05	4.54-4.11	4.52(0.23)	4.50(0.02)	4.19	4.46(0.25)
$a^1A_{1g} \rightarrow a^1T_{1g}$	$2t_{2g} \rightarrow 6e_g$	4.99	5.15	4.85	4.60	4.98	5.50	
$a^1A_{1g} \rightarrow b^1E_u$	$2t_{2g} \rightarrow 2t_{2u}$	5.35	5.18		4.63			
$a^1A_{1g} \rightarrow a^1A_{1u}$	$2t_{2g} \rightarrow 2t_{2u}$	5.42	5.26		4.76			
$a^1A_{1g} \rightarrow b^1T_{2u}$	$2t_{2g} \rightarrow 2t_{2u}$	5.64	5.48	4.32-4.43	5.05	4.79	4.50	
$a^1A_{1g} \rightarrow a^1T_{2g}$	$2t_{2g} \rightarrow 6e_g$	5.43	5.58	5.08	4.91	5.69	5.90	
$a^1A_{1g} \rightarrow b^1T_{1g}$	$2t_{2g} \rightarrow 3t_{2g}$	5.72	5.81					
$a^1A_{1g} \rightarrow a^1E_g$	$2t_{2g} \rightarrow 3t_{2g}$	5.88	5.94					
$a^1A_{1g} \rightarrow b^1T_{2g}$	$2t_{2g} \rightarrow 9a_{1g}$		5.99					
$a^1A_{1g} \rightarrow b^1T_{1u}$	$2t_{2g} \rightarrow 2t_{2u}$	6.24(0.664)	6.07	5.07-5.20	5.41(0.81)	6.01(0.59)	5.76	5.53(2.3)
$a^1A_{1g} \rightarrow c^1T_{2g}$	$2t_{2g} \rightarrow 3t_{2g}$	6.28	6.38					
$a^1A_{1g} \rightarrow c^1T_{2u}$	$2t_{2g} \rightarrow 10t_{1u}$		6.64					
$a^1A_{1g} \rightarrow c^1T_{1u}$	$2t_{2g} \rightarrow 10t_{1u}$		6.64					
$a^1A_{1g} \rightarrow b^1A_{2u}$	$2t_{2g} \rightarrow 10t_{1u}$		6.68					
$a^1A_{1g} \rightarrow c^1E_u$	$2t_{2g} \rightarrow 10t_{1u}$		6.72					
$a^1A_{1g} \rightarrow d^1T_{2g}$	$2t_{2g} \rightarrow 2t_{1g}$		7.23					
$a^1A_{1g} \rightarrow c^1T_{1g}$	$2t_{2g} \rightarrow 2t_{1g}$		7.25					
$a^1A_{1g} \rightarrow b^1E_g$	$2t_{2g} \rightarrow 2t_{1g}$	7.12	7.39					
$a^1A_{1g} \rightarrow a^1A_{1g}$	$2t_{2g} \rightarrow 3t_{2g}$	7.63	7.72					
$a^1A_{1g} \rightarrow c^1A_{2u}$	$2t_{2g} \rightarrow 1a_{1u}$		9.42					

Table 3.4: EOM-CCSD transition energies (in eV) to the low lying singlet states of $\text{Cr}(\text{CO})_6$ compared to the TD-DFT and (MS)-CASPT2 values. The calculated oscillator strengths are given in parenthesis.

Chapter 4

Quantum chemical study of the electronic structure of MCH_2^+ ($M=Fe,Co,Ni$)

DURING the last two decades, the MCH_2^+ series was widely studied experimentally as well as theoretically. The aim of these studies is to collect fundamental informations about unsaturated transition metal complexes and their properties. These complexes are very important to understand mechanisms involving in the catalytic reactions like alkanes formation:



This catalytic scheme is strongly dependent on the choice of the metal center. For instance, this process is endothermic with a first row transition metal but exothermic with a third row metal [85–89].

Theoretical studies have mainly focused on the metal-carbon bond strength of MCH_2^+ series, which can be compared to the experimental data of gas-phase experiments. Bauschlicher et al. looked at the first and second row metal complexes [90] using *modified coupled pair functional* (MCPF) and *internally contracted averaged coupled pair functional* (ICACPF) while Irikura and Goddard studied the third row transition metal complexes [91] using *generalized valence bond* (GVB) pairs. The nature of the bond was also widely stud-

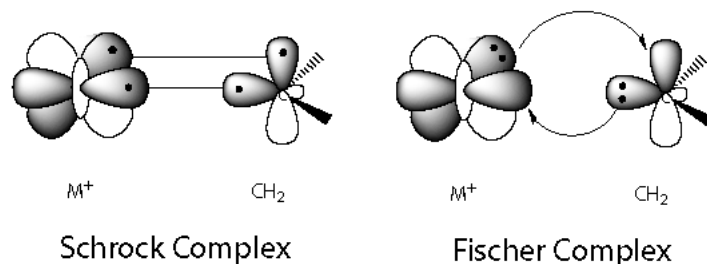


Figure 4.1: Schrock and Fischer type complex. see text for details

ied [92–94]. Depending on the metal center, the nature of the bond varies between two extreme cases: a purely covalent or a purely dative interaction. In the covalent situation, the σ bond involves one electron in an hybrid orbital ($s+d$) of the metal center and one electron in a sp^2 hybrid orbital of the carbon atom while the π bond involves an overlap of a d orbital of the metal with a p orbital of the carbon (see Figure 4.1). These types of complexes are usually referred to as Schrock type complexes or metal-methyldene complex [95]. In the dative situation, a doubly occupied sp^2 orbital of the carbon overlaps an empty ($s+d$) orbital of the metal center while a doubly occupied d orbital of the metal overlaps with an empty p orbital of the methylene. These types of complexes are referred to as Fischer type complexes or metal-carbene complexes [96]. Metal-carbene and metal-methyldene complexes show different reactivity: Schrock type complexes take part in nucleophilic reactions as catalysts for the polymerization of olefins [97, 98]; Fischer type complexes behave as electrophilic centers [99, 100] and can be used as catalysts for other kinds of chemical reactions.

In contrast, little attention has been devoted to the spectroscopic properties of metal-methylene complexes. These systems are known to be characterized by a high density of electronic states within a small energy window with several nearly degenerate states. Musaev, Morokuma and coworkers studied several electronic states of the iron and cobalt complexes [92, 94, 101]. The ground state of $FeCH_2^+$ is described by a pair of nearly degenerate 4B_1 and 4B_2 states with a 4A_2 state very close. Whereas the electronic ground state of $CoCH_2^+$ is described by two nearly degenerate 3A_1 and 3A_2 states and $NiCH_2^+$ by a 2A_1 state. An accurate description of the structure and the energetics of the low-lying electronic states is required to clarify and determine the ground state of each complex and the nature of the $M-C$ bond which depends on the occupation of the molecular orbitals. Recently, photofragment spectroscopy experiments have shown that the MCH_2^+ ($M=Fe, Co, Ni$) cations have three different dissociation channels [102]. The loss of CH_2 is the most favorable but the departure of H or H_2 was also reported (see Fig. 4.2). This behaviour gives us an interesting set of small transition metal complexes with a few number of degrees of freedom to study the competition between dissociation channels. The size of the system, on one hand, is reasonable and can be treated with highly correlated methods, particularly CC methods like $CCSD$ and $EOM-CCSD$. The complexity of the electronic

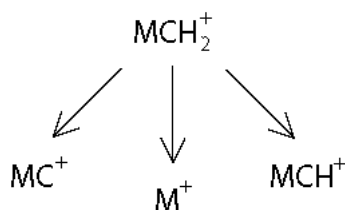


Figure 4.2: The different dissociation channels of MCH_2^+ : CH_2 , H_2 or H loss corresponding to the detection of the daughter fragments M^+ , MC^+ and MCH^+ respectively. [102]

structure (open shell, nearly degenerate states, unsaturated valence shell of the metal), on the other hand, is a challenge to apply CC methods which have not yet been used so much for this kind of problems.

This chapter reviews a preliminary study of the electronic structure of MCH_2^+ ($M=Fe, Co, Ni$) complexes at the CCSD and EOM-CCSD level of theory with high quality basis sets. This work is the necessary first step to clarify the Franck-Condon region and the electronic structure, to determine the absorbing state(s), to collect some hints on the dissociation pathways, and to help us in the choice of the relevant coordinates to build potential energy surfaces. We also discuss the spin contamination occurring in these open shell systems when using an unrestricted Hartree Fock wave function and we propose a solution to reduce it.

4.1 Computational Details

4.1.1 Geometry Optimization

Each complex was optimized within the C_{2v} symmetry constraint with the C-H bond length fixed at 1.09 Å. Previous studies have shown that the C-H bond length does not change significantly with the level of CC theory used [103]. It is also interesting to keep the C-H bond length fixed in order to compare the geometries of the complexes. Under these conditions, only two degrees of freedom remain to be optimized, the bond length between the metal center and the carbon atom and the angle between M, C and one of the H atoms as shown in figure 4.3. We optimized the parameters at the CCSD level with two different ROHF references based on HF or KS orbitals using two different basis sets. The first basis set is composed by a Wachters+f basis set on the metal and the cc-pVDZ basis sets on C and H. We improved the basis set by replacing the cc-pVDZ by a cc-pVTZ set.

The results are presented in Table 4.1. The metal methylene distances are in good agreement with previous work. The values are in the range 1.80-1.85 Å which is usual for this type of bond. It has also to be noted that the distances are shortened when we

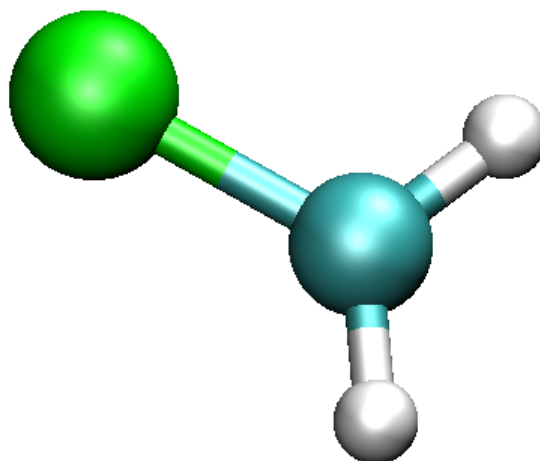


Figure 4.3: Geometry of the MCH_2^+ series.

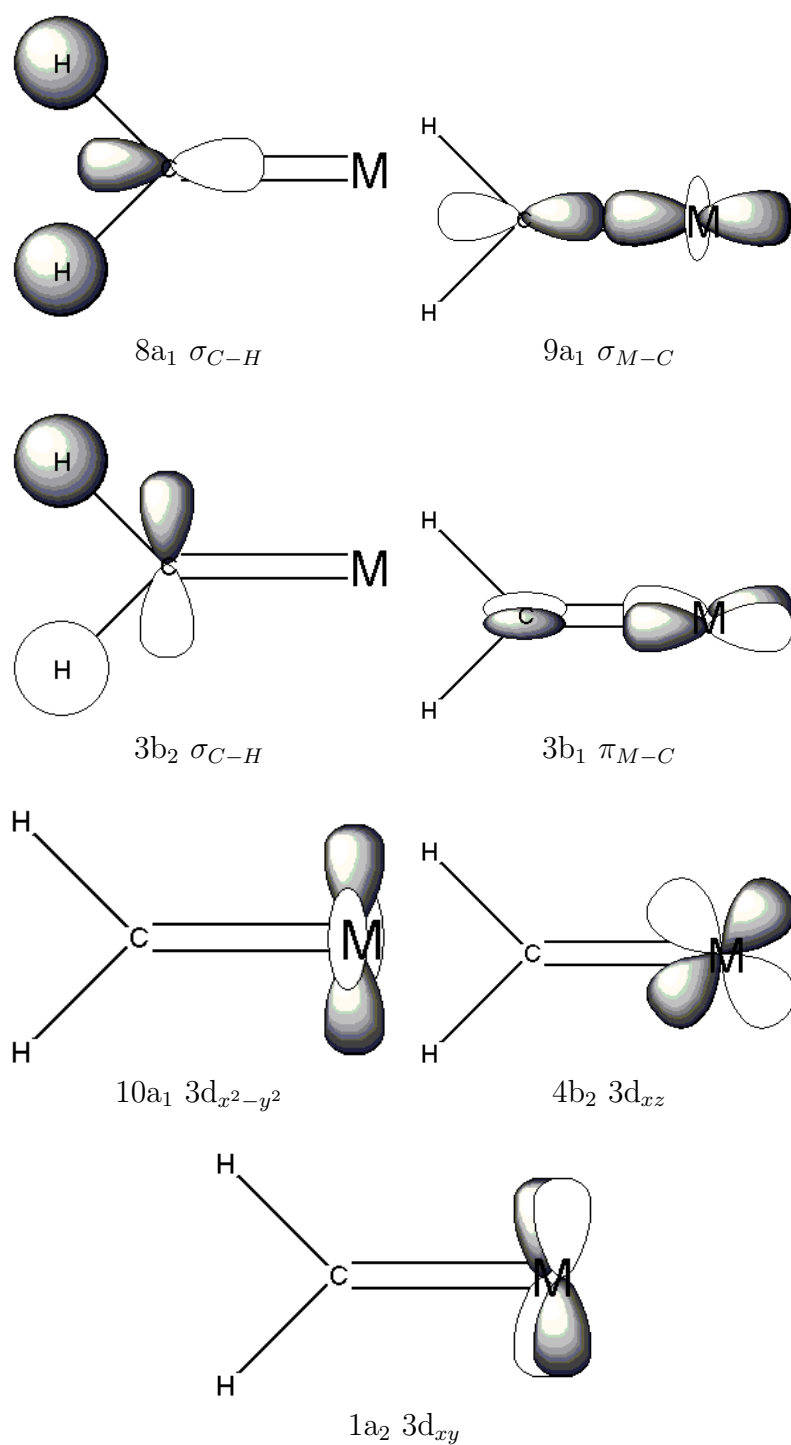
increase the size of the basis set which is a well known trend when one increase the CC level. The angle is very stable from one complex to the next one around 123-125 degrees. The iron complex shows a longer metal-methylene bond length than the cobalt and nickel complexes which have almost the same value when using the cc-pVTZ basis sets. This trend was also observed by Bauschlicher et al. [90].

The electronic study reported in the next section is based on the CCSD/ROHF geometries and is performed with Wachters+f/cc-pVTZ basis sets.

4.2 Results

4.2.1 Electronic Structure

In this section, the electronic structure of each complex is presented. These complexes are characterized by an open-shell ground state which is nearly degenerate with one or several states. The theoretical study is complicated by the occurrence of a high density of states in a small energy window. Schematic orbitals of the MCH_2^+ (M=Fe, Co, Ni) are plotted in Figure 4.4.

Figure 4.4: Schematic orbitals of the MCH_2^+ complexes.

		MCPF	CCSD/HF		CCSD/KS	
		[90]	cc-pVDZ	cc-pVTZ	cc-pVDZ	cc-pVTZ
$FeCH_2^+$	Fe-C	1.808	1.861	1.850	1.863	1.852
	Fe-C-H	124.0	123.12	123.19	123.40	123.40
$CoCH_2^+$	Co-C	1.791	1.818	1.802	1.822	1.806
	Co-C-H	124.3	124.09	124.05	124.23	124.16
$NiCH_2^+$	Ni-C	1.790	1.824			1.808
	Ni-C-H	124.05	124.50			124.85

Table 4.1: Optimized bond lengths and bond angles (in \AA and $^\circ$) of MCH_2^+ (M= Fe, Co, Ni). Wachters+f basis set has been used for the metal center in all systems.

Electronic ground state and spectroscopy of $FeCH_2^+$

The low-lying 4B_2 , 4B_1 , 4A_2 , and 4A_1 states of $FeCH_2^+$ were computed at the CCSD level of theory using different reference wave functions (see Table 4.2). The ground state is a nearly degenerate pair of 4B_2 and 4B_1 as expected. The CCSD/ROHF using a HF reference gives the 4B_1 state as the ground state with the 4B_2 only 44 cm^{-1} higher in energy while the CCSD/ROHF based on a KS reference gives a reverse order with 18 cm^{-1} between the two states. The 4A_2 state is at 816 cm^{-1} with the HF reference and 804 cm^{-1} higher in energy with the KS reference. The 4A_1 is higher in energy (see Table 4.4).

The electronic configuration of the 4B_1 state is $(8a_1)^2 (9a_1)^2 (3b_2)^2 (3b_1)^2 (10a_1)^1 (4b_2)^1 (1a_2)^1$ corresponding to $(\sigma_{C-H})^2 (\sigma_{C-H})^2 (\sigma_{Fe-C})^2 (\pi_{Fe-C})^2 (3d_{xy})^1 (3d_{xz})^1 (3d_{x^2-y^2})^1$ while the electronic configuration of the 4B_2 state is $(8a_1)^2 (3b_2)^2 (3b_1)^2 (1a_2)^2 (9a_1)^1 (10a_1)^1 (4b_2)^1$ corresponding to $(\sigma_{C-H})^2 (\sigma_{C-H})^2 (3d_{xy})^2 (\pi_{Fe-C})^2 (\sigma_{Fe-C})^1 (3d_{xz})^1 (3d_{x^2-y^2})^1$. The σ_{Fe-C} is an overlap of the $3d_{z^2}$ of Fe and the $2p_z$ of C while the π_{Fe-C} is a π overlap of the $3d_{yz}$ of Fe and the $2p_y$ of C (see Fig. 4.4). This $2p_y$ is the only 2p orbital of the carbon atom available to make a π -bond since the $2p_x$ participates to σ_{C-H} bonds while the $2p_z$ participates to the σ_{Fe-C} bond (see Fig. 4.4). According to the electronic configuration the 4B_1 should be the ground state corresponding to a double bond between the iron atom and the methylene fragment. The 4B_2 is then an excited state corresponding to a $\sigma_{Fe-C} \rightarrow 3d_{xy}$ excitation. A careful analysis of the HF orbitals of the UHF 4B_1 shows that the double occupation of π_{Fe-C} orbital (in the ROHF case with both HF or KS orbital) becomes a single occupation of the $3d_{yz}$ orbital of Fe and of the $2p_y$ orbital of C without any overlap. This wrong description of the electronic structure may lead to the observed spin contamination and the poor quality of the reference wave function. The same kind

state	electronic configuration	HF		KS	
		spin mult. (ref)	CCSD/UHF Energy	spin mult. (ref)	CCSD/UHF Energy
4B_1	$\sigma_{Fe-C}^2 \pi_{Fe-C}^2 3d_{xy}^1 3d_{xz}^1 3d_{x^2-y^2}^1$	4.34 (4.48)	-1301.885061	?	-1301.869632
4B_2	$\pi_{Fe-C}^2 3d_{xy}^2 \sigma_{Fe-C}^1 3d_{xz}^1 3d_{x^2-y^2}^1$	4.34 (4.47)	-1301.885019	4.23 (4.25)	-1301.878677
4A_2	$\pi_{Fe-C}^2 3d_{xz}^2 \sigma_{Fe-C}^1 3d_{xy}^1 3d_{x^2-y^2}^1$	4.34 (4.49)	-1301.880751	?	-1301.865884
4A_1		4.62 (4.43)	-1301.802479	?	?

Table 4.2: Comparison of CCSD Energies (in a.u.) and multiplicities (reference multiplicities are given in parenthesis) with UHF and ROHF references for the $FeCH_2^+$ complex. The two σ_{C-H} orbitals are omitted in the electronic configuration. Several states (marked as ?) have shown convergence difficulties and are not yet characterized.

state	electronic configuration	HF				KS		
		spin mult. (ref)	CCSD/UHF Energy	CCSD/ROHF Energy	spin mult. (ref)	CCSD/UHF Energy	CCSD/ROHF Energy	
3A_2	$\sigma_{Co-C}^2 \pi_{Co-C}^2 3d_{xz}^2 3d_{xy}^1 3d_{x^2-y^2}^1$	3.387 (3.601)	-1420.869260	-1420.862941	?	?	-1420.855395	
3A_1	$\pi_{Co-C}^2 3d_{xy}^2 3d_{xz}^2 \sigma_{Co-C}^1 3d_{x^2-y^2}^1$?	?	-1420.861286	?	?	-1420.853232	
3B_2	$\sigma_{Co-C}^2 \pi_{Co-C}^2 3d_{xy}^2 3d_{xz}^1 3d_{x^2-y^2}^1$?	?	-1420.850856	?	?	-1420.844123	
3B_1	$\sigma_{Co-C}^2 \pi_{Co-C}^2 3d_{x^2-y^2}^2 3d_{xy}^1 3d_{xz}^1$	3.106 (3.257)	-1420.848952	-1420.848162	?	?	-1420.842161	

Table 4.3: Comparison of CCSD Energies (in a.u.) and multiplicities with UHF and ROHF references (reference multiplicities are given in parenthesis) for the $CoCH_2^+$ complex. The two σ_{C-H} orbitals are omitted in the electronic configuration. Several states (marked as ?) have shown convergence difficulties and are not yet characterized.

of effect has been identify for the nickel analog [103] and it has been shown that the KS orbital correct this error.

Electronic ground state and spectroscopy of CoCH_2^+

The low lying 3A_2 , 3A_1 , 3B_1 , 3B_2 , and the first 1A_1 states of CoCH_2^+ were calculated and are presented in Table 4.3. The electronic ground state of the cobalt complex is a 3A_2 and is nearly degenerate with the 3A_1 state as expected but with a reverse order compared to the results found by Musaev and coworkers [94]. Its electronic configuration is $(8a_1)^2 (9a_1)^2 (3b_1)^2 (3b_2)^2 (4b_2)^2 (10a_1)^1 (1a_2)^1$ corresponding to $(\sigma_{C-H})^2 (\sigma_{C-H})^2 (\sigma_{Fe-C})^2 (\pi_{Fe-C})^2 (3d_{xz})^2 (3d_{xy})^1 (3d_{x^2-y^2})^1$. This configuration can be view as the electronic configuration of the 4B_1 ground state of FeCH_2^+ where we have added one electron in the $3d_{xz}$ orbital. The 3A_1 is quasi degenerated with the ground state and lies at only 363 cm^{-1} with ROHF reference based of HF orbitals and at 475 cm^{-1} with KS orbitals (see Table 4.4). Its electronic configuration is $(8a_1)^2 (3b_1)^2 (3b_2)^2 (4b_2)^2 (1a_2)^2 (9a_1)^1 (10a_1)^1$ corresponding to $(\sigma_{C-H})^2 (\sigma_{C-H})^2 (\pi_{Fe-C})^2 (3d_{xz})^2 (3d_{xy})^2 (\sigma_{Fe-C})^1 (3d_{x^2-y^2})^1$. The two other triplet 3B_2 and 3B_1 are higher in energy, at 2652 cm^{-1} (2474 cm^{-1} with KS orbitals) and 3244 cm^{-1} (2905 cm^{-1} with KS orbitals) respectively. The singlet states is higher in energy. The singlet states are not contaminated since a UHF or RHF calculations are equivalent in this particular case. In this case, the spin contamination dos not play an important role in the order of the electronic states like in the iron analog. However, the spin contamination can be explain in the same way. A close analysis of the occupied orbital in the UHF reference wave function shows that the π_{Co-C} is badly described by two single occupied $3d_{yz}$ of the cobalt and $2p_y$ of the carbon atoms instead of one doubly occupied π -bonding orbital.

Electronic ground state and spectroscopy of NiCH_2^+

The reader is invited to read the article at the end of this chapter. The study of the electronic structure of NiCH_2^+ was already studied with a small difference, namely the choice of the basis sets used. This difference dos not much affect the general conclusion made with FeCH_2^+ and CoCH_2^+ .

Comparison between the different complexes

The MCH_2^+ series shows the same characteristics in their electronic structures. The electronic ground state configuration of FeCH_2^+ is $(\sigma_{C-H})^2 (\sigma_{C-H})^2 (\sigma_{Fe-C})^2 (\pi_{Fe-C})^2 (3d_{xy})^1 (3d_{xz})^1 (3d_{x^2-y^2})^1$. By adding one electron in a single occupied d-type orbital (the $3d_{xz}$ in this case), we obtain the electronic ground state configuration of the CoCH_2^+ , namely $(\sigma_{C-H})^2 (\sigma_{C-H})^2 (\sigma_{Fe-C})^2 (\pi_{Fe-C})^2 (3d_{xz})^2 (3d_{xy})^1 (3d_{x^2-y^2})^1$. Applying the addition of one electron in a d-type orbital (the $3d_{xy}$) of the electronic ground state of CoCH_2^+ , we get the electronic ground state configuration of the NiCH_2^+ , $(\sigma_{C-H})^2 (\sigma_{C-H})^2 (\sigma_{Fe-C})^2 (\pi_{Fe-C})^2 (3d_{xz})^2 (3d_{xy})^2 (3d_{x^2-y^2})^1$.

	FeCH ₂ ⁺	CoCH ₂ ⁺	NiCH ₂ ⁺
Ground state	0	0	0
First excited state	18	475	2200
Second excited state	804	2474	3000
Third excited state	?	2905	8870

Table 4.4: Transition energies of the first excited states of the MCH_2^+ series at the CCSD level with ROHF reference and KS orbitals (except for the nickel where we present the CCSD transition energies with an UHF reference and a different basis set [103]). The energies are given in cm^{-1} and relative to the ground state of each complex.

These additions of electrons directly influence the energy gap between the ground state and the first excited state of the MCH_2^+ series (M=Fe, Co, Ni) (see Table 4.4. Starting from $FeCH_2^+$ with a nearly degenerate ground state, the addition of one electron separates by 475 cm^{-1} the ground state and the first excited state of $CoCH_2^+$ and the addition of a second electron separates by 2200 cm^{-1} (calculated with a different basis set [103]) the ground state and the first excited state of $NiCH_2^+$.

4.2.2 Spin Contamination

The calculations, performed with an UHF reference (with either HF or KS orbitals) have shown large spin contamination in all MCH_2^+ systems. One may argue that the use of a *Restricted Open-shell Hartree Fock* (ROHF) reference avoids by itself the spin contamination and could solve this problem. But our aim is to study the spectroscopy and the photodissociation of the MCH_2^+ , namely compute the transition energies and oscillator strengths. At this time, the only way to compute the oscillator strengths within a CC framework is to use the EOM-CCSD strategy which gives relevant results only with RHF or UHF references but not with ROHF.

In this particular case of the MCH_2^+ series, the UHF reference based on KS orbital is a good choice since the wave function is less contaminated than its HF counterpart in the majority of states. The CC correction to the spin contamination amounts at 0.2-0.4. The calculations based on KS reference are less spin contaminated than the UHF based CC as it had been shown in our previous study on $NiCH_2^+$. [103]. KS References are already

less contaminated than the CC corrected spin multiplicities of the UHF references, giving *a fortiori* a less contaminated CCSD/KS multiplicity than the CCSD/HF. This strategy may be employed, in principle, each time we are facing a spin contamination of the reference wave function.

The inclusion of the triple excitations (CCSDT) or at least a CCSD augmented by perturbative correction for the connected triple excitations (CCSD(T)) will remove the remaining spin contamination of the CCSD wave function as observed in NiCH_2^+ [103]. This treatment will also more accurately describe the nearly degeneracy in the FeCH_2^+ system. These calculations are on the way.

4.3 Conclusion

The electronic structure of MCH_2^+ (M=Fe, Co, Ni) has been investigated in detail by means of the Coupled Cluster approach based either on Hartree Fock orbitals or on Kohn-Sham orbitals. The electronic ground states of each complex have been characterized, showing that the metal center is double bonded with the methylene fragment. The σ_{M-C} is characterized by an overlap between the $3d_{z^2}$ of the metal and the $2p_z$ orbital of the carbon atom while the π_{M-C} is characterized by a π -overlap between the $3d_{yz}$ of the metal with the $2p_y$ orbital of the carbon atom.

When based on UHF references, the CC calculations are spin contaminated. An analysis of the reference wave function and the occupation of the Hartree-Fock orbitals shows a wrong description of the π_{M-C} orbital which is replaced by a singly occupied $3d_{yz}$ on the metal center and a singly occupied $2p_y$ orbital on the carbon atom. This bad description can be corrected by the use of Kohn-Sham orbitals which do not have this deficiency. The new CCSD wave function obtained with the KS orbitals is still contaminated but the contamination is reduced. The inclusion of the triple excitations should remove the remaining contamination and best describe the electronic structure. These calculations are on the way.

The energy gap between the ground state and the first excited state of the MCH_2^+ series (M=Fe, Co, Ni) has been rationalized by means of an analysis of the 3d occupations of the metal center. The number of holes in the 3d orbital occupations of the metal center directly influence the energy gap. Starting with a 3-holes situation in the 3d orbitals of the electronic ground of FeCH_2^+ to a 1-hole situation in the case of NiCH_2^+ , the energy gap grows from a nearly degenerate ground state of FeCH_2^+ to more than 2200 cm^{-1} for NiCH_2^+ .

From this work, a computational strategy may be proposed to calculate the low-lying PES describing the various observed photofragmentation channels of MCH_2^+ . This work complemented by wave packet propagations will be the subject of a further study. Only the few low-lying states will be retained in these simulations.

[Signalement bibliographique ajouté par : ULP – SCD – Service des thèses électroniques]

Quantum chemical study of the electronic structure of NiCH₂⁺ in its ground state and low-lying electronic excited states

Sébastien Villaume, Chantal Daniel and Alain Strich

The Journal of Chemical Physics, 2005, Vol. 122

La publication présentée ici dans la thèse est soumise à des droits détenus par un éditeur commercial.

Pour les utilisateurs ULP, il est possible de consulter cette publication sur le site de l'éditeur :
http://scitation.aip.org/journals/doc/JCPSA6-ft/vol_122/iss_4/044313_1-div0.html

Il est également possible de consulter la thèse sous sa forme papier ou d'en faire une demande via le service de prêt entre bibliothèques (PEB), auprès du Service Commun de Documentation de l'ULP: peb.sciences@scd-ulp.u-strasbg.fr

Chapter 5

Emission spectroscopy of metal-to-ligand-charge-transfer states of $\text{HRe}(\text{CO})_3(\text{H-DAB})$

THE emission spectroscopy of $(\text{L})\text{Re}(\text{CO})_3(\alpha\text{-diimine})$ complexes ($\text{L}=\text{Methyl, Ethyl, Benzyl}$) has been widely studied in the literature (see PhD. Thesis [104, 105]). These complexes are representative of this class of molecules possessing low-lying Metal-to-Ligand-Charge-Transfer states as far as their spectroscopic properties are concerned. The model system $\text{HRe}(\text{CO})_3(\text{H-DAB})$ is particularly adequate to simulate absorption and emission spectra since it combines a relative simple potential energy curves scheme with interesting spectroscopic features.

[Signalement bibliographique ajouté par : ULP – SCD – Service des thèses électroniques]

Emission spectroscopy of metal-to-ligand-charge-transfer states of $\text{HRe}(\text{CO})_3(\text{H-dab})$, model system for α -diimine rhenium tricarbonyl complexes

Sébastien Villaume and Chantal Daniel

Comptes Rendus Chimie, 2005, Volume 8, N° 9-10, Pages 1453-1460

Pages 1453 à 1460 :

La publication présentée ici dans la thèse est soumise à des droits détenus par un éditeur commercial.

Pour les utilisateurs ULP, il est possible de consulter cette publication sur le site de l'éditeur : <http://dx.doi.org/10.1016/j.crci.2004.10.037>

Il est également possible de consulter la thèse sous sa forme papier ou d'en faire une demande via le service de prêt entre bibliothèques (PEB), auprès du Service Commun de Documentation de l'ULP: peb.sciences@scd-ulp.u-strasbg.fr

Chapter 6

Photochemistry of $\text{RCo}(\text{CO})_4$ ($\text{R}=\text{H}, \text{CH}_3$)

THE photochemistry of $\text{RCo}(\text{CO})_4$ has been extensively studied as a model system to understand and explain dissociation of carbonyl ligand occurring after a irradiation. Low temperature matrix experiments on $\text{HCo}(\text{CO})_4$ have concluded that the loss of a carbonyl is more favorable than the homolysis of the Co-H bond with a 8 to 1 branching ratio [106–108]. However, the theoretical studies, coupling computed *ab initio* Potential Energy Surfaces (PES) with wave packet propagation, failed to reproduce the CO loss but have put in evidence the Co-H homolysis [109–113].

The ground state properties and reactivity have been studied by means of DFT calculations [114–117] while the electronic spectroscopy, photochemistry and quantum dynamics of $\text{HCo}(\text{CO})_4$ have been investigated by accurate *ab initio* methods and wave packet propagations [109–113]. These simulations consisted of wave packet propagation on 2 dimensional PES along Co-H and Co- CO_{axial} bond elongations computed at the CASSCF level of theory with a limited active space. Only three states were included, the electronic ground state $^1\text{A}_1$, the first absorbing state ^1E corresponding to an $3d_{\text{CO}} \rightarrow \sigma_{\text{Co-H}}^*$ excitation and a low lying triplet state $^3\text{A}_1$ which corresponds to a $\sigma_{\text{Co-H}} \rightarrow \sigma_{\text{Co-H}}^*$ excitation. The ^1E and $^3\text{A}_1$ states are dissociative along both coordinates but it was shown that the photolysis of the Co-H bond occurs in less than 20fs after absorption to the ^1E state, with 80% of population transferred via inter-system crossing within 50ps to the $^3\text{A}_1$. From the $^3\text{A}_1$ state, the Co-H bond breaks to produce the diradicals $\text{H}\bullet + \bullet\text{Co}(\text{CO})_4$. Recently, the umbrella motion of the equatorial carbonyls (see Fig 6.1) has also been included in the study but the results remained unchanged [118].

This study which does not reproduce the low temperature matrices experimental observations, should be revisited taking into account the limitations of this first investigation performed ten years ago. The first limitation was the number of degrees of freedom that were effectively taken into account, namely the Co-H and Co- CO_{axial} . Other degrees of freedom, leading to Jahn-Teller or pseudo Jahn-Teller deformations, might influence the photochemistry and the different dissociation channels. The second limitation was the number of states included in the simulation, the $^1\text{A}_1$, ^1E , and $^3\text{A}_1$ states. When the first

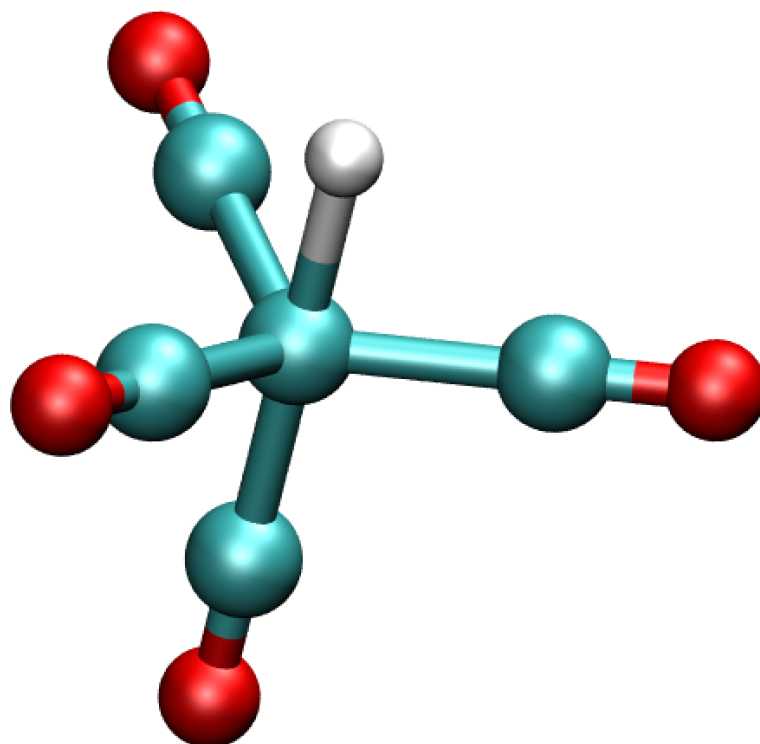


Figure 6.1: $\text{HCo}(\text{CO})_4$ adopts a trigonal bi-pyramidal structure. The equatorial carbonyls make an umbrella in the direction of the hydrogen atom.

simulation was done, the computational cost did not permit to compute a lot of states. Nowadays, a dozen of electronic excited states can be computed in average CASSCF calculations and can be followed by a MS-CASPT2 treatment to include both static and dynamical electronic correlation effects. Finally the choice of the active space, limited by computational cost at that time, might be extend to include all d-shell orbitals of the cobalt atom and all π_{CO}^* of the carbonyls in order to have a balanced description of the electronic structure.

In this part, we present a new study of the electronic structure of $\text{RCo}(\text{CO})_4$ ($\text{R}=\text{H}, \text{CH}_3$) based on new large CASSCF/MS-CASPT2 calculations with high quality basis set. We compare these results with TD-DFT which enabled for the calculation of several tens of electronic states with a very small computational effort. This study is a preliminary investigation in the perspective of revisiting the quantum dynamics. The second part of this chapter is devoted to a preliminary quantum dynamical 2D simulation on $\text{HCo}(\text{CO})_4$.

6.1 Computational Details

The electronic calculations have been performed in C_s symmetry under the C_{3v} symmetry constraint. An experimental structure is available for $\text{HCo}(\text{CO})_4$, but there is no experi-

mental informations concerning $\text{CH}_3\text{Co}(\text{CO})_4$. Thus, The geometry of $\text{CH}_3\text{Co}(\text{CO})_4$ was optimized within C_s symmetry at DFT (B3LYP) level of theory. This geometry was validated by comparison with the optimized and the experimental geometries of $\text{HCo}(\text{CO})_4$. The electronic ground state configuration of $\text{RCo}(\text{CO})_4$ is described by the following occupation $(\sigma_{\text{Co-R}})^2 (3d_\pi)^4 (3d_\delta)^4$. The $\sigma_{\text{Co-R}}$ orbital is a σ overlap between the d_{z^2} orbital of Co and a p_z orbital of the CH_3 fragment or the $1s$ orbital of the H atom in the case of $\text{HCo}(\text{CO})_4$. The low lying vacant orbitals are the π_{CO}^* of the carbonyls and the $\sigma_{\text{Co-R}}^*$ anti-bonding orbitals. The active space is chosen to include all d-shell orbitals (including the $\sigma_{\text{Co-R}}$ orbital) of Co and the vacant orbitals cited above. For the hydride complex, 16 active electrons have been correlated into 13 orbitals whereas in the methyl complex, 16 active electrons have been correlated into 14 orbitals (we included 1 extra vacant orbital corresponding to the $\sigma_{\text{Co-CO}_{axial}}^*$ orbital in the active space). The atomic natural orbitals basis sets (ANO-Small) have been used for both complexes. The CASSCF and the MS-CASPT2 calculations have been performed in the C_s symmetry group in which the E states in the true C_{3v} symmetry gives degenerate states in A' and A'' in C_s . We computed 9 averaged roots in the A' symmetry and 9 averaged roots in A''. The TD-DFT calculation have been performed using the B3LYP functional and 6-31G(d) basis sets on the optimized geometries of both complexes and on the experimental geometry of $\text{HCo}(\text{CO})_4$.

6.2 Results

6.2.1 Geometry optimization

The optimized and the experimental parameters are presented in Table 6.1. We fixed the Co-C-O bond angles in both structures at 180° . The comparison between experimental and optimized structure of $\text{HCo}(\text{CO})_4$ gives a reasonable agreement. The angle of the umbrella is 81.0° in the optimized DFT structure while it has been measured at 80.3° . The main deviation arises from the axial bond lengths, the Co-H bond length is overestimated while the Co- CO_{axial} bond length is underestimated. However, these results are in good agreement with the DFT structure of Ziegler et al. [114,115]. On the basis of these observations, it is reasonable to think that the optimized geometry of $\text{CH}_3\text{Co}(\text{CO})_4$ is of good quality and can be used in subsequent calculations. The comparison of the complexes $\text{HCo}(\text{CO})_4$ and $\text{CH}_3\text{Co}(\text{CO})_4$ shows that structures are very close except that the calculated value of Co- CH_3 and Co-H differs from 0.592 \AA . This difference is consistent with the difference observed for $\text{RMn}(\text{CO})_5$ analogs [114,115]. This shorter Co-R bond length in the Hydride complex was expected and is related to the weakness of Co- CH_3 bond compared to the Co-H bond.

parameters	$\text{CH}_3\text{Co}(\text{CO})_4$	$\text{HCo}(\text{CO})_4$	$\text{HCo}(\text{CO})_4$ (exp)
Co-R	2.086	1.494	1.556
Co- C_{axial}	1.812	1.812	1.764
Co- C_{eq}	1.806	1.801	1.818
C-0	1.170	1.141	1.141
R-Co- C_{eq}	83.8	81.0	80.3

Table 6.1: Most relevant geometrical parameters of the $\text{RCo}(\text{CO})_4$ optimized at DFT (B3LYP) level of theory and the experimental parameters of $\text{HCo}(\text{CO})_4$ (Bond lengths and bond angles in Å and $^\circ$).

6.2.2 Absorption Spectroscopy of $\text{RCo}(\text{CO})_4$ ($\text{R}=\text{H}, \text{CH}_3$)

The MS-CASPT2 and TD-DFT transition energies of $\text{HCo}(\text{CO})_4$ and $\text{CH}_3\text{Co}(\text{CO})_4$ complexes are reported in Table 6.2 together with oscillator strengths. Both complexes absorb at 254 nm ($39\,400\text{ cm}^{-1}$) [106,107]. The absorption spectrum of $\text{HCo}(\text{CO})_4$ is characterized by an intense band at $44\,000\text{ cm}^{-1}$ preceded by a shoulder at $34\,000\text{ cm}^{-1}$.

The MS-CASPT2 results show that the theoretical spectrum starts at about $35\,500\text{ cm}^{-1}$ for $\text{HCo}(\text{CO})_4$ and about $34\,000\text{ cm}^{-1}$ for $\text{CH}_3\text{Co}(\text{CO})_4$. For both complexes, the four low-lying states calculated between $35\,740$ and $42\,040\text{ cm}^{-1}$ ($\text{HCo}(\text{CO})_4$) and $33\,980$ and $42\,340\text{ cm}^{-1}$ ($\text{CH}_3\text{Co}(\text{CO})_4$) contribute to the first band observed around $40\,000\text{ cm}^{-1}$. The TD-DFT does not give the same order of transitions than the MS-CASPT2 for both complexes, the b^1E state is higher in energy. It corresponds to a $3d_\pi \rightarrow \sigma_{\text{Co-R}}^*$ excitation for both complexes, showing that this type of excitation is not described adequately in TD-DFT.

For $\text{HCo}(\text{CO})_4$, the transition to the d^1E state is responsible of the intense peak observed at $44\,000\text{ cm}^{-1}$ observed in the experimental spectrum. This band is shifted to higher energy in the methyl complex ($48\,200\text{ cm}^{-1}$). Finally, $\text{CH}_3\text{Co}(\text{CO})_4$ complex shows a peak of intermediate intensity around $50\,000\text{ cm}^{-1}$ corresponding to a sigma bond to ligand charge transfer (SBLCT) state which is absent in its hydride counterpart and replaced by a metal to ligand charge transfer (MLCT) state around $48\,000\text{ cm}^{-1}$.

The TD-DFT transition energies are underestimated by more than 0.5eV. This trend is usually observed in a number of transition metal complexes [119].

6.3 Potential Energy Surfaces

In a preliminary computation of the 3D-PES for the hydride complex $\text{HCo}(\text{CO})_4$ including the umbrella motion (θ angle) together with the elongation of the Co-H and Co- CO_{axial}

STATE	Main configuration	MS-CASPT2		TD-DFT (exp.)		TD-DFT (opt.)	
		ΔE	f	ΔE	f	ΔE	f
R=H							
$a^1A_1 \rightarrow a^1E$	$3d_\delta \rightarrow \sigma_{Co-H}^*$	35 740	0.0013	30 860	0.0	30 560	0.0
$a^1A_1 \rightarrow b^1E$	$3d_\pi \rightarrow \sigma_{Co-H}^*$	40 280	0.0013	37 580	0.0012	36 900	0.0016
$a^1A_1 \rightarrow c^1E$	$3d_\delta \rightarrow \pi_{CO}^*$	41 320	0.04	35 150	0.0056	34 400	0.002
$a^1A_1 \rightarrow b^1A_1$	$3d_\delta \rightarrow \pi_{CO}^*$	42 040	0.08	36 410	0.0233	35 900	0.028
$a^1A_1 \rightarrow d^1E$	$3d_\delta \rightarrow \pi_{CO}^*$	44 190	0.08	38 945	0.0360	38 100	0.0326
$a^1A_1 \rightarrow e^1E$	$3d_\pi \rightarrow \pi_{CO}^*$	49 900	0.04	43 280	0.0002		
R=CH ₃							
$a^1A_1 \rightarrow a^1E$	$3d_\delta \rightarrow \sigma_{Co-CH_3}^*$	33980	0.0024	29345	0.0009		
$a^1A_1 \rightarrow b^1E$	$3d_\pi \rightarrow \sigma_{Co-CH_3}^*$	38390	0.0032	34650	0.0008		
$a^1A_1 \rightarrow c^1E$	$3d_\delta \rightarrow \pi_{CO}^*$	40720	0.0178	33120	0.0029		
$a^1A_1 \rightarrow b^1A_1$	$3d_\delta \rightarrow \pi_{CO}^*$	42340	0.0140	34740	0.0158		
$a^1A_1 \rightarrow d^1E$	$3d_\pi \rightarrow \pi_{CO}^*$	48200	0.0364	37790	0.024		
$a^1A_1 \rightarrow e^1E$	$\sigma_{Co-CH_3} \rightarrow \pi_{CO}^*$	52290	0.0200	45750	0.0676		

Table 6.2: CASSCF/MS-CASPT2 and TD-DFT transition energies in cm^{-1} of the low lying electronic states of $\text{RCo}(\text{CO})_4$ ($\text{R}=\text{H}, \text{CH}_3$) and corresponding oscillator strengths f.

bonds, we have concluded that angular deformation leads to nearly harmonic shape of the potential along this coordinate [120]. Consequently, this deformation can be neglected in the computation of the PES. As far as the methyl complex is concerned, the study is performed in collaboration with the Freie Universitat Berlin where the calculations are on the way in the group of J. Manz in the perspective of ultra-fast laser experiments performed in the group of L. Woste. In order to study the competition between the loss of the axial carbonyl and the homolysis of the metal-hydrogen bond, we computed PES of the electronic ground state and the two low lying ^1E states at the CASSCF level using a reduced active space of 10 electrons correlated in 11 active orbitals for $\text{HCo}(\text{CO})_4$. All 5 d-shell orbitals of the metal, the $\sigma_{\text{Co-H}}^*$ and 5 π_{CO}^* constitute this active space.

The geometry parameters of $\text{HCo}(\text{CO})_4$ have been fixed to the experimental values except the two coordinates of interest, namely Co-H and Co- CO_{axial} bond lengths. We computed 400 CASSCF points for each surface by means of averaged CASSCF on the three roots (a^1A_1 , a^1E , b^1E) in C_s symmetry using C_{3v} symmetry constraint to keep the degeneracy of the ^1E states. For the Co-H bond, the grid is composed by 0.9, 1.2, 1.4, 1.5, 1.556, 1.7, 1.8, 1.9, 2.0, 2.1, 2.4, 2.7, 3.0, 3.3, 3.7, 4.2, 5.0, 7.0, 10.0, and 15.0 Å while we used 1.3, 1.5, 1.6, 1.7, 1.764, 1.9, 2.0, 2.1, 2.3, 2.5, 2.7, 3.0, 3.3, 3.7, 4.2, 5.0, 7.0, 10.0, and 15.0 Å for the Co- CO_{axial} bond. The surfaces which was fitted using splines technique, are presented at the end of this chapter (Fig. 6.6, 6.7, and 6.8).

As expected, the first excited state a^1E is dissociative in both directions. The second excited state b^1E has the same shape than a^1E . Surface cuts are presented (see Fig. 6.2 and 6.3) to clarify the position of the excited states relative to the ground state.

Using these potentials, we performed a preliminary dynamical study.

6.4 Quantum Dynamics

The dynamical simulation was carried out using the three potential a^1A_1 (ground state), a^1E (first excited state) and b^1E (second excited state). The grid parameters used in the simulation are presented in Table 6.3. We used the Fourier Grid Hamiltonian method to discretize the system and we have computed the ten first vibrational eigenfunctions of the electronic ground state. The eight first eigenstates are plotted in Figure 6.4.

We used the vibrational eigenstate $\nu=(0,0)$ to as initial wave packet of the simulation. This wave packet is photo excited with a laser field with the following parameters: a field frequency of 0.150 a.u. is chosen in order to lie between a^1E and b^1E with a pulse duration of 100fs. The ground state is coupled to the excited states through transition dipole moments computed at the CASSCF level of theory.

As an approximation in this preliminary work, we used constant transition dipole moments, namely the value at the equilibrium geometry. In future simulations, we will use transition dipole moments depending on the coordinates and discretized on the same grid than the PES and the Hamiltonian.

We used the Chebichev propagator to compute and to evaluate the evolution of the wave packet in time.

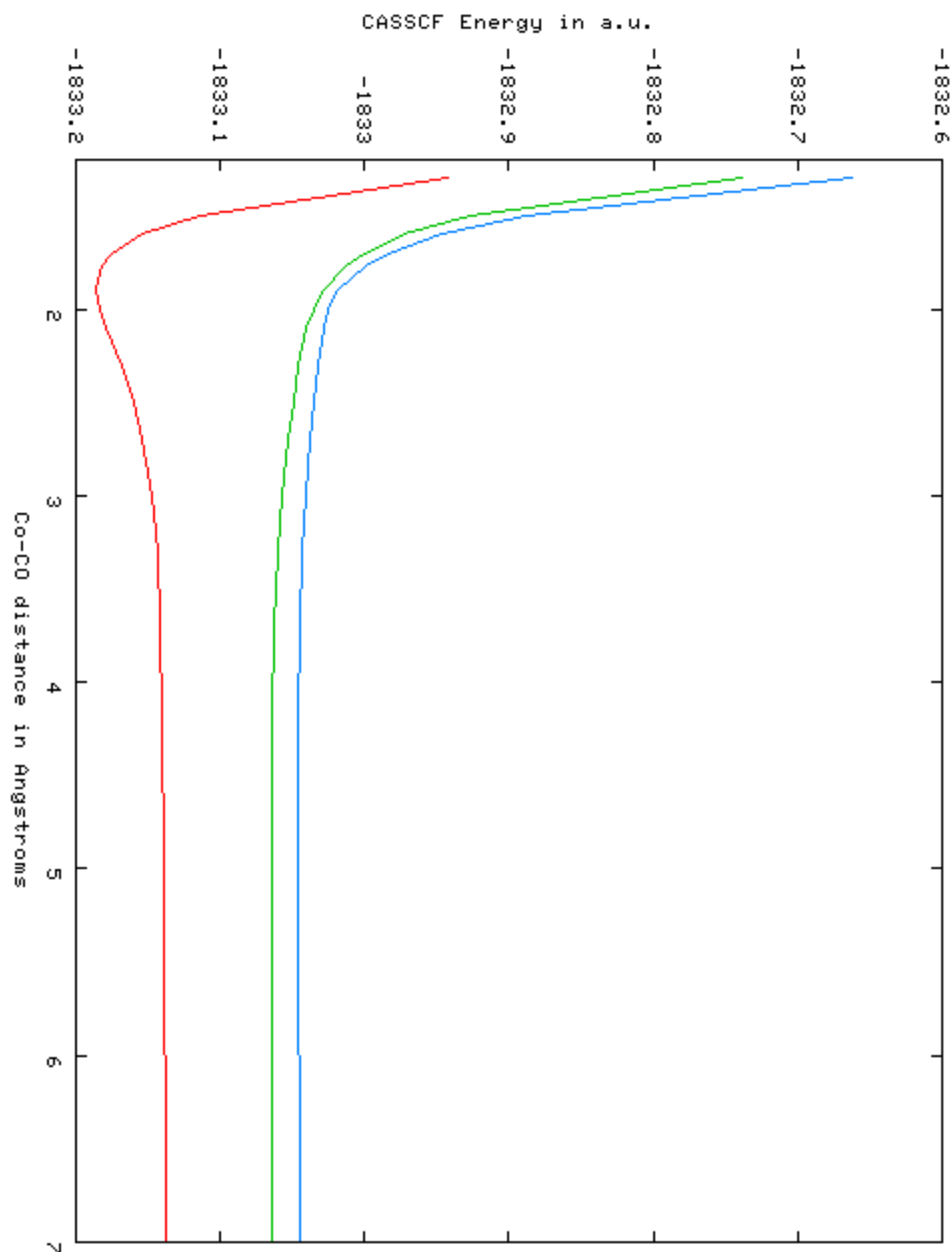


Figure 6.2: Potential Energy Curve along the Co-CO coordinate.

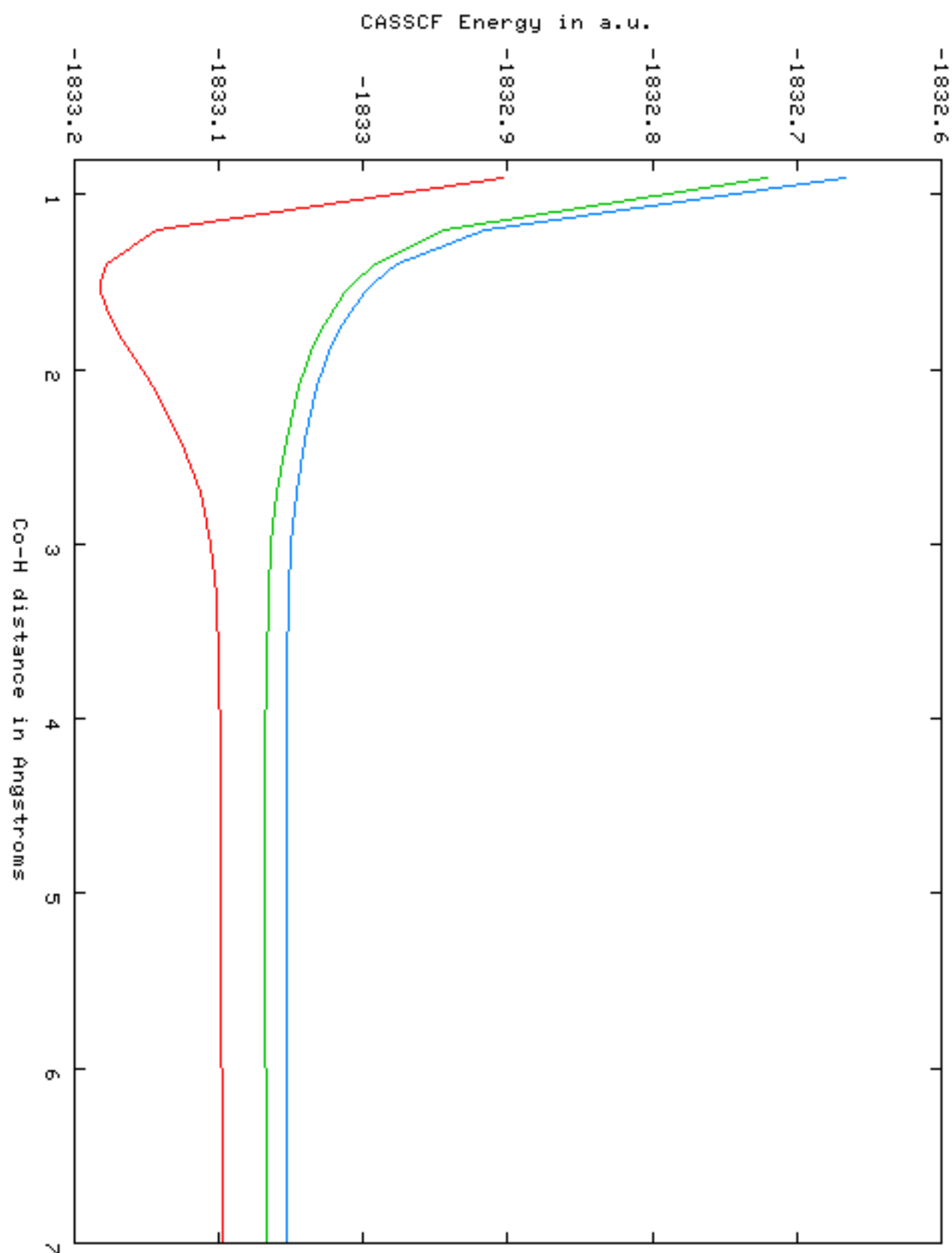


Figure 6.3: Potential Energy Curve along the Co-H coordinate.

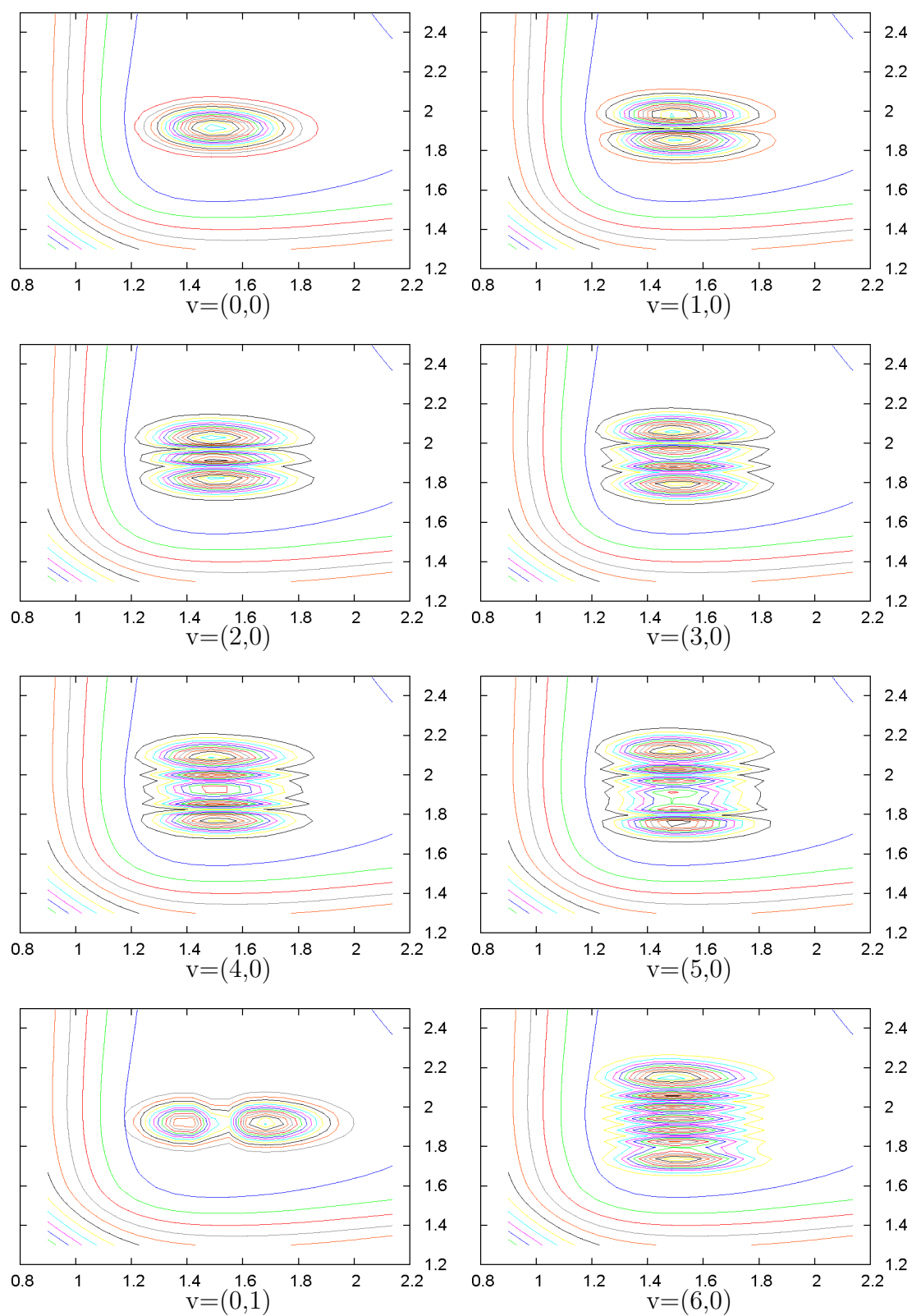


Figure 6.4: The eight first eigenstate of the electronic ground state a^1A_1 of $HCo(CO)_4$.

	Number of grid points	q_0	q_f	ΔQ
Co-H	64	0.9	5.0	0.064
Co-CO _{axial}	128	1.3	5.0	0.0289

Table 6.3: Grid parameters used in the simulation.

6.4.1 Results

The low-lying vibrational excited state of the electronic ground state correspond to the excitation of the Co-CO_{axial} bond. The first vibrational excited state of the Co-H bond ($v=0,1$) is higher in energy (seventh). According to the Hooke's Law, this is not surprising since the reduced mass between Co and H is very small compared to the reduced mass between Co and CO. We used the vibrational ground state as initial wave packet since one may consider that the main population of the system is usually in the vibrational ground state at room temperature.

Snapshots of the simulation are presented in Figure 6.5 at time $t = 0, 10, 20,$ and 30fs for both excited states. At $t = 0\text{fs}$, The wave packet is still on the ground state and nothing appears on excited states. At $t = 5\text{fs}$, under the influence of the laser field, both $a^1\text{E}$ and $b^1\text{E}$ are populated. The major part of the population stay on the ground state, less than 5% of the initial wave packet goes to excited states. After less than 20fs , the wave packet starts to dissociate along the CO-H coordinate for both excited states. It has to be noted a small displacement of the wave packet along the Co-CO_{axial} coordinate but this effect is negligible compared to the displacement along the Co-H coordinate. After 35fs , we can see for both excited states a wave packet "train": the laser field is still populating both states in the Franck Condon region while the front of the wave packet goes to higher bond length. This preliminary simulation show that the homolysis of the Co-H bond is ultra fast and very efficient. The experimental CO loss is not reproduced and need more investigation. One possible way is to include more than two electronic excited states. The MS-CASPT2 study and the experimental spectrum have shown an intense absorption around 44000 cm^{-1} which might correspond to the $d^1\text{E}$ state. Following this idea, we are computing 5 new CASSCF potential energy surfaces with an increased active space of 10 electrons correlated in 14 orbitals. This work requires a large computer effort and is still in progress.

6.5 Conclusion

The electronic structure of $\text{RCo}(\text{CO})_4$ complexes ($\text{R}=\text{H}, \text{CH}_3$) has been studied by means of MS-CASPT2 and TD-DFT. The MS-CASPT2 transition energies are in good agreement with the experimental spectrum while the TD-DFT underestimates the transition energies by more than 0.5eV . The main feature of the experimental spectrum, namely shoulders

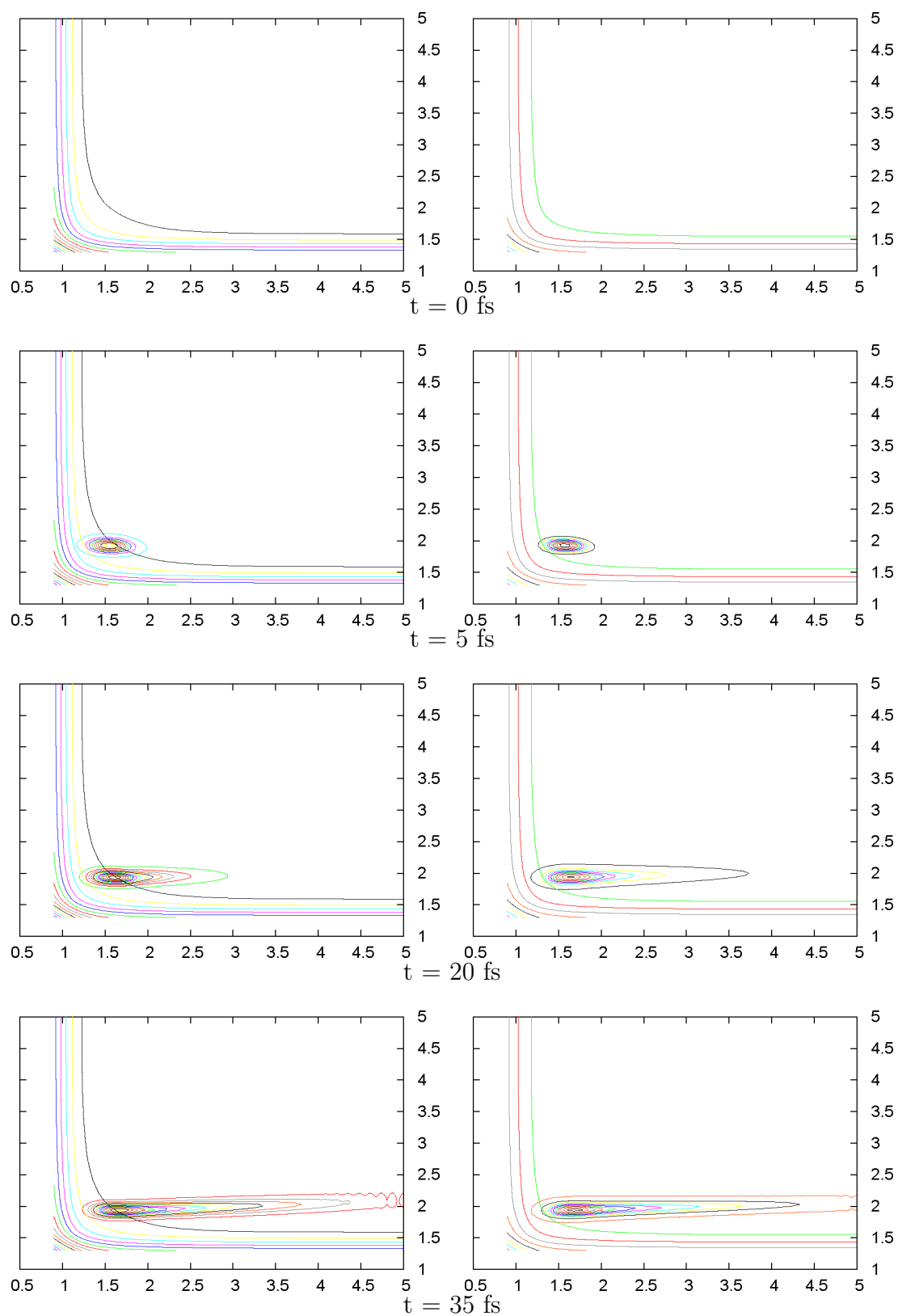


Figure 6.5: Snapshots of the dynamical simulation. The a^1E excited state is on the left and b^1E is on the right.

and intense peak, are qualitatively reproduced.

Potential energy surfaces of $\text{HCo}(\text{CO})_4$ were computed using 400 single point calculations at the averaged CASSCF(10e/11a) level of theory. We considered the elongations of the Co-H and Co-CO_{axial} bond while the umbrella motion was not included in this preliminary work. The a¹E and the b¹E are dissociative in both directions.

The wave packet propagation on these calculated PES did not reproduce the CO loss observed experimentally. However, our simulation has shown that the Co-H bond breaks either from the a¹E or b¹E states. This discrepancy may come from a lack of flexibility due to the limited size of the active space used to compute the potential energy surfaces. This may also come from the limited number of excited states we have used in the simulation. The experimental absorption spectrum of $\text{HCo}(\text{CO})_4$ shows an intense band at 44 000cm⁻¹ corresponding to the transition from a¹A₁ → d¹E state. Following these considerations, we are computing more PES using an increased active space. [120]

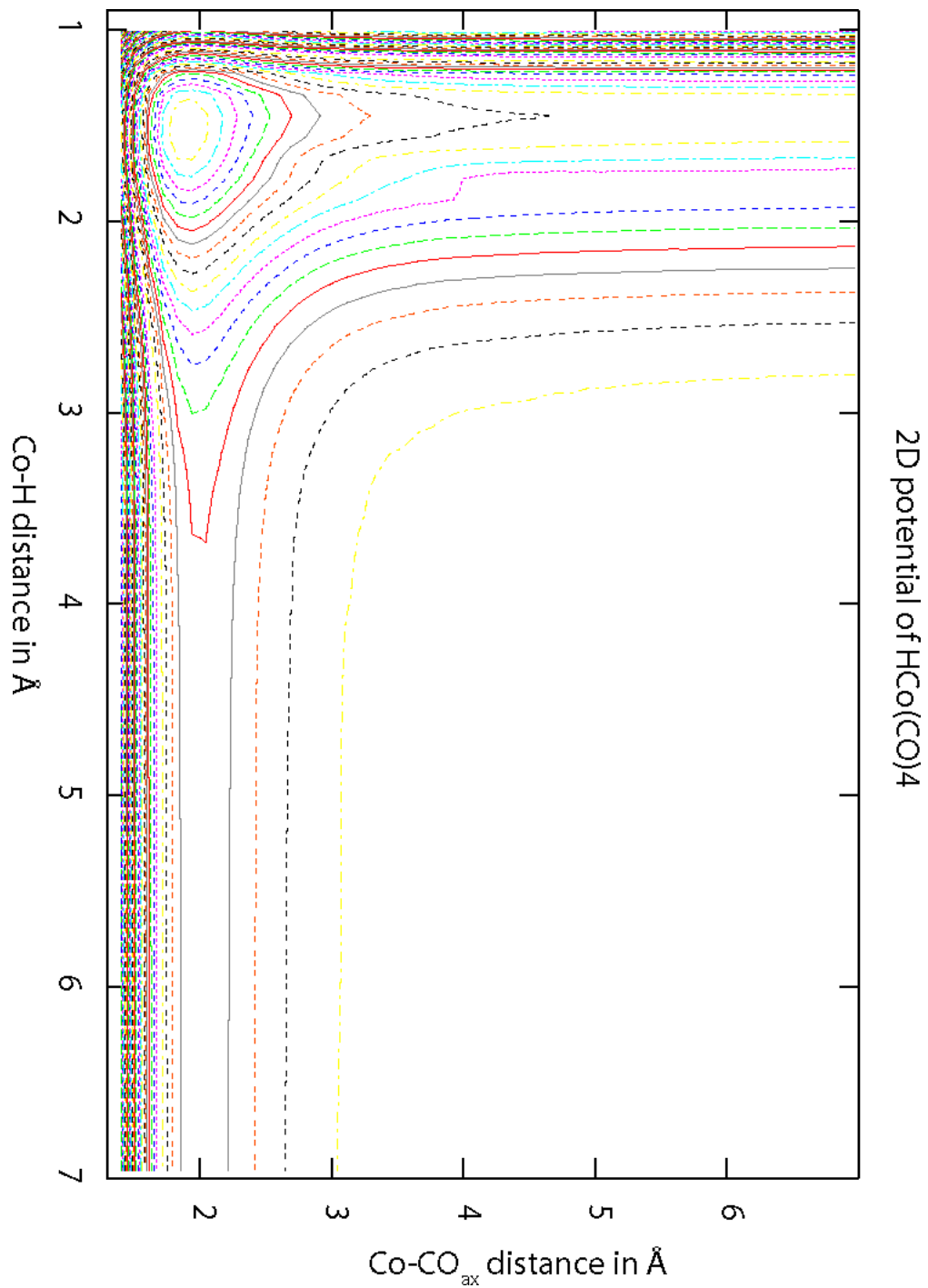


Figure 6.6: ground state.

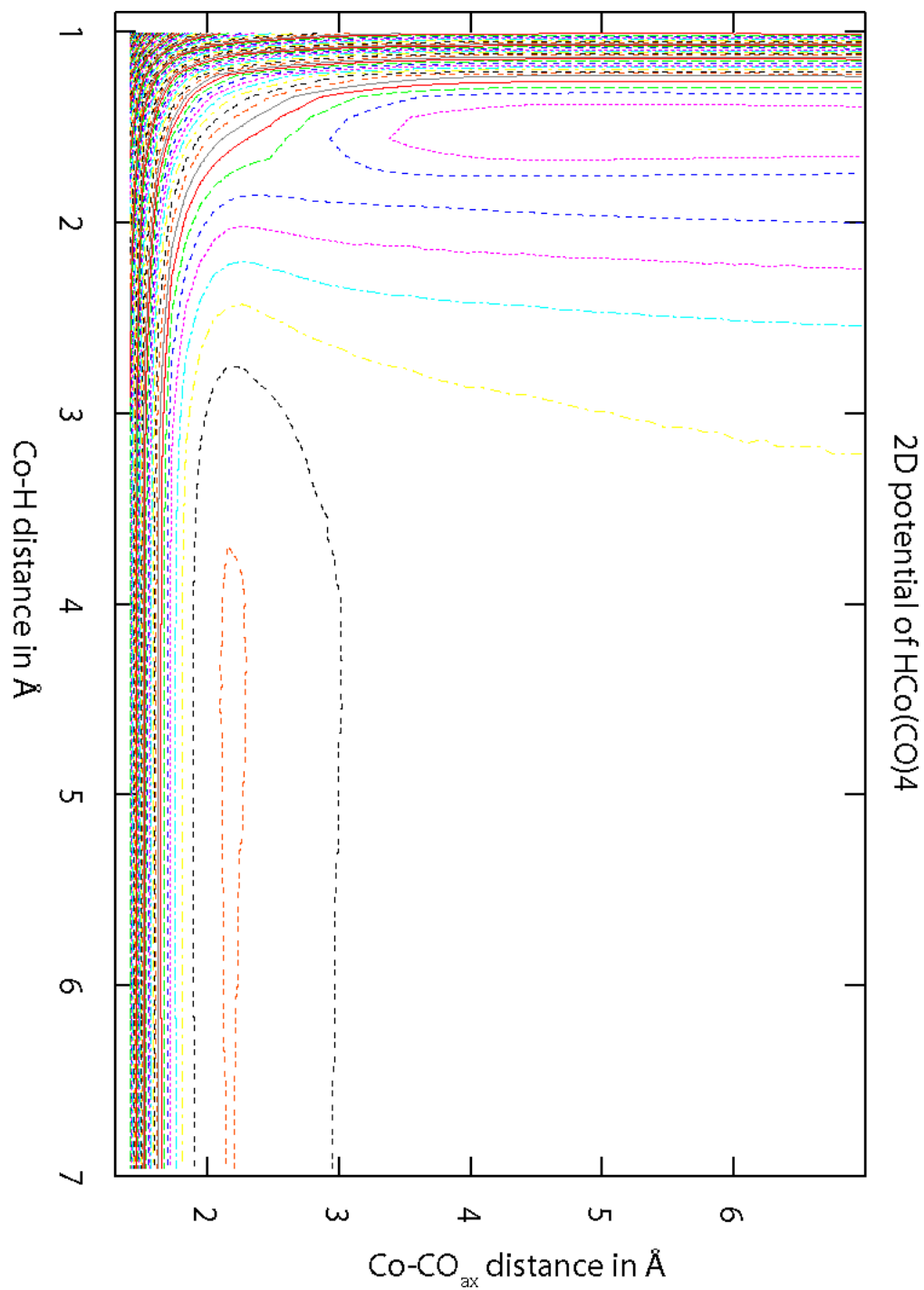


Figure 6.7: first excited state.

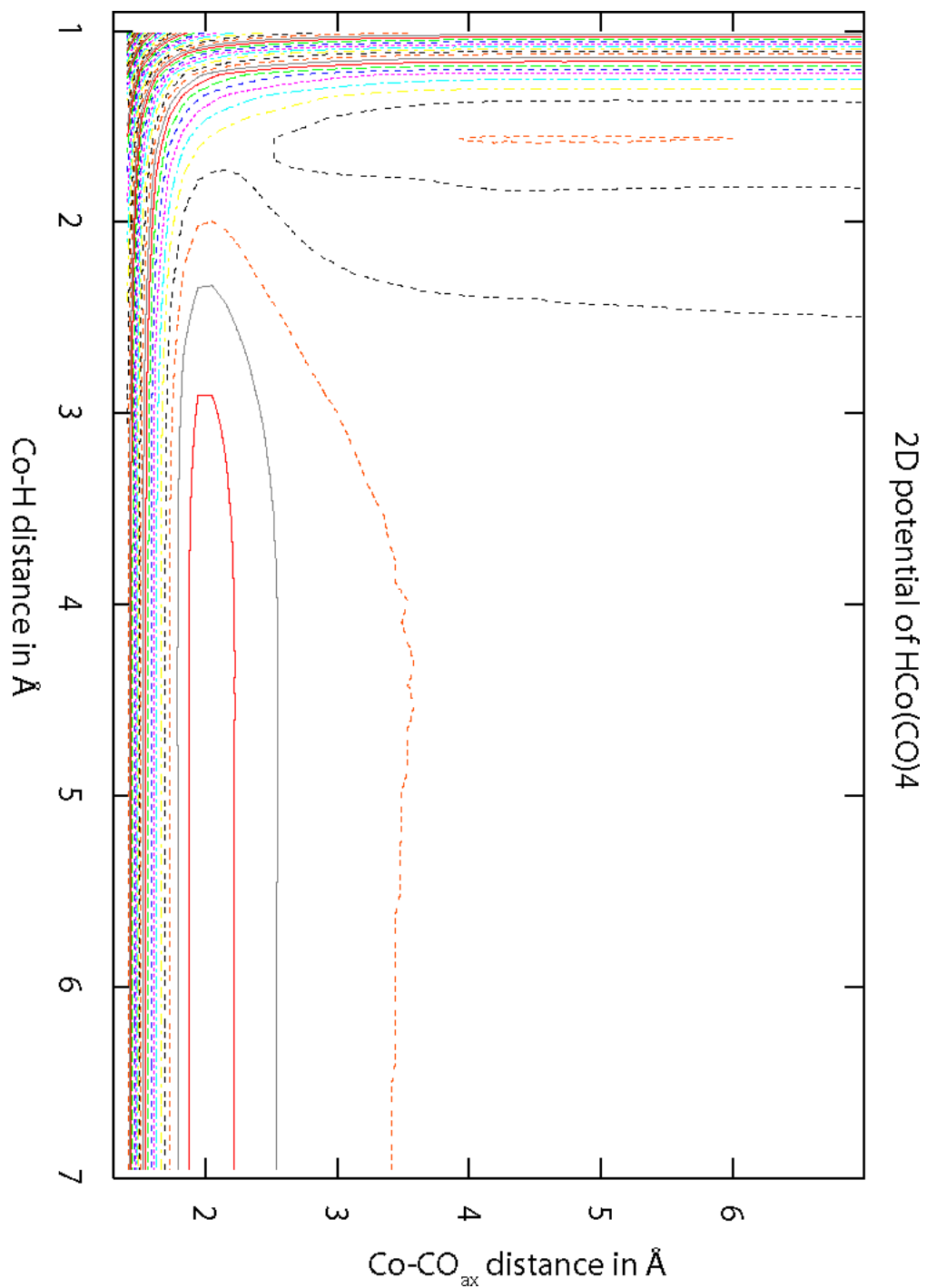


Figure 6.8: second excited state.

Conclusion

THE ultimate goal of this work was to investigate the electronic spectroscopy and the photochemistry of transition metal complexes by means of Coupled Cluster calculations and wave packet propagation.

In the first part, the intra-molecular rearrangements in trifluorophosphorane PH_2F_3 have been studied. This molecule was used to assess the quality of CC calculations. The structure of the stable isomers and the transition states connecting them were optimized at the CCSD(T) level of theory and cc-pVTZ basis sets. The optimized structure of the most stable isomer TBP1 show a good agreement with experimental data. The activation barriers of the two possible modes of rearrangement were calculated at 9.70 kcal mol⁻¹ (M_2) and 7.24 kcal mol⁻¹ (M_4), showing that the M_4 mode is the most favorable. The harmonic vibrational spectrum of TBP1 has been calculated at the CCSD(T) level of theory. The frequencies as well as the relative intensities are in good agreement with experiment.

The CC approach was also applied to the investigation of the electronic structure of $\text{Cr}(\text{CO})_6$. This system is known to be a tough case and the assignment of its absorption spectrum is subject of controversy. Transition energies have been calculated at the CCSD level with mixed Wachters+f/cc-pVDZ basis sets. Our results show that these transition energies are systematically shifted by 0.5eV to higher energy (with respect to the experimental spectrum). Calculations including the correction of the triple excitations are running to estimate the missing correlation. The qualitative recent assignment by CASPT2 and TDDFT approaches with a series of low-lying MLCT states below the MC states has been confirmed by the present study. Moreover refined CASSCF/MS-CASPT2 and Coupled Cluster calculations have put in evidence the near degeneracy of the a^1T_{1u} MLCT absorbing state with the a^1T_{1g} MC state which should be responsible for the ultra-fast (fs timescale) carbonyl loss of $\text{Cr}(\text{CO})_6$.

The study of the MCH_2^+ series (M=Fe, Co, Ni) has been performed to clarify the Franck-Condon region and the electronic structure of these complexes. This study is the starting point in the understanding of different dissociation pathways and the determination of the relevant coordinates to build potential energy surfaces. These systems are characterized by

open-shell configurations and nearly degenerate ground states with large spin contamination. The CC treatment reduces the spin contamination by 0.2-0.4 but is unable to remove it completely. The use of a reference based on Kohn-Sham orbitals gives less contaminated states since the reference wave function is already less contaminated. This technique may help in tough cases where the results are very sensitive to the quality of the reference wave function. The low-lying states have been put in evidence for each molecule. The photoactive states potentially responsible for the photofragmentation of the molecules as well as the energy windows of irradiation have been determined without ambiguity.

The second aspect of this work deals with the use of wave packet propagation as a tool to simulate the absorption/emission spectroscopy and the study of photochemical processes. The main difficulty is usually the dimensionality and the choice of the relevant coordinates that have to be included in the dynamical simulation to reproduce the experimental data. In the field of transition metal complexes, the building of the potential energy surfaces may lead to several complications.

In this work, we have presented two different aspects of the photochemistry of transition metal complexes. The first part focuses on the electronic spectroscopy of the $\text{HRe}(\text{CO})_3(\text{H-DAB})$ complex. Theoretical absorption and emission spectra have been computed using the information contained by the autocorrelation function. A time resolved stimulated emission spectrum has been calculated, showing the fine structure of the vibrational states and the split of the wave packet in time. Other effects, such as spontaneous emission, were not taken into account.

The electronic spectroscopy and the photodissociation dynamics of $\text{HCo}(\text{CO})_4$ was revisited in order to improve the description of the electronic problem and to investigate the role of the umbrella motion in the dissociation scheme. Two ^1E absorbing states have been included in the computation of the 2D-PES on the basis of the computation of nine electronic states 1D-PEC calculated for the Co-H and Co-CO_{axial} bonds elongations. Preliminary dynamics simulation does not modify significantly our previous conclusion, namely a fast direct bond breaking of the cobalt-hydrogen bond. In order to prepare new simulations of laser control experiments on $\text{RCo}(\text{CO})_4$ (R=H, CH₃), we have performed dynamics with the laser coupled to the vibrational states of the molecule.

The purpose of this work was to investigate the potential of the Coupled Cluster method for the description of complex electronic structure problems of transition metals compounds. The calculations performed were far from being routine calculations. In contrast, coding has to be performed at each step. It has been shown that the use of KS orbitals as references could help in the case of large spin contamination. As soon as the atomic basis sets include enough electronic correlation effects, their influence on the Coupled Cluster calculations seems to be modest. The crucial point seems to be the addition of the triple excitations. Another aspect which will be investigated in future work will be the description of bond breakings by Coupled cluster methods. From this point of view, $\text{Cr}(\text{CO})_6$ or $\text{HCo}(\text{CO})_4$ are very good model complexes to go further.

Bibliography

- [1] J. Michl, V. Bonacic-Koutecky, *Electronic aspects of Organic Photochemistry*, (John Wiley & sons Inc., 1990).
- [2] S. D. Vartak, N. M. Lawandy, *Opt. Comm.* **120**, 184 (1995).
- [3] H. Stapelfeldt, E. Constant, C. P. B., *Prog. Crystal Growth and Charact.* **33**, 209 (1996).
- [4] A. H. Zewail, *Phys. Today* **33**, 27 (1980).
- [5] N. Bloembergen, A. H. Zewail, *J. Phys. Chem.* **88**, 5459 (1984).
- [6] A. H. Zewail, *J. Phys. Chem.* **100**, 12701 (1996).
- [7] E. T. Sleva, I. M. Xavier, A. H. Zewail, *J. Opt. Soc. Am. B* **3**, 483 (1986).
- [8] W. S. Warren, A. H. Zewail, *Laser Chem.* (1983).
- [9] A. Assion, T. Tautert, M. Bergt, B. Brixner, T. Kiefer, V. Seyfried, M. Strehle, G. Gerber, *Science* **282**, 919 (1998).
- [10] T. Brixner, M. Strehle, G. Gerber, *Appl. Phys. B* **68**, 281 (1991).
- [11] T. Baumert, R. Grosser, M. Thalweiser, G. Gerber, *Phys. Rev. Letters* **67**, 3753 (1991).
- [12] T. Baumert, G. Gerber, *Adv. At. Mol. Opt. Phys.* **35**, 163 (1995).
- [13] T. Baumert, T. Brixner, V. Seyfried, M. Strehle, G. Gerber, *Appl. Phys. B* **65**, 779 (1997).
- [14] T. Baumert, R. Thalweiser, G. Gerber, *Chem. Phys. Lett.* **209**, 29 (1993).
- [15] T. Brixner, G. Gerber, *Opt. Lett.* **26**, 557 (2001).
- [16] T. Brixner, A. Oehrlein, M. Strehle, G. Gerber, *Appl. Phys. B* **70**, S119 (2000).
- [17] T. Brixner, N. H. Damrauer, P. Niklaus, G. Gerber, *Nature* **414**, 57 (2001).

- [18] M. Erdmann, O. Rubner, V. Engel, *J. Organomet. Chem.* **661**, 191 (2002).
- [19] M. Erdmann, Z. Shen, E. V., *Chem. Phys. Lett.* **352**, 275 (2002).
- [20] S. Vajda, A. Bartelt, E.-C. Kaposta, T. Leisner, C. Lupulescu, S. Minemoto, P. Rosendo-Francisco, L. Wöste, *Chem. Phys.* **267**, 231 (2001).
- [21] C. Daniel, J. Full, L. Gonzalez, C. Kaposta, M. Krenz, C. Lupulescu, J. Manz, S. Minemoto, M. Oppel, P. Rosendo-Francisco, S. Vajda, L. Wöste, *Chem. Phys.* **267**, 247 (2001).
- [22] R. S. Judson, H. Rabitz, *Phys. Rev. Letters* **68**, 1500 (1992).
- [23] D. Goswami, *Phys. Rev.* **374**, 385 (2003).
- [24] S. K. Kim, S. Pedersen, A. H. Zewail, *Chem. Phys. Lett.* **233**, 500 (1995).
- [25] S. A. Trushin, W. Fuss, W. E. Schmid, L. Kompa, *J. Phys. Chem. A* **102**, 4129 (1998).
- [26] S. A. Trushin, W. Fuss, W. E. Schmid, L. Kompa, *J. Phys. Chem.* **104**, 1997 (1997).
- [27] L. Banares, T. Baumert, M. Bergt, B. Kiefer, G. Gerber, *J. Chem. Phys.* **108**, 5799 (1997).
- [28] M. Gutmann, J. M. Janello, M. S. Dickebohm, M. Grossekatheofer, J. Lindener-Roennecke, *J. Phys. Chem.* **102**, 4138 (1998).
- [29] D. R. Yarkony, *J. Phys. Chem. A* **105**, 6277 (2001).
- [30] D. R. Yarkony, *J. Phys. Chem. A* **105**, 2642 (2001).
- [31] S. Matsika, D. R. Yarkony, *J. Chem. Phys.* **115**, 2038 (2001).
- [32] M. Born, R. Oppenheimer, *Ann. Phys.* **84**, 457 (1927).
- [33] A. Szabo, N. S. Ostlund, *Modern Quantum Chemistry: Introduction to Advanced Electronic Structure Theory*, (Macmillan, New York, 1982).
- [34] W. Koch, M. C. Holthausen, *A Chemist's guide to Density Functional Theory*, (Wiley, 2000).
- [35] P. E. M. Siegbahn, J. Almlöf, A. Heiberg, B. O. Roos, *J. Phys. Chem.* **74**, 2384 (1981).
- [36] T. Helgaker, P. Jorgensen, J. Olsen, *Molecular Electronic Structure Theory*, (John Wiley & Sons Inc., 2000).

- [37] J. Finley, P.-A. Malmqvist, B. O. Roos, L. Serrano-Andres, *Chem. Phys. Lett.* **288**, 299 (1998).
- [38] J. F. Stanton, R. J. Bartlett, *J. Chem. Phys.* **102**, 3629 (1995).
- [39] R. Schinke, *Photodissociation Dynamics*, (Cambridge University Press, 1993).
- [40] H.-D. Meyer, U. Manthe, L. S. Cederbaum, *Chem. Phys. Lett.* **165**, 73 (1990).
- [41] E. J. Heller, *Acc. Chem. Res.* **14**, 368 (1981).
- [42] E. J. Heller, *J. Chem. Phys.* **62**, 1544 (1975).
- [43] C. C. Marston, G. G. Balint-Kurti, *J. Chem. Phys.* **91**, 3571 (1989).
- [44] H. Tal-Ezer, R. Kosloff, *J. Chem. Phys.* **81**, 3967 (1984).
- [45] R. Kosloff, *Ann. Rev. Phys. Chem.* **45**, 145 (1994).
- [46] J. W. Gilje, R. W. Braun, A. H. Cowley, *J. Chem. Soc., Chem. Commun.*, 15 (1974).
- [47] D. Christen, J. Kadel, A. Liedtke, R. Minkwitz, H. Oberhammer, *J. Phys. Chem.* **93**, 6672 (1989).
- [48] A. Strich, *Inorg. Chem.* **17**, 942 (1978).
- [49] R. S. Berry, *J. Chem. Phys.* **32**, 933 (1960).
- [50] I. Ugi, D. Marquarding, H. Klusaceck, P. Gillespie, F. Ramirez, *Acc. Chem. Res.* **4**, 288 (1971).
- [51] J. I. Musher, *J. Am. Chem. Soc.* **94**, 5662 (1972).
- [52] R. R. Holmes, R. N. Storey, *Inorg. Chem.* **5**, 2146 (1966).
- [53] R. R. Holmes, C. J. Hora Jr., *Inorg. Chem.* **11**, 2506 (1972).
- [54] P. M. Treichel, R. A. Goodrich, S. B. Pierce, *J. Am. Chem. Soc.* **89**, 2017 (1967).
- [55] F. Keil, W. Kutzelnigg, *J. Am. Chem. Soc.* **97**, 3623 (1975).
- [56] J. Breidung, W. Thiel, A. Komornicki, *J. Phys. Chem.* **92**, 5603 (1988).
- [57] H. Wasada, K. Hirao, *J. Am. Chem. Soc.* **114**, 16 (1992).
- [58] C. J. Cerjan, W. H. Miller, *J. Chem. Phys.* **75**, 2800 (1981).

- [59] J. F. Stanton, J. Gauss, S. A. Perera, A. D. Yau, J. D. Watts, M. Nooijen, N. Oliphant, P. G. Szalay, W. J. Lauderdale, S. R. Gwaltney, S. Beck, A. Balková, D. E. Bernholdt, K.-K. Baeck, P. Rozyczko, H. Sekino, C. Huber, J. Pittner, R. J. Bartlett. Aces ii is a program product of the quantum theory project, university of florida., Integral packages included are VMOL (J. Almlöf and P. R. Taylor); VPROPS (P. R. Taylor); ABACUS (T. Helgaker, H. J. Aa. Jensen, P. Jørgensen, J. Olsen, and P. R. Taylor).
- [60] E. L. Muetterties, W. Mahler, R. Schmutzler, *Inorg. Chem.* **2**, 613 (1963).
- [61] R. J. Gillespie, *J. Chem. Educ.* **47**, 18 (1970).
- [62] L. A. Barnes, M. Rosi, C. W. Bauschlicher, *J. Chem. Phys.* **94**, 2031 (1991).
- [63] L. A. Barnes, B. Liu, R. Lindh, *J. Chem. Phys.* **98**, 3978 (1993).
- [64] B. J. Persson, B. O. Roos, *J. Chem. Phys.* **101**, 6810 (1994).
- [65] J. Li, G. Schreckenbach, T. Ziegler, *J. Phys. Chem.* **98**, 4838 (1994).
- [66] B. Delley, M. Wrinn, H. P. Luthi, *J. Chem. Phys.* **100**, 5785 (1994).
- [67] J. Li, G. Schreckenbach, T. Ziegler, *J. Am. Chem. Soc.* **117**, 486 (1995).
- [68] V. Jonas, W. Thiel, *J. Chem. Phys.* **102**, 8474 (1995).
- [69] A. W. Ehlers, G. Frenking, E. J. Baerends, *Organometallics* **16**, 4896 (1997).
- [70] A. W. Ehlers, Y. Ruiz-Morales, E. J. Baerends, T. Ziegler, *Inorg. Chem.* **36**, 5031 (1997).
- [71] K. G. Spears, *J. Phys. Chem. A* **101**, 6273 (1997).
- [72] T. Szymanska-Buzar, *Coord. Chem. Rev.* **159**, 205 (1997).
- [73] N. A. Beach, H. B. Gray, *J. Am. Chem. Soc.* **90**, 5713 (1968).
- [74] K. Pierloot, E. Tsokos, L. G. Vanquickenborne, *J. Phys. Chem.* **100**, 16545 (1996).
- [75] A. Rosa, E. J. Baerends, S. J. A. Van Gisbergen, E. Van Lenthe, J. A. Groeneveld, J. G. Snijders, *J. Am. Chem. Soc.* **121**, 10356 (1999).
- [76] M. Guttman, J. M. Janello, M. S. Dickebohm, M. Grossekathefer, J. Lindener-Roeneke, *J. Phys. Chem. A* **102**, 4138 (1998).
- [77] M. J. Paterson, P. A. Hunt, M. A. Robb, *J. Phys. Chem. A* **106**, 10494 (2002).
- [78] B. N. Figgis, A. N. Sobolev, *Acta. Cryst. E* **60**, i93 (2004).

- [79] B. Rees, A. Mitschler, *J. Am. Chem. Soc.* **98**, 7918 (1976).
- [80] A. Jost, B. Rees, W. Yelon, *Acta. Cryst. B* **31**, 2649 (1975).
- [81] H.-J. Werner, P. J. Knowles, R. Lindh, M. Schütz, P. Celani, T. Korona, F. R. Manby, G. Rauhut, R. D. Amos, A. Bernhardsson, A. Berning, D. L. Cooper, M. J. O. Deegan, A. J. Dobbyn, F. Eckert, C. Hampel, G. Hetzer, A. W. Lloyd, S. J. McNicholas, W. Meyer, M. E. Mura, A. Nicklass, P. Palmieri, R. Pitzer, U. Schumann, H. Stoll, A. J. Stone, R. Tarroni, T. Thorsteinsson. Molpro, version 2002.6, a package of ab initio programs, (2003), see <http://www.molpro.net>.
- [82] N. Ben Amor, S. Villaume, D. Maynau, C. Daniel. to be submitted.
- [83] S. Villaume, A. Strich, C. Daniel, S. A. Perera, R. J. Bartlett. to be published.
- [84] V. Vallet, A. Strich, C. Daniel, *Chem. Phys.* **311**, 13 (2005).
- [85] K. Eller, H. Schwarz, *Chem. Rev.* **91**, 1121 (1991).
- [86] K. K. Irikura, J. L. Beauchamp, *J. Am. Chem. Soc.* **111**, 75 (1989).
- [87] S. W. Buckner, T. J. MacMahon, G. D. Byrd, G. D. Freiser, *Inorg. Chem.* **28**, 3511 (1989).
- [88] K. K. Irikura, J. L. Beauchamp, *J. Am. Chem. Soc.* **113**, 2769 (1991).
- [89] K. K. Irikura, J. L. Beauchamp, *J. Phys. Chem.* **95**, 8344 (1991).
- [90] C. W. Bauschlicher, H. Partridge, J. A. Sheehy, S. R. Langhoff, M. Rosi, *J. Phys. Chem.* **96**, 6969 (1992).
- [91] K. K. Irikura, W. A. Goddard III, *J. Am. Chem. Soc.* **116**, 8733 (1994).
- [92] D. G. Musaev, K. Morokuma, N. Koga, *J. Chem. Phys.* **99**, 7859 (1993).
- [93] F. Ogliaro, S. D. Loades, D. L. Cooper, P. B. Karadakov, *J. Phys. Chem. A* **104**, 7091 (2000).
- [94] D. G. Musaev, K. Morokuma, N. Koga, K. A. Nguyen, M. S. Gordon, T. R. Cundari, *J. Phys. Chem.* **97**, 11435 (1993).
- [95] R. R. Schrock, *Acc. Chem. Res.* **12**, 98 (1979).
- [96] E. O. Fischer, *Adv. Organomet. Chem.* **14**, 1 (1976).
- [97] H. W. Turner, R. R. Schrock, *J. Am. Chem. Soc.* **104**, 2331 (1982).
- [98] J. Levisalles, F. Rose-Munsch, H. Rudler, J.-C. Daran, Y. Dromzee, Y. J. Jeannin, *J. Am. Chem. Soc. Commun.* **15** (1981).

- [99] E. O. Fischer, K. H. Dotz, *Chem. Ber.* **103**, 1273 (1970).
- [100] K. H. Dotz, E. O. Fischer, *Chem. Ber.* **105**, 1356 (1972).
- [101] D. G. Musaev, K. Morokuma, *J. Chem. Phys.* **101**, 10697 (1994).
- [102] J. Husband, F. Aguirre, C. J. Thompson, C. M. Laperle, R. B. Metz, *J. Phys. Chem. A* **104**, 2020 (2000).
- [103] S. Villaume, C. Daniel, A. Strich, S. A. Perera, R. J. Bartlett, *J. Chem. Phys.* **122**, 044313 (2005).
- [104] I. Bruand-Cote, thesis, Université Louis Pasteur, Strasbourg, (2002).
- [105] D. Guillaumont, thesis, Université Louis Pasteur, Strasbourg, (1998).
- [106] R. L. Sweany, F. N. Russel, *Organometallics* **7**, 719 (1988).
- [107] R. L. Sweany, *Inorg. Chem.* **21**, 752 (1982).
- [108] S. P. Church, M. Poliakoff, J. A. Timney, J. J. Turner, *Inorg. Chem.* **22**, 3259 (1983).
- [109] A. Veillard, A. Strich, *J. Am. Chem. Soc.* **110**, 3793 (1988).
- [110] C. Daniel, M. C. Heitz, L. Lehr, J. Manz, T. Schroder, *J. Phys. Chem.* **97**, 12485 (1993).
- [111] M. C. Heitz, C. Ribbing, C. Daniel, *J. Chem. Phys.* **106**, 1421 (1997).
- [112] C. Daniel, *J. Am. Chem. Soc.* **114**, 1625 (1992).
- [113] M. R. Hachey, C. Daniel, *Inorg. Chem.* **37**, 1387 (1998).
- [114] T. Ziegler, V. Tschinke, A. Becke, *J. Am. Chem. Soc.* **109**, 1351 (1987).
- [115] E. Folga, T. Ziegler, *J. Am. Chem. Soc.* **115**, 5169 (1993).
- [116] V. Jonas, W. Thiel, *J. Chem. Phys.* **105**, 3636 (1996).
- [117] S. K. Goh, D. S. Marynick, *Organometallics* **21**, 2262 (2002).
- [118] E. Orel, Y. Zhao, O. Kuhn, *J. Chem. Phys.* **112**, 94 (2000).
- [119] C. Daniel, *Chem. Rev.* **238-239**, 143 (2003).
- [120] S. Villaume, C. Daniel. to be published.

Appendix A

Acronym Glossary

ANO	Atomic natural orbital
B3LYP	Adiabatic connection method using Becke exchange and Lee-Yang-Parr correlation functional
CAS	Complete active space
CASPT2	Complete active space second-order perturbation theory
CASSCF	Complete active space self-consistent field
CC	Coupled cluster
CCSD	Coupled cluster with single and double excitation operators
CCSD(T)	CCSD with perturbative estimate for connected triples
CCSDT	Coupled cluster with single, double, and triple excitation operators
CCSDTQ	Coupled cluster with single, double, triple, and quadruple excitation operators
CI	Configuration interaction
CISD	Configuration interaction including single and double electronic excitation
DFT	Density functional theory
EOM-CC	Equation-of-motion coupled cluster
EA-EOM-CC	Electron-attachment equation-of-motion coupled cluster
FGH	Fourier grid hamiltonian method
GVB	Generalized valence bond
H-DAB	1,4-diaza-1,3-butadiene
HF	Hartree-Fock
HOMO	Highest occupied molecular orbital
ICACPF	Internally contracted average coupled-pair functional
IL	Intra-ligand
IP-EOM-CC	Ionization-potential equation-of-motion coupled cluster
KS	Kohn-Sham
LLCT	Ligand-to-ligand charge transfer
LMCT	Ligand-to-metal charge transfer
LUMO	Lowest occupied molecular orbital
MC	Metal centered
MCTDH	Multiconfiguration time dependent Hartree theory

MCPF	Modified coupled-pair functional
MLCT	Metal-to-ligand charge transfer
MP n	Møller-Plesset perturbation theory of order n
MRCI	Multireference configuration interaction
MS-CASPT2	Multistate complete active space second order perturbation theory
NMR	Nuclear magnetic resonance
PEC	Potential energy curve
PES	Potential energy surface
RHF	Restricted Hartree-Fock
ROHF	Restricted open-shell Hartree-Fock
STEOM-CC	Similarity transformed equation-of-motion coupled cluster
TD-DFT	Time dependent density functional theory
TDH	Time dependent Hartree theory
TBP	Trigonal bipyramid
TP	Tetragonal bipyramid
UHF	Unrestricted Hartree-Fock

Spectroscopie électronique et photochimie de petits complexes de métaux de transition étudiés par des méthodes Coupled Cluster et propagation de paquets d'ondes.

Cette thèse de chimie informatique et théorique porte sur la spectroscopie électronique et la photochimie de petits complexes de métaux de transition. Ces molécules sont caractérisées par une grande densité d'états électroniques excités de nature très diverse dans le domaine énergétique UV-Visible. La position relative de ces états est contrôlée par la nature du centre métallique et des ligands, ce qui influe sur la réactivité induite par la lumière. L'étude théorique de la photochimie de ces systèmes nécessite l'emploi de méthodes de chimie quantique prenant en compte la corrélation électronique. La première partie de la thèse décrit les méthodes *ab initio* et de dynamique quantique que nous avons utilisées. Le second chapitre présente une étude des réarrangements intramoléculaires dans PH_2F_3 . La troisième partie rapporte une étude détaillée de la spectroscopie électronique de $\text{Cr}(\text{CO})_6$ ainsi que la photodissociation conduisant au départ d'un ligand carbonyle. Le quatrième chapitre porte sur l'étude de la structure électronique de la famille des petits complexes MCH_2^+ ($\text{M}=\text{Fe}, \text{Co}, \text{Ni}$) par des calculs Coupled Cluster. L'avant-dernière partie concerne la spectroscopie d'absorption et plus particulièrement d'émission des états à transfert de charge métal vers ligands du complexe $\text{HRe}(\text{CO})_3(\text{H-DAB})$. Enfin le dernier chapitre propose une nouvelle étude de la photochimie des complexes $\text{RCo}(\text{CO})_4$ ($\text{R}=\text{H}, \text{CH}_3$) par des calculs *ab initio* et TD-DFT ainsi qu'une simulation par dynamique quantique de la photodissociation compétitive des ligands axiaux CO et H dans le cas de $\text{HCo}(\text{CO})_4$.

Electronic spectroscopy and photochemistry of small transition metal complexes studied via Coupled Cluster calculations and wavepacket propagation.

The scope of this thesis in computational and theoretical chemistry is the study of the electronic spectroscopy and the photochemistry of transition metal compounds. These molecules are characterized by a high density of electronic excited states of different nature in the UV-Visible energy window. The relative position and the character of these excited states are controlled by the nature of the metal center and surrounding ligands which influence light-induced reactivity. The theoretical study of the photochemistry of these systems requires approaches based on highly correlated methods of quantum chemistry. The first part of the thesis describes quantum chemical methods and quantum dynamical formalism used in this work. The second chapter presents the study of the intramolecular rearrangement in trifluorophosphorane PH_2F_3 . The third part focuses on the electronic spectroscopy of $\text{Cr}(\text{CO})_6$ the photodissociation processes that lead to the departure of a carbonyl. The fourth chapter deals with the detailed study of the electronic structure of the MCH_2^+ ($\text{M}=\text{Fe}, \text{Co}, \text{Ni}$) series. The fifth part is dedicated to the absorption and emission spectroscopy of a metal to ligand charge transfer states of $\text{HRe}(\text{CO})_3(\text{H-DAB})$. The last part is devoted to the photochemistry of $\text{RCo}(\text{CO})_4$ ($\text{R}=\text{H}, \text{CH}_3$) studied via *ab initio* and TD-DFT calculations and a quantum dynamical simulation of the competitive photodissociation of axial ligands CO and H in the case of $\text{HCo}(\text{CO})_4$.